universität wien

MASTERARBEIT / MASTER'S THESIS

Titel der Masterarbeit / Title of the Master's Thesis

„Colour-Flow Evolution at Next-to-leading Order "

verfasst von / submitted by

Ines Ruffa, BSc

angestrebter akademischer Grad / in partial fulfilment of the requirements for the degree of

Master of Science (MSc)

Wien, 2020 / Vienna, 2020

Studienkennzahl lt. Studienblatt / degree programme code as it appears on the student record sheet:	A 066 876 [2]
Studienrichtung lt. Studienblatt / degree programme as it appears on the student record sheet:	Masterstudium Physik
Betreut von / Supervisor:	Univ.-Prof. Dr. André Hoang
Mitbetreut von / Co-Supervisor:	Dr. Simon Plätzer

Table of contents

Abstract

This thesis aims to investigate soft gluon evolution at next-to-leading order (NLO), i.e. adding soft gluon corrections, both real emissions and virtual exchanges to a hard, short-distance scattering process. In this context "soft" refers to gluons emitted at an energy scale much smaller than the one of the hard process.

The main part of this work is thus dedicated to analyse the one-loop/one-emission and two-loop Feynman diagrams involving soft gluons in order to provide the basic ingredients if one aims to perform soft gluon evolution and to resum non-global logarithms at next-to-leading logarithmic level as well as beyond the large-N limit of QCD. The analysis of the diagrams is separated into two parts - the colour structure and the kinematical part.

Treating the amplitude as a vector in colour space, it is decomposed in terms of the colour-flow basis. The general form of the soft anomalous dimension matrix at one-loop/one-emission and two-loop order in the colour-flow basis is determined by analysing the colour structures. As a result of this analysis structures of special importance at two-loop order are obtained which extend the sum over two-parton correlations, usually referred to as "dipoles", to include three-parton correlations as well.

Using the Feynman tree theorem (FTT) to treat the kinematical part allows one to efficiently rewrite the loop integrals in the form of phase-space integrals. In this way it is possible to combine the loop integrals with the emission contributions at the integrand level of a cross-section in order to demonstrate the cancellation of infrared (IR) divergences. In particular, the FTT is reformulated such that one can use it in the presence of eikonal propagators as well as at the two-loop level.

Zusammenfassung

Diese Arbeit befasst sich mit der Entwicklung von Streuamplituden durch das Hinzufügen von soften Gluon Korrekturen - virtuelle Beiträge („Loops") sowie auch reelle Emissionen - in nächstführender Ordnung in perturbativer Störungstheorie zu einem harten Prozess. Softe Gluonen sind durch eine Energieskala charakterisiert, die weitaus kleiner als die Skala des harten Prozesses ist.

Der Hauptteil widmet sich der Analyse der relevanten Ein-Loop/Ein-Emissisons und Zwei-Loop Feynman-Diagrammen mit soften Gluonen. Die Kenntnis ihrer Form gestattet die Resummation von nicht-globalen Logarithmen zu nächstführender logarithmischer Ordnung und ermöglicht es außerdem, Beiträge zu berücksichtigen, die mit der Anzahl der Farbladungen unterdrückt sind. Die Analyse der Diagramme besteht aus zwei Teilen - der Farbstruktur und der kinematischen Abhängigkeit.

Behandelt man die Streuamplitude als Vektor im Farbraum, so verlangt es nach Wahl einer Basis dieses Vektorraums, um konkrete Berechnungen durchzuführen. In dieser Arbeit wird die Farbflussbasis gewählt. Durch die eingehende Betrachtung der Farbstrukturen wird die Form der soften anomalen Dimension zur Ein-Loop/Ein-Emissions und Zwei-Loop Ordnung bestimmt. In Zwei-Loop Ordnung treten Strukturen auf, die nahelegen, die Summe über Zwei-Parton Korrelationen, sogenannte „Dipole", auf eine zu erweitern, die auch Drei-Parton Korrelationen berücksichtigt.

Das Feynman Tree Theorem (FTT) wird angewendet, da es in effizienter Weise erlaubt, die Loop-Integrale in Form von Phasenraum-Integralen darzustellen. Damit lässt sich die Kanzellierung der infrarot (IR) Divergenzen zwischen virtuellen und reellen Beiträgen explizit zeigen. Im Speziellen wird das FTT umformuliert, um die Anwendung bei eikonalen Propagatoren sowie für Zwei-Loop Diagramme zu ermöglichen.

1 Overview

For some hard, short-distance scattering process the most important radiative QCD corrections are given by collinear and soft gluons in a perturbative treatment. The latter are the subject of this thesis, soft gluon corrections of the hard external lines of QCD amplitudes. In this context "hard" refers to a high-energy scale, while the energy scale at which "soft" gluons are emitted is very small compared to the hard scale.

For totally inclusive observables (e.g. total e^+e^- cross-section) infrared (IR) divergences introduced by the softness of the massless gluon completely cancel between virtual exchange and real emission soft corrections; a fixed-order calculation leads to sufficiently precise predictions. Observables for which the real emissions are restricted in some way, i.e. for non-global observables [1], the IR divergences still cancel (by virtue of the Bloch-Nordsieck theorem/Kinoshita-Lee-Nauenberg theorem), however, a resummation of the perturbative series is needed, since large logarithms (between the scale provided by the constraint on the real emission and some hard scale) appear. This resummation can be achieved by soft gluon evolution equations [2, 3] formulated in colour space.

In this work the main focus lies on the virtual soft gluon corrections at one-loop/one-emission and two-loop order in perturbation theory. These provide input to construct the evolution equations at next-to-leading order (NLO) such that resummation of non-global next-to-leading logarithms (NLL) is made possible, as well as to include contributions subleading in the number of colours N.

The thesis is structured as follows:

At first some basic concepts like the QCD Lagrangian, important relations concerning colour algebra, renormalisation and the eikonal approximation for soft four-momenta are briefly reviewed.

Following up on this general introduction, a more specific and detailed one concerned with the methods and techniques relevant to this work is given. These include the colour-space formalism [4, 5] as the framework in which scattering amplitudes can be treated and the colour-flow basis [2, 5, 6] which is the basis of choice of the colour vector space in this work. It is elucidated how to translate colour factors obtained from the conventional QCD Feynman rules to the colour-flow basis, which allows for an immediate physical interpretation in terms of the flow of the colour charges in a process. This flow of colour charges can then be intuitively depicted with the help of colour-line diagrams.

After focussing on the efficient formulation of the colour structure of the amplitudes, their kinematic part is addressed. For the purposes of this work it is beneficial to be able to rewrite the loop integrals in the form of real-emission phase-space integrals in order to combine the virtual soft gluon exchange corrections with the real emission diagrams leading to a cancellation of IR divergences. The rewriting can be most conveniently achieved by applying the Feynman tree theorem (FTT) [7, 8]. In particular, it is reformulated in order to apply it in the presence of eikonal propagators.

In the last part of the introductory sections the soft gluon evolution equations [2, 3, 9], which allow for resummation of non-global logarithms, are introduced. The evolution proceeds in colour space at amplitude level which allows to formulate an IR-finite evolution operator since the cancellation of IR divergences already takes place at the integrand level and an expression for the soft anomalous dimension matrix is found. Thus, for this part the concepts of the prior sections can already be put to use.

The fourth section is dedicated to investigate the structure of the soft anomalous dimension matrix at leading order. The colour structure is analysed in the colour-flow basis in detail, leading to an expression for the matrix element of the colour-correlator [2, 6]. For the kinematic part the FTT is applied to the soft virtual exchange diagram, the result is combined with the corresponding soft emission process, the IR singularities indeed cancel.

The fifth section provides ingredients for a next-to-leading order as well as next-to-leading colour soft evolution. At first the one-loop/one-emission diagrams which contribute in the soft limit are analysed, an expression for the building blocks of the soft anomalous dimension concerning its colour structure in the colour-flow basis is given at this order. The FTT is used to obtain expressions for the cut-contributions of the loop integrals.

In the same way the colour structure for the two-loop diagrams is analysed as well. Further, a procedure to apply the FTT at two-loop level is discussed in detail and graphically illustrated in the case of the double virtual soft gluon exchange. This procedure is then applied to the other two-loop diagrams contributing in the eikonal limit, in this way expressions for the cut-contributions of the diagrams are obtained. By filtering out the radiative cuts in the loop momenta and combining them with the squared real emission diagrams the cancellations of IR divergences between them for each of the different colour structures is shown.

The self-energy contributions ("bubble-diagrams") demand a slightly modified treatment concerning their kinematic part due to the appearance of double propagators. A cutting rule for such cases is introduced and by using this modified cutting rule the FTT is applied to the loop integrand and the radiative cancellations of IR divergences are shown for the self-energy diagrams as well.

A short summary and an outlook conclude the main part of the thesis. The appendices provide more detailed calculations on Jacobian determinants and the soft two-loop current [10]. The conventions which are used in this work concerning the Feynman rules are briefly summarised. Moreover, the lengthy results for the matrix elements in the colour-flow basis of the one-loop/one-emission and two-loop colour structures which lead to the results of the colour part of the soft anomalous dimension are explicitly given. Finally, a list of kinematically forbidden cuts appearing in the course of the FTT cutting procedure is provided.

All the diagrams and illustrations in this work have been prepared using JaxoDraw [11].

2 Preliminaries

2.1 QCD Lagrangian and colour algebra

This introductory section aims to briefly summarise the basic ingredients of the locally gauge-invariant QCD Lagrangian as well as establish the conventions of signs and normalisation concerning the colour algebra, which will be used in later sections. This section is based on the corresponding chapters in [12, 13].

The central object of QCD is its Lagrangian density given by

$$\mathcal{L}_{\mathrm{QCD}} = -\frac{1}{4} F^a_{\mu\nu} F^{\mu\nu\,a} + \sum_{f=1}^{n_f} \bar{\psi}^j_f \left(i \not{D}^i{}_j - m\delta^i_j \right) \psi_{f,i} \ . \tag{2.1}$$

The contribution to the Lagrangian of the quark fields ψ is subject to a sum over flavours (with the total number of flavours n_f) and the covariant derivative $(D^\mu)^i{}_j$ is, in terms of components, given by

$$(D^\mu)^i{}_j = \partial^\mu \delta^i_j + igA^{\mu\,a}(t^a)^i{}_j \ , \tag{2.2}$$

with the (anti-)fundamental indices $i, j = 1, ..., N$. It is convenient to explicitly distinguish fundamental and anti-fundamental indices, since in the following sections of this work a main focus lies on the flow of the colour charges.
The use of the covariant derivative instead of just the partial derivative ensures that the kinetic term of the quark fields is not only invariant under global transformations but under local gauge transformations as well. This can be established by noticing the invariance of the QCD Lagrangian under local $\mathrm{SU}(N)$ gauge transformations for each flavour of the quark field $\psi(x)$

$$\psi(x) \to \psi'(x) = \exp\left[\theta^a(x) t^a\right] \psi(x) \equiv U(\vec{\theta}(x))\psi(x) \ , \tag{2.3}$$

where the generators are in the fundamental representation and the $\theta^a(x)$ are local functions in space-time, they parameterise the group.
The kinetic term of the gauge fields A^a_μ is written in terms of the non-Abelian field-strength tensor $F^a_{\mu\nu}$ which has the following form

$$F^a_{\mu\nu}(x) = \partial_\mu A^a_\nu(x) - \partial_\nu A^a_\mu(x) - g f^{abc} A^b_\mu(x) A^c_\nu(x) \ . \tag{2.4}$$

At variance with the Abelian case, self-interactions are introduced due to the presence of the last term in the equation above. The gluon field $\mathcal{A}_\mu = t^a A^a_\mu$ transforms according to the adjoint representation

$$\mathcal{A}_\mu \to \mathcal{A}'_\mu = U(\vec{\theta}(x))\mathcal{A}_\mu(x)U^{-1}(\vec{\theta}(x)) + \frac{i}{g}\partial_\mu \left[U(\vec{\theta}(x))\right] U^{-1}(\vec{\theta}(x)) \ . \tag{2.5}$$

Therefore, the field-strength tensor $\mathcal{F}_{\mu\nu} = F^a_{\mu\nu} t^a$ transforms in the adjoint representation as well and hence it is not gauge-invariant by itself in the non-Abelian case. But of course the combination $(F^a_{\mu\nu} F^{a\,\mu\nu})$ appearing in the Lagrangian is gauge-invariant.

Due to the arbitrariness of the gauge field, which is caused by its gauge transformation property, an additional gauge-fixing term has to be introduced to the Lagrangian. For covariant gauges it is of the form

$$\mathcal{L}_{\mathrm{gauge-fixing}} = -\frac{1}{2\xi}\,(\partial_\mu A^{\mu\,a})^2 \ . \tag{2.6}$$

Throughout this work the Feynman-t'Hooft gauge is used, i.e. the gauge parameter is assigned the value $\xi = 1$.

In addition to the gauge-fixing term one needs to include a Faddeev-Popov ghost field Lagrangian in order to eliminate contributions from unphysical polarisations of the gluons, in covariant gauge it reads

$$\mathcal{L}_{\mathrm{ghost}} = (\partial_\mu \bar{\eta}^a)\,(D^\mu_{ab}\eta^b) \ , \tag{2.7}$$

where the covariant derivative in the adjoint representation is given by

$$D^\mu_{ab} = \partial^\mu \delta_{ab} + g f_{abc} A^{\mu\,c} \ . \tag{2.8}$$

The (anti-)ghost fields η^a and $\bar{\eta}^a$ are Grassmann-valued fields, i.e. they are Lorentz-scalars but they anti-commute.

The set of generators obey the relation

$$\left[t^a, t^b\right] = i f^{abc} t^c \ , \tag{2.9}$$

with f^{abc}, the structure constants. The commutation relation implies that the structure constants can be expressed in terms of the fundamental generators

$$f^{abc} = -2i\mathrm{Tr}\left[t^a t^b t^c - t^b t^a t^c\right] \ . \tag{2.10}$$

In the course of this work this relation will be used repeatedly, it is very convenient when one aims to rewrite the colour factor either purely in terms of fundamental generators or adjoint ones (see sections 3.1 and 3.2).

As a normalisation convention of the fundamental generators it is used here that $T_R = 1/2$ and thus

$$\mathrm{Tr}\left[t^a t^b\right] = T_R \delta^{ab} \ . \tag{2.11}$$

Furthermore, for the adjoint representation generators $(t^a_{\mathrm{adj}})^{bc} = -i f^{abc}$ one has

$$\mathrm{Tr}\left[t^a_{\mathrm{adj}} t^b_{\mathrm{adj}}\right] = N \delta^{ab} \ . \tag{2.12}$$

These normalisation properties can be used to find the following relations

$$\begin{aligned} (t^a)^i{}_j (t^a)^j{}_k &= C_F\, \delta^i_k \ , \\ (t^a_{\mathrm{adj}})^{bc} (t^a_{\mathrm{adj}})^{cd} &= C_A\, \delta^{bd} \ , \end{aligned} \tag{2.13}$$

with the Casimir invariants $C_F = (N^2-1)/2N$ and $C_A = N$. The Fierz identity is used frequently in this work; it reads

$$(t^a)^i{}_j (t^a)^l{}_k = \frac{1}{2}\left[\delta^i_k \delta^n_j - \frac{1}{N}\delta^l_k \delta^i_j\right] \,, \tag{2.14}$$

which can be established by using the general form of an arbitrary matrix M of SU(N), i.e. $M = \exp[i\theta^a t^a]$ or, written as an expansion, $M = \theta^0 \mathbb{1} + \theta^a t^a$ and determining the coefficients. Note that there is an implicit sum over two equal adjoint indices.

2.2 Renormalisation

In this introductory section a brief overview of multiplicative renormalisation is given. It is based on the corresponding chapters in [12, 14] and lecture notes by Simon Plätzer of the lecture "Particle Physics III" [15].

In general the loop integrals encountered when evaluating amplitudes of radiative corrections are ultraviolet (UV) and/or infrared (IR) divergent. A convenient way to handle such ill-defined integrals in a first step is to perform dimensional regularisation in order to extract the leading singularities by changing the number of dimensions to $d = 4 - 2\varepsilon$ and performing an expansion around $\varepsilon = 0$. As a consequence, the necessity to introduce a dimensionful parameter, the t'Hooft parameter μ, arises. This ensures that the mass-dimension of the integral (measure) remains unchanged. For example, if one writes for the loop momentum $k = (k^0, E\vec{n}(\theta, \varphi))$ where $\vec{n}^2 = 1$, one may rewrite the d-dimensional integration measure in the following way

$$\mu^{4-d} \int \mathrm{d}^d k = \int_{-\infty}^{\infty} \mathrm{d}k^0 \int \mathrm{d}E \left(\frac{\mu}{E}\right)^{2\varepsilon} E^2\, \theta(E) \int \mathrm{d}\Omega^{(d-2)} \,, \tag{2.15}$$

where

$$\int \mathrm{d}\Omega^{(d-2)} = \int_{-1}^{1} \mathrm{d}\cos\theta \left(1 - \cos^2\theta\right)^{-\varepsilon} \int \mathrm{d}\Omega^{(d-3)} \,. \tag{2.16}$$

Consult appendix A for details on the calculation of the Jacobian determinant in this particular case. Concerning the angular integration in equation (2.16) with its Jacobian factor, it is noteworthy that for real emission integrands, which are typically of the form $(1-\cos\theta)^{-1}$ the collinear divergence will be regularised as well, in addition to the soft divergence of the energy integration.

When specifying a loop integrand and performing the k^0 integration for the loop integral measure given in equation (2.15), then one will typically find some $1/E$ factors pertaining to the propagators which combine with the factor E^2 from the Jacobian determinant such that in the end one is left with a logarithmic energy integration $(\mathrm{d}E/E) \times (\mu/E)^{2\varepsilon}$ (see section 4.3 for a particular example). This leads to a pattern of divergences of the form $(\text{poles in}\, \varepsilon) \times (\mu/Q)^{2\varepsilon}$, where Q is a scale involved in the process one aims to describe, for instance the hard scale of the hard, short-distance process. Thus, one finds the same divergence structure as it can be obtained by performing Feynman parameter integrals for massless particles.
At this point it shall be remarked that dimensional regularisation preserves gauge invariance and Lorentz invariance.
After having made the divergences explicit in terms of poles in the parameter ε for letting $\varepsilon \to 0$

one can perform the renormalisation procedure in order to deal with the UV divergences. The renormalisation proceeds through the redefinition of “bare”, i.e. unrenormalised, quantities of the Lagrangian in terms of renormalised ones. These quantities can be identified with fields, masses and couplings, which have to be redefined. As a result the bare Lagrangian $\mathcal{L}_{\text{bare}}$ is expressed as a sum of the renormalised Lagrangian $\mathcal{L}_{\text{ren}}$ and a counterterm Lagrangian $\mathcal{L}_{\text{ct}}$,

$$\mathcal{L}_{\text{bare}} = \mathcal{L}_{\text{ren}} + \mathcal{L}_{\text{ct}} \ . \tag{2.17}$$

The renormalisation transformations from bare to renormalised quantities effectively subtract the divergent parts. For a multiplicative renormalisation a multiplicative factor, a renormalisation factor Z_i, is introduced in the transformation, absorbing the UV divergence. Expanding the renormalisation factor leads to a removal of the UV divergences order by order in perturbation theory. There is, however, some freedom of how to define this divergent part. The renormalisation scheme characterises this freedom. For instance, in the minimal subtraction (MS) scheme, only the UV-pole in ε is removed, while in the $\overline{\text{MS}}$-scheme the constant $\ln(4\pi) - \gamma_E$, appearing due to an expansion of the gamma function, is eliminated as well.

Crucially, a theory is renormalisable if the (finite) number of the parameters, which are used to absorb the UV divergences, remain the same at each order in perturbation theory.

For any renormalisation scheme one has to introduce a renormalisation scale μ_R describing at which momentum scale the renormalisation is to be performed. It is important to remark that for amplitudes which exhibit both UV and IR divergences or processes involving multiple scales it is beneficial to explicitly distinguish the arbitrary renormalisation scale μ_R from the t'Hooft scale μ, the latter will always have cancelled in the final result. As mentioned previously, the structure of the divergences originating from the loop-integration is $(\text{poles in}\, \varepsilon) \times (\mu/Q)^{2\varepsilon}$. Performing the renormalisation procedure provides one with the same structure but with an opposite sign and μ_R as the scale, i.e. $(-\text{poles in}\, \varepsilon) \times (\mu/\mu_R)^{2\varepsilon}$. Therefore, expanding in ε, one is left with a logarithm of the form $\ln(\mu_R^2/Q^2)$ relating the two scales μ_R and Q, the pole in ε has cancelled.

For a general quantity X which gets renormalised one can formulate

$$X^{\text{bare}}(\mu, \varepsilon) = Z_X(\mu, \mu_R, \varepsilon) X(\mu_R) \ , \tag{2.18}$$

which leads to the conclusion that the renormalised quantity $X(\mu_R) = \lim_{\varepsilon\to 0}(Z_X^{-1}(\mu, \mu_R, \varepsilon)$ $X^{\text{bare}}(\mu, \varepsilon))$ is finite. Further, for the renormalisation factor Z_X one can establish the expansion

$$Z_X(\mu, \mu_R, \varepsilon) = 1 + \left(\frac{\mu}{\mu_R}\right)^{2\varepsilon} g\, Z_X^{(1)} + \left(\frac{\mu}{\mu_R}\right)^{4\varepsilon} g^2 Z_X^{(2)} + \dots \ , \tag{2.19}$$

where g is the renormalised coupling. For the coupling itself it may also prove useful to adopt an alternative (but equivalent) way of defining the renormalisation transformation. In particular, with the equations (2.18) and (2.19) one can write

$$g^{\text{bare}}(\mu, \varepsilon) = Z_g(\mu, \mu_R, \varepsilon)\, g(\mu_R) = \left[1 + \left(\frac{\mu}{\mu_R}\right)^{2\varepsilon} g(\mu_R) Z_g^{(1)} + \left(\frac{\mu}{\mu_R}\right)^{4\varepsilon} g^2(\mu_R) Z_g^{(2)} + \dots\right] g(\mu_R) \ . \tag{2.20}$$

For convenience one can now absorb the factor of $(\mu/\mu_R)^{2\varepsilon}$ into the coupling. Hence, letting $g \to g \times (\mu_R/\mu)^{2\varepsilon}$ one can reformulate equation (2.20) such that one obtains

$$g^{\text{bare}}(\mu, \varepsilon) = \left[1 + g(\mu_R)\tilde{Z}_g^{(1)} + g^2(\mu_R)\tilde{Z}_g^{(2)} + ...\right] \left(\frac{\mu_R}{\mu}\right)^{2\varepsilon} g(\mu_R) \ , \tag{2.21}$$

or equivalently,

$$\mu^{2\varepsilon} g^{\text{bare}}(\mu, \varepsilon) = \tilde{Z}_g(\mu, \mu_R, \varepsilon)\, \mu_R^{2\varepsilon}\, g(\mu_R) \ . \tag{2.22}$$

In this way of writing one may define $\mu^{2\varepsilon} g^{\text{bare}}(\mu, \varepsilon)$ as the bare coupling in dimensional regularisation with correct mass dimension and, in the same sense, $\mu_R^{2\varepsilon}\, g(\mu_R)$ can be recognised as the renormalised coupling.

For QCD the parameters which get renormalised are the gluon field A_α^a, the quark field ψ, the ghost field η^a, the coupling and, in principle, the masses of the quarks

$$\begin{aligned}
A_\alpha^{a,\text{bare}} &= Z_3^{1/2} A_\alpha^a \ , \\
\psi^{\text{bare}} &= Z_2^{1/2} \psi \ , \\
\eta^{a,\text{bare}} &= Z_\eta^{1/2} \eta^a \ , \\
g^{\text{bare}} &= Z_g g \ , \\
m^{\text{bare}} &= Z_m m \ ,
\end{aligned} \tag{2.23}$$

where the dependence on μ and μ_R are suppressed to avoid clutter. As explicitly written before, the renormalised parameters depend on the renormalisation scale μ_R, while the bare parameters depend on μ and their use leads to the divergence in ε.

In principle one has to take into account the renormalisation of the gauge-fixing parameter ξ as well, however, its renormalisation factor coincides with the one for the gluon field, Z_3, due to the transversality of the gluon vacuum polarisation tensor ("bubble-diagram"). Consequently, the gauge-fixing term of the Lagrangian does not get renormalised.

Using equation (2.23) one can rewrite the bare QCD Lagrangian as

$$\begin{aligned}
\mathcal{L}_{\text{QCD}}^{\text{bare}} = &-\frac{1}{4} F_{\alpha\beta}^a F^{a,\alpha\beta} + \bar{\psi}(i\partial\!\!\!/ - g A\!\!\!/^a t^a - m)\psi - \frac{1}{2\xi}(\partial_\alpha A^{a,\alpha})^2 - \bar{\eta}^a \partial^\alpha \partial_\alpha \eta^a + g\,\bar{\eta}^a f^{abc} \partial_\alpha A^{b,\alpha} \eta^c \\
&+ \bar{\psi}\, i\partial\!\!\!/\, \psi (Z_2 - 1) - g\,\bar{\psi} A\!\!\!/^a t^a \psi\, (Z_{1F} - 1) - m\bar{\psi}\,\psi(Z_m Z_2 - 1) \\
&- \bar{\eta}^a \partial^\alpha \partial_\alpha \eta^a (Z_\eta - 1) + g\, f^{abc} \bar{\eta}^a \partial_\alpha A^{b,\alpha} \eta^c (Z_1' - 1) \\
&- \frac{i}{4} \left(\partial_\alpha A_\beta^a - \partial_\beta A_\alpha^a\right) \left(\partial^\alpha A^{a,\beta} - \partial^\beta A^{a,\alpha}\right) (Z_3 - 1) \\
&+ \frac{1}{2} g\, f^{abc} A^{b,\alpha} A^{c,\beta} \left(\partial_\alpha A_\beta^a - \partial_\beta A_\alpha^a\right) (Z_1 - 1) - \frac{1}{4} g^2\, f^{abc} f^{ade} A^{b,\alpha} A^{c,\beta} A_\alpha^d A_\beta^e (Z_4 - 1) \ ,
\end{aligned} \tag{2.24}$$

where one defines the renormalisation constants for the triple gluon vertex Z_1, for the quartic gluon vertex Z_4, for the quark-gluon coupling Z_{1F} and for the ghost-gluon coupling Z_1' in the counterterm Lagrangian. Making use of the universality of the coupling g one can establish

$$\begin{aligned} Z_{1F} &= Z_g\, Z_2\, Z_3^{1/2}, \\ Z_1 &= Z_g\, Z_3^{1/2}, \\ Z_1' &= Z_g\, Z_3^{1/2}\, Z_\eta, \\ Z_4 &= Z_g^2\, Z_3^2\ . \end{aligned} \tag{2.25}$$

These results lead to the Slavnov-Taylor identities

$$\frac{Z_{1F}}{Z_2} = \frac{Z_1}{Z_3} = \frac{Z_1'}{Z_\eta} = \left(\frac{Z_4}{Z_3}\right)^{\frac{1}{2}} , \tag{2.26}$$

which fix the relations between the different Green functions, similar to the Ward identity in QED and hold to all orders in perturbation theory.
Due to the dependence of the renormalised parameters on the renormalisation scale, one can formulate renormalisation group equations (RGE) by differentiating with respect to μ_R. A bare, truncated n-point Green function G^{bare} can be brought into relation with the renormalised one, G_R, in the following way

$$G^{\text{bare}}(g^{\text{bare}}, m^{\text{bare}}, \mu; p_1, ..., p_n) = Z_\varphi^{-\frac{n}{2}}\,(\mu, \mu_R)\, G_R\,(g(\mu_R), m(\mu_R), \mu_R; p_1, ..., p_n)\ , \tag{2.27}$$

where the field renormalisation factor Z_φ stands for a product of the gluon, quark and ghost renormalisation factors. Differentiating with respect to μ_R leads to the Callan-Symanzik equation

$$\left(\mu_R \frac{\partial}{\partial \mu_R} + \beta_g \frac{\partial}{\partial g} + m\, \gamma_m \frac{\partial}{\partial m} - n\gamma_\varphi\right) G_R(g(\mu_R), m(\mu_R), \mu_R; p_1, ..., p_n) = 0\ , \tag{2.28}$$

where the β-function and the so-called anomalous dimensions for mass and fields are given by

$$\begin{aligned} \beta_g &= \mu_R \frac{\partial g}{\partial \mu_R}\ , \\ \gamma_m &= \frac{\mu_R}{m} \frac{\partial m}{\partial \mu_R}\ , \\ \gamma_\varphi &= \frac{1}{2} Z_\varphi^{-1} \mu_R \frac{\partial}{\partial \mu_R} Z_\varphi\ , \end{aligned} \tag{2.29}$$

respectively. Defining

$$\mathrm{d}t \equiv \frac{\mathrm{d}\overline{\mu}_R}{\overline{\mu}_R} = \frac{\mathrm{d}\overline{g}}{\beta_g(\overline{g}, \frac{\overline{m}}{\overline{\mu}_R}, \varepsilon)} = \frac{\mathrm{d}\overline{m}}{\overline{m}\gamma_{\overline{m}}}\ , \tag{2.30}$$

with the initial conditions $\overline{\mu}_R(t=0) = \mu_R$, $\overline{g}(t=0) = g$ and $\overline{m}(t=0) = m$ one can rewrite equation (2.28) as

$$\left[\frac{\mathrm{d}}{\mathrm{d}t} - n\gamma_\varphi\right] G_R\,(\overline{g}(\overline{\mu}_R), \overline{m}(\overline{\mu}_R), \overline{\mu}_R; p_1, ..., p_n) = 0\ . \tag{2.31}$$

Solving this differential equation and taking into account the initial conditions one obtains

$$G_R(g, m, \mu_R; p_1, ..., p_n) = G_R(\overline{g}, \overline{m}, \overline{\mu}_R; p_1, ..., p_n) \exp\left[-n \int_g^{\overline{g}} \mathrm{d}x \frac{\gamma_\varphi(x)}{\beta_g(x)}\right] , \tag{2.32}$$

which provides the relation of the truncated Green function at different scales/couplings. This principle described for amputated Green functions also holds for general operators, in particular also for observables like cross-sections.
In this way, by solving the renormalisation group equation for the coupling α_s, one finds one of the defining properties of QCD: asymptotic freedom. It also allows one to approximate up-, down- and strange-quarks (u-, d-, s-quarks) as massless for sufficiently high μ_R. The RGE for the quark mass in the $\overline{\text{MS}}$-scheme can be written as

$$\mu_R \frac{\mathrm{d}}{\mathrm{d}\mu_R} m(\mu_R) = \gamma_m \alpha_s^{\overline{\text{MS}}}(\mu_R) m(\mu_R) , \tag{2.33}$$

and its solution provides one with the fact that $m(\mu_R)$ decreases as the renormalisation scale increases. According to this reasoning the quark masses for u-, d- and s-quarks can be neglected in the high-energy limit, since their masses, e.g. in the $\overline{\text{MS}}$-scheme, are much smaller than Λ_{QCD}, the scale up to which perturbation theory can be safely performed. Thus, the high-energy limit coincides with a "zero-mass" limit for u-, d- and s-quarks.

2.3 Eikonal approximation

Previously, UV divergences have been introduced, in this section IR divergences (soft and collinear singularities) are discussed. In particular, the eikonal approximation, i.e. the approximation for soft gluons, is reviewed [12].

Consider the emission of a soft gluon of momentum k off a massless quark line i, with some amplitude $\mathcal{M}_0$ of a hard, short-distance process depicted by the "blob"

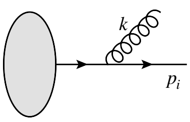

$$\equiv \mathcal{M}^\mu = ig\, t_i^a \bar{u}(p_i)\gamma^\mu \frac{i(\not{p}_i + \not{k})}{[(p_i + k)^2]} \mathcal{M}_0(p_i + k) . \tag{2.34}$$

The soft gluon approximation is now implemented by letting $k \to \lambda k$, followed by $\lambda \to 0$. Performing the limit $k \to \lambda k$ gives

$$\mathcal{M}^\mu = -g t_i^a \bar{u}(p_i)\gamma^\mu \left[\frac{1}{\lambda} \frac{\not{p}_i}{[2p_i \cdot k + \lambda k^2]} + \frac{\not{k}}{[2p_i \cdot k + \lambda k^2]}\right] \mathcal{M}_0(p_i + \lambda k) . \tag{2.35}$$

For the eikonal approximation only terms of the lowest order in λ, i.e. of $\mathcal{O}\left(\frac{1}{\lambda}\right)$, are kept. Hence, one finds

$$\mathcal{M}^\mu_{\text{eikonal}} = -g\, t_i^a \bar{u}(p_i) \frac{1}{\lambda} \frac{p_i^\mu}{[p_i \cdot k]} \mathcal{M}_0(p_i) , \tag{2.36}$$

where the Dirac equation was used such that $\bar{u}(p_i)\gamma^\mu \not{p}_i = 2p_i^\mu \bar{u}(p_i)$ and for the amplitude $\mathcal{M}_0$ one can approximate $\mathcal{M}_0(p_i + \lambda k) = \mathcal{M}_0 + \mathcal{O}(\lambda)$. Also note that for a polarisation vector in the soft limit it holds that $\varepsilon_\mu(k) \to \varepsilon_\mu(k) + \lambda k_\mu$ and $\lambda \to 0$. From equation (2.36) one can observe

that in addition to the soft divergence for $\lambda \to 0$, there is also a collinear divergence, if the angle θ between $\vec{p_i}$ and $\vec{k}$ tends to zero.
For the eikonal Feynman rule the spin of the fermion (in this case the quark) which emits the soft gluon is not relevant anymore; in the soft limit one finds the structure of a Feynman rule for a scalar particle.
To obtain the so-called next-to-eikonal approximation one takes terms of $\mathcal{O}(\lambda^0)$ into account as well. Thus, one finds

$$\mathcal{M}^\mu_{\mathrm{next-to-eik.}} = -g t_i^a \bar{u}(p_i) \left[\frac{1}{\lambda} \frac{p_i^\mu}{[p_i \cdot k]} + \frac{\gamma^\mu \not{k}}{[2 p_i \cdot k]} - k^2 \frac{2 p_i^\mu}{[(2 p_i \cdot k)^2]} \right] \mathcal{M}_0(p_i + \lambda k) \;, \tag{2.37}$$

where in this case also the dependence of the amplitude $\mathcal{M}_0$ on λ has to be taken into consideration. Furthermore, at variance with the eikonal approximation, there is now a dependence on the spin of the fermion.

In this work only the leading singularity is of interest, hence it is sufficient to use the eikonal approximation. This is the case since, if the absolute value squared of the amplitude is calculated leading to an expression for a cross-section, only the term in the amplitude of order λ^{-1} will contribute a $1/\varepsilon$ pole or, equivalently, it will give a logarithmically enhanced contribution. For example, when expressing the measure in the variable of energy $\mathrm{d}\Pi_k \propto \mathrm{d}^d k \, \delta(k^2) \propto \mathrm{d}E \, E^{d-2} \frac{1}{E}$ (neglecting the angular integration), then one finds a behaviour of the energy integration of $\frac{\mathrm{d}E}{E} \frac{1}{E^{2\varepsilon}}$ for the cross-section (see also section 4.3).

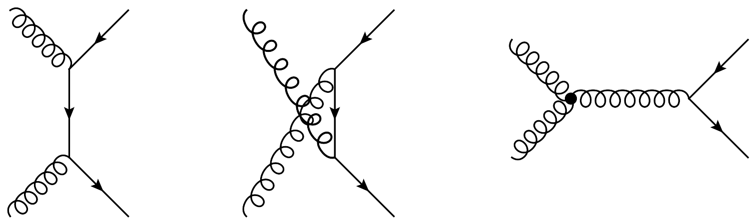

Figure 1: Tree-level Feynman diagrams for the process $gg \to q\bar{q}$

3 Introduction

3.1 Colour-space formalism

The colour-space formalism provides a toolbox in order to systematically treat amplitudes with many partons involved, such that the underlying physics remains transparent. In the following sections the operators which are used to formulate the soft gluon evolution equations "live" in a colour vector space.

When it comes to determining amplitudes with many partons involved the difficulty of this task, i.e. the number of Feynman diagrams which need to be considered, increases as a factorial of the number of external parton lines. Therefore, different techniques are beneficial in order to facilitate the calculation of such multi-parton amplitudes and to make the physics more transparent.

Such a simplification is the colour-space formalism, where the amplitude is split up into its SU(N) colour structure with the corresponding indices of the gauge group and a partial amplitude, which depends on the four-momenta of the partons involved. Stripping off the colour structure will leave behind a partial amplitude which can be built from "QED-type" Feynman rules.

As an illustration consider the process $gg \to q\bar{q}$ at tree-level. In order to establish a more concise notation, the amplitude is treated as a component in the colour vector space. The three different channels which contribute to this process are depicted in Figure 1. For this tree-level process, the amplitude can be written as

$$\begin{aligned} \mathcal{M}^{i}{}_{\bar{i}}{}^{a_1 a_2}(...) &= \mathcal{M}_1(...)(t^{a_1}t^{a_2})^{i}{}_{\bar{i}} + \mathcal{M}_2(...)(t^{a_2}t^{a_1})^{i}{}_{\bar{i}} \\ &= \sum_{\sigma} \mathcal{M}_\sigma(...) C_{\sigma}{}^{i}{}_{\bar{i}}{}^{a_1 a_2} \ , \end{aligned} \tag{3.1}$$

where the ellipsis in the arguments of the amplitudes indicate their momentum dependence. The sum over σ introduced in the last line of equation (3.1) can be understood as a sum over the different orderings of the generators which are absorbed into the colour factor C which carries the colour indices.

Generalising this example to a process with a number of n_q quarks and anti-quarks, as well as a number of n_g gluons, one can write

$$
\begin{aligned}
\mathcal{M}^{i_1 \cdots i_{n_q}\; a_1 \ldots a_{n_g}}_{\bar{i}_1 \cdots \bar{i}_{n_q}}(\ldots) &= \sum_\sigma \mathcal{M}_\sigma(\ldots)\; C^{i_1 \ldots i_{n_q}\; a_1 \ldots a_{n_g}}_{\sigma\; \bar{i}_1 \ldots \bar{i}_{n_q}} \\
&= \sum_\sigma \mathcal{M}_\sigma(\ldots)\, \langle c_1 \ldots c_{2n_q+n_g} | \sigma \rangle \\
&= \langle c_1 \ldots c_{2n_q+n_g} | \mathcal{M}_{2n_q+n_g}(\ldots) \rangle \ .
\end{aligned} \tag{3.2}
$$

In equation (3.2) the colour factor is written as a projection of the colour basis σ onto the abstract basis of the colour space, the latter being a collection of the gauge indices (labelled by $c_1, \ldots, c_{2n_q+n_g}$) of the external particles which are involved in the process. In this particular case there is a total number of $2n_q + n_g$ indices. The colour basis σ then projects out a certain ordering of these indices (cf. equation (3.1)). In the last step of equation (3.2) the following relation/definition for the amplitude vector in colour space is used [6]

$$
|\mathcal{M}_\mathrm{N}\rangle = \sum_\sigma \mathcal{M}_{\mathrm{N},\sigma}\, |\sigma\rangle \ . \tag{3.3}
$$

The object $|\mathcal{M}_\mathrm{N}\rangle$ is a vector in a N-parton colour space. To represent the colour structures in colour space it is efficient to use colour charge operators, $\mathbf{T}^a_i$ for a parton line labelled by i, which are defined by their action onto colour space in the following way [5]

$$
\langle c_1 \ldots c_i \ldots c_n |\, \mathbf{T}^a_i | d_1 \ldots d_i \ldots d_n \rangle = \delta^{c_1}_{d_1} \ldots (T^a)^{c_i}{}_{d_i} \ldots \delta^{c_n}_{d_n} \ , \tag{3.4}
$$

where the $(T^a)^{c_i}{}_{d_i}$ denotes the generator of a quark $(T^a)^{c_i}{}_{d_i} = (t^a)^{c_i}{}_{d_i}$, an antiquark $(T^a)^{c_i}{}_{d_i} = (\overline{t^a})^{c_i}{}_{d_i} = -(t^a)^{c_i}{}_{d_i}$ or a gluon $(T^a)^{c_i}{}_{d_i} = i f^{a c_i}{}_{d_i}$ depending on which type of parton i the operator acts on.

The inner products of the colour charges give the usual Casimir invariants

$$
\mathbf{T}_i \cdot \mathbf{T}_i = C_R \ , \tag{3.5}
$$

where $C_R = C_A, C_F$ depending on whether the parton line is a gluon or a quark/an anti-quark. The inner product of two different parton lines with labels i and j is given by $\mathbf{T}^a_i \mathbf{T}^a_j = \mathbf{T}_i \cdot \mathbf{T}_j$. The important property of colour conservation can be written as [5]

$$
\sum_{i=1}^{n} \mathbf{T}_i\, |\mathcal{M}(p_1, \ldots, p_n)\rangle = 0 \ , \tag{3.6}
$$

which is, however, not an operator identity. It is only satisfied if the colour charges act onto a gauge-invariant amplitude-vector. Formulated differently, the conservation property follows from the fact that the amplitude is invariant under gauge transformations, i.e. acting a gauge transformation on the amplitude-vector for each external line gives (internally, the gauge transformations compensate each other)

$$
e^{i \sum_i \theta_a T^a_i}\, |\mathcal{M}\rangle = |\mathcal{M}\rangle \ . \tag{3.7}
$$

In order to be able to explicitly write down a matrix representation of the colour charges one has to specify a basis of the colour space. In general, there are three prominent basis choices for the colour space, namely the trace basis, the adjoint basis and the colour-flow basis, the latter will be used in this work and it will be introduced in detail in section 3.2.
For the trace basis one rewrites the colour structure purely in terms of fundamental representation generators, for the adjoint basis, as the name suggests, in terms of structure constants, which can be especially useful for processes which involve gluons only. As an example consider an n-gluon amplitude; for the trace basis the colour factor can be written in the following way (using relation (2.10) of section 2.1 in order to rewrite the structure constants as a trace of fundamental generators) [4]

$$\mathcal{M}(\text{n-gluons}) = \sum_{\sigma(2,\ldots,\text{n})} \text{Tr}[t^{a_1} \ldots t^{a_\text{n}}]\mathcal{M}_\sigma(1,\ldots,\text{n}) \ , \tag{3.8}$$

with a sum over the $(\text{n}-1)!$ different permutations of the indices.
For the n-gluon process in the adjoint basis, the colour factor takes the form [4]

$$\begin{aligned}\mathcal{M}(\text{n-gluons}) &= \sum_{\sigma(2,\ldots,(\text{n}-1))} (F^{a_2}F^{a_3}\ldots F^{a_{\text{n}-1}})^{a_1}{}_{a_\text{n}}\mathcal{M}_\sigma(1,\ldots,\text{n}) \\ &= \sum_{\sigma(2,\ldots,(\text{n}-1))} (-if^{a_2 a_1}{}_{\hat{a}_1})(-if^{a_3\hat{a}_1}{}_{\hat{a}_2})\ldots(-if^{a_{\text{n}-1}\hat{a}_{\text{n}-2}}{}_{a_\text{n}})\mathcal{M}_\sigma(1,\ldots,\text{n}) \ .\end{aligned} \tag{3.9}$$

3.2 Colour-flow basis

The colour-flow basis is a spanning set of the colour vector space, which provides a straightforward physical interpretation in terms of the flow of colour in a QCD-process as well as the possibility to give a unified description for quarks, anti-quarks and gluons. Due to these reasons and the fact that it is based on permutations of colour labels of the partons the colour-flow basis is especially well suited for numerical amplitude evolution.

In the colour-flow basis the colour structure is written in terms of colour-flow Kronecker deltas which symbolise the flow of colour in a QCD Feynman diagram. This immediate physical interpretation, as well as the possibility of a unifying description for the different types of partons make the usage of the colour-flow basis very advantageous, in particular for numerical soft gluon evolution.

To start with, there are two approaches for translating the colour factor to the colour-flow basis. One may want to start at the level of the QCD Lagrangian; rewriting the gluon field as a $N \times N$ matrix. Instead of writing the $A_{\mu a}$ and the generators separately, one combines them to obtain $(A_{\mu\, a}(t^a)^i{}_j) \equiv \frac{1}{\sqrt{2}}(\mathcal{A}_\mu)^i{}_j$. With this convention, the Lagrangian (not considering the gauge-fixing and ghost part of the QCD Lagrangian) takes the following form [4]

$$\mathcal{L} = -\frac{1}{4}(\mathcal{F}_{\mu\nu})^i{}_j(\mathcal{F}^{\mu\nu})^j{}_i + \bar{\psi}^j\left(\delta^i_j i\partial\!\!\!/ - \frac{g}{\sqrt{2}}\gamma^\mu(\mathcal{A}_\mu)^i{}_j - m\delta^i_j\right)\psi_i \ , \tag{3.10}$$

where the field-strength tensor is now given by [4]

$$(\mathcal{F}_{\mu\nu})^i{}_j = \partial_\mu(\mathcal{A}_\nu)^i{}_j - \partial_\nu(\mathcal{A}_\mu)^i{}_j + \frac{ig}{\sqrt{2}}\left[(\mathcal{A}_\mu)^i{}_l(\mathcal{A}_\nu)^l{}_j - (\mathcal{A}_\nu)^i{}_l(\mathcal{A}_\mu)^l{}_j\right] \;, \tag{3.11}$$

Due to this form it is sensible to absorb the factor of $1/\sqrt{2}$ into the coupling. The Feynman rules which follow from the Lagrangian in equation (3.10) do not explicitly contain any fundamental generators or structure constants anymore; they are listed for completeness in appendix C. Note however, that using the Lagrangian method to derive the colour-flow Feynman rules proceeds by introducing a colour-flow gluon field which has N^2 degrees of freedom (one has to add an additional generator). In order to restrict U(N) to SU(N) the implementation of a U(1) gluon field is required, it acts as a subtraction term of the extra degrees of freedom [16, 17].

As an alternative to the "Lagrangian-approach" one can chose to rewrite the colour structures directly, this is the approach taken throughout this work. The rewriting proceeds by primarily using the following three identities

$$\begin{aligned}
&\mathrm{Tr}[t^a t^b] = T_R\,\delta^{ab} \;, \\
&B_a D^a = B_a\delta^{ab}D_b = \frac{1}{\sqrt{T_R}}(B^a t^a)^i{}_j\frac{1}{\sqrt{T_R}}(D^b t^b)^j{}_i \;, \\
&(t^a)^i{}_j(t^a)^k{}_l = T_R\left[\delta^i_l\delta^k_j - \frac{1}{N}\delta^i_j\delta^k_l\right] \;,
\end{aligned} \tag{3.12}$$

where the last line in equation (3.12) is the Fierz identity (compare equation (2.14)) with N being the number of colours. Its second term conveniently takes care of implementing the tracelessness condition. Hence, as opposed to the Lagrangian-approach, the SU(N) condition is immediately taken into account by the Fierz identity. The objects B_a and D_a represent general objects with an adjoint index a, for instance polarisation vectors or fundamental generators. How these relations are used in order to rewrite the colour structure in the colour-flow basis is exemplified in the following.
Consider the emission of a soft gluon from a hard parton line. Starting with a quark line with label i the colour structure corresponding to the emission of a soft gluon can be translated to the colour-flow basis in the following way (the equal sign is meant purely in terms of colour structure of the diagram)

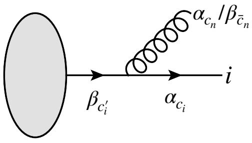

$$\begin{aligned}
&= \varepsilon^*_a(t^a)^{\alpha_{c_i}}{}_{\beta_{c_i'}} = \varepsilon^*_a\delta^{ab}(t^b)^{\alpha_{c_i}}{}_{\beta_{c_i'}} = \frac{1}{\sqrt{T_R}}(\varepsilon^*)^{\beta_{\bar{c}_n}}{}_{\alpha_{c_n}}\left[(t^a)^{\alpha_{c_i}}{}_{\beta_{c_i'}}(t^a)^{\alpha_{c_n}}{}_{\beta_{\bar{c}_n}}\right] \\
&= \lambda_i(\varepsilon^*)^{\beta_{\bar{c}_n}}{}_{\alpha_{c_n}}\left(\delta^{\alpha_{c_i}}_{\beta_{\bar{c}_n}}\delta^{\alpha_{c_n}}_{\beta_{c_i'}} - \frac{1}{N}\delta^{\alpha_{c_i}}_{\beta_{c_i'}}\delta^{\alpha_{c_n}}_{\beta_{\bar{c}_n}}\right) \;,
\end{aligned} \tag{3.13}$$

where α/β denote the fundamental/anti-fundamental indices of the partons. Additionally, there are colour labels $c_i/c_i'/c_n$ and an anti-colour label $\bar{c}_n$. In this work the colour label with the prime is always used to indicate that this label belongs to a parton from the hard, short-distance process, prior to any soft gluon emission/exchange. The polarisation tensor is written

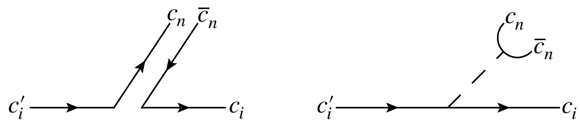

Figure 2: Colour-line diagrams for the emission of a soft gluon from a hard quark line i, colour labels are explicitly written.

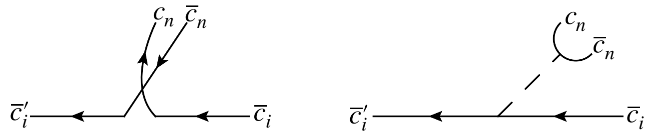

Figure 3: Colour-line diagrams for the emission of a soft gluon from a hard anti-quark line i.

as a combination with a generator, i.e. $\sqrt{T_R}(\varepsilon^*)^{\beta_{\bar{c}n}}_{\alpha_{cn}} = \varepsilon^*_a(t^a)^{\beta_{\bar{c}n}}_{\alpha_{cn}}$. The factor of λ_i in equation (3.13) which has been chosen to replace the factor $\sqrt{T_R}$ will be explained shortly.
In Figure 2 the two expressions of colour-flow Kronecker deltas in equation (3.13) are depicted in terms of colour-line/colour-flow diagrams.

The two parts in this result come from the usage of the Fierz identity, which implements the fact that the SU(N) gluon propagator has been decomposed into a U(N) and a U(1) part. The latter symbolises a gluon which is colour-connected to itself, this contribution gets subtracted from the U(N) gluon colour-flow. The dashed line of the second diagram in Figure 2 is used to represent this U(1) part, it is suppressed in the number of colours.
When considering a soft gluon emission off an anti-quark one finds that

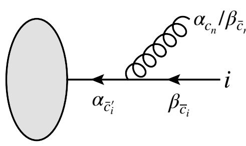

$$= -\varepsilon^*_a(t^a)^{\alpha_{\bar{c}'_i}}_{\ \beta_{\bar{c}_i}} = -\bar{\lambda}_i(\varepsilon^*)^{\beta_{\bar{c}n}}_{\alpha_{cn}}\left(\delta^{\alpha_{\bar{c}'_i}}_{\beta_{\bar{c}n}}\delta^{\alpha_{cn}}_{\beta_{\bar{c}_i}} - \frac{1}{N}\delta^{\alpha_{\bar{c}'_i}}_{\beta_{\bar{c}_i}}\delta^{\alpha_{cn}}_{\beta_{\bar{c}n}}\right) , \tag{3.14}$$

where, in the colour-line notation, this result can be depicted by the flow of colour in the way one can see in Figure 3. Finally, for a hard gluon line i radiating a soft gluon one finds

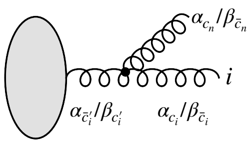

$$\begin{aligned} &= -\varepsilon^*_a\varepsilon^*_b i f^{abc}\frac{1}{\sqrt{T_R}}(t^c)^{\alpha_{\bar{c}'_i}}_{\ \beta_{c_i}} \\ &= (\varepsilon^*)^{\beta_{\bar{c}n}}_{\alpha_{cn}}(\varepsilon^*)^{\beta_{\bar{c}_i}}_{\alpha_{c_i}}\left(\lambda_i\delta^{\alpha_{\bar{c}'_i}}_{\beta_{\bar{c}_i}}\delta^{\alpha_{cn}}_{\beta_{c'_i}}\delta^{\alpha_{c_i}}_{\beta_{\bar{c}n}} - \bar{\lambda}_i\delta^{\alpha_{\bar{c}'_i}}_{\beta_{\bar{c}n}}\delta^{\alpha_{cn}}_{\beta_{\bar{c}_i}}\delta^{\alpha_{c_i}}_{\beta_{c'_i}}\right) , \end{aligned} \tag{3.15}$$

where the $\delta^{\alpha_{\bar{c}'_i}}_{\beta_{\bar{c}_i}}$ and $\delta^{\alpha_{c_i}}_{\beta_{c'_i}}$ Kronecker deltas can be dropped, as they simply describe the "spectator" colour lines, i.e. there occurs no change in the colour label, which can be seen from the colour-line diagrams in Figure 4. Note that in this case there is a gluon propagator, for this reason one writes an additional generator (t^c) in equation (3.15), which has been extracted from the vertex of the hard process, such that one can ensure that all of the adjoint indices in the expression are contracted.
It turns out that for the triple gluon vertex one finds a simplified colour structure, since all of

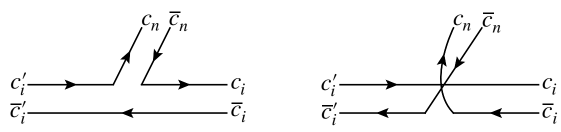

Figure 4: Colour-line diagrams for the emission of a soft gluon from a hard gluon line i.

the $1/N$-terms cancel, as they should.

These considerations lead to a unifying description of the colour charge operator of line i [2]

$$\mathbf{T}_i = \lambda_i \mathbf{t}_{c_i} - \bar{\lambda}_i \bar{\mathbf{t}}_{\bar{c}_i} - \frac{1}{N}(\lambda_i - \bar{\lambda}_i)\mathbf{s} \ . \tag{3.16}$$

The variables λ_i and $\bar{\lambda}_i$ encode the information on the type of the hard parton i. When comparing with the results in equations (3.13), (3.14) and (3.15) it becomes clear, that $\lambda_i = \sqrt{T_R}$ in the case that i is a quark or a gluon line and zero otherwise and $\bar{\lambda}_i = \sqrt{T_R}$ for an anti-quark or a gluon line i.

The operators $\mathbf{t}_{c_i}$, $\bar{\mathbf{t}}_{\bar{c}_i}$ and $\mathbf{s}$ are specified by their action on the colour basis $|\sigma\rangle$ in the following way [2]

$$\begin{aligned}
\mathbf{t}_i\,|\sigma\rangle &= \mathbf{t}_i \left| \begin{array}{ccccc} 1 & \dots & i & \dots & n \\ \sigma(1) & \dots & \sigma(i) & \dots & \sigma(n) \end{array} \right\rangle = \left| \begin{array}{cccccc} 1 & \dots & i & \dots & n & n+1 \\ \sigma(1) & \dots & n+1 & \dots & \sigma(n) & \sigma(i) \end{array} \right\rangle , \\
\bar{\mathbf{t}}_{\bar{i}}\,|\sigma\rangle &= \mathbf{t}_{\sigma^{-1}(\bar{i})} \ , \\
\mathbf{s}\,|\sigma\rangle &= \mathbf{s} \left| \begin{array}{ccc} 1 & \dots & n \\ \sigma(1) & \dots & \sigma(n) \end{array} \right\rangle = \left| \begin{array}{cccc} 1 & \dots & n & n+1 \\ \sigma(1) & \dots & \sigma(n) & n+1 \end{array} \right\rangle ,
\end{aligned} \tag{3.17}$$

where for the colour-flow basis states one uses [2, 6]

$$|\sigma\rangle = \left| \begin{array}{ccc} 1 & \dots & n \\ \sigma(1) & \dots & \sigma(n) \end{array} \right\rangle , \tag{3.18}$$

with $\sigma(a)$ being the permutation of the colour label a. Thus, when writing $|\sigma\rangle$ the whole basis vector is referred to, while the $\sigma(a)$ denotes a permutation of colour labels which characterise the basis vector. The variable n stands for the number of the colour lines of quarks and gluons and it has to be equal to the number of anti-quark plus the gluon colour lines, i.e. $n = n_q + n_g = n_{\bar{q}} + n_g$. The number of colour lines n also gives the dimensionality of the basis vector. Due to the number of permutations of the colour labels one has $n!$ different basis states.

Note that the colour labels $1, \dots, n$ are equivalent to the c, c' and $\bar{c}$ labels which were used before. The colour labels are simply numbers, they enumerate the partons involved in a process. One counts colour and anti-colour labels separately, for instance, for a colour line i of a quark one can set $c_i = 1$ and $\bar{c}_i = 0$. In addition, if there is a gluon involved in the process one can identify $c_g = 2$ and $\bar{c}_g = 1$.

From equation (3.17) one can also nicely see that emitting a parton brings us from a lower to a higher dimension in colour space since after the emission one has $(n+1)$ colour labels.

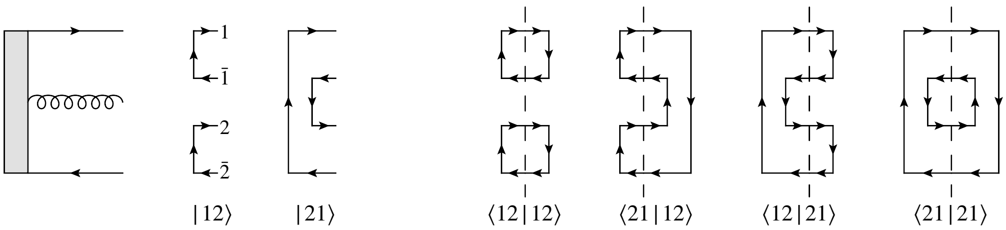

Figure 5: On the left hand side: Example for a basis with $n = 2$ colour lines and its two basis states. On the right hand side: Scalar products of the different basis states in the form of colour-line diagrams. This figure has been adapted from [6] and [2].

To obtain the colour-flow Kronecker deltas, one can act with the abstract basis onto the colour-flow basis vector such that

$$\langle c|\sigma\rangle = \left\langle \begin{array}{ccc} 1 & \dots & n \\ 1 & \dots & n \end{array} \middle| \begin{array}{ccc} 1 & \dots & n \\ \sigma(1) & \dots & \sigma(n) \end{array} \right\rangle = \delta^{\alpha_1}_{\beta_{\sigma(1)}} \dots \delta^{\alpha_n}_{\beta_{\sigma(n)}} \ , \tag{3.19}$$

where the α/β are again the fundamental/anti-fundamental indices.

The colour-flow basis is not orthogonal, for this reason the scalar product between two different basis vectors, say σ and τ, does not give a $\delta_{\sigma\tau}$ but the components which build up the scalar product matrix are [2, 6]

$$S_{\sigma\tau} = \langle\sigma|\tau\rangle = \delta^{\alpha_1}_{\beta_{\tau(1)}} \dots \delta^{\alpha_n}_{\beta_{\tau(n)}} \delta^{\beta_{\sigma(1)}}_{\alpha_1} \dots \delta^{\beta_{\sigma(n)}}_{\alpha_n} = N^{n-\#\text{transpositons}} = N^{\#(\text{colour}-\text{loops})} \ . \tag{3.20}$$

Here, the exponent of N, "number of transpositions", refers to the minimum number of transpositions between the two basis permutations of the vectors $|\sigma\rangle$ and $|\tau\rangle$.

After the last equal sign in equation (3.20), the exponent of the number of colours gives the result for a diagrammatic evaluation of the components of the scalar product matrix of two different basis vectors. Such a diagrammatic approach proceeds as follows. Take the example of the basis states depicted in Figure 5, there one has $n = 2$ colour lines and thus two basis states for which the following short-hand notation is used

$$|12\rangle = \left| \begin{array}{cc} 1 & 2 \\ 1 & 2 \end{array} \right\rangle , \quad |21\rangle = \left| \begin{array}{cc} 1 & 2 \\ 2 & 1 \end{array} \right\rangle \ . \tag{3.21}$$

Further, on the right hand side of Figure 5 the scalar products of the basis states are diagrammatically represented, which clarifies the expression "colour-loops" in equation (3.20). Every closed colour line contributes a colour-loop, such that, according to equation (3.20), the scalar products evaluate to $\langle 12|12\rangle = N^2$, $\langle 21|12\rangle = N$, $\langle 12|21\rangle = N$ and $\langle 21|21\rangle = N^2$. Since, as already mentioned, the colour-flow basis is not orthogonal one can introduce dual basis vectors such that one can write down a completeness relation in the "usual" form [2]

$$\sum_\sigma |\sigma\rangle\,[\sigma| = \sum_\sigma |\sigma]\,\langle\sigma| = \mathbb{1} \ , \tag{3.22}$$

and further [2]

$$\langle\sigma|\tau] = [\tau|\sigma\rangle = \delta_{\sigma\tau} \ . \tag{3.23}$$

In this sense one can also write basis-independent objects/operators in the following way [2]

$$\mathbf{A} = \sum_{\sigma,\tau} \mathcal{A}_{\sigma\tau} |\tau\rangle \langle\sigma| = \sum_{\sigma,\tau} [\tau|\mathbf{A}|\sigma] |\tau\rangle \langle\sigma| \ , \tag{3.24}$$

and a trace of an operator in colour space can be written as [2]

$$\mathrm{Tr}[\mathbf{A}] = \sum_{\tau} [\tau|\mathbf{A}|\tau\rangle = \sum_{\sigma,\tau} [\tau|\mathbf{A}|\sigma] \langle\sigma|\tau\rangle = \mathrm{Tr}[\mathcal{A}S] = \sum_{\sigma,\tau} \mathcal{A}_{\tau\sigma} S_{\sigma\tau} \ . \tag{3.25}$$

In particular, when expressing the amplitude as a vector in the colour vector space (see equation (3.3)), the amplitude squared gives with the considerations above

$$|\mathcal{M}|^2 = \langle\mathcal{M}|\mathcal{M}\rangle = \mathrm{Tr}\left[|\mathcal{M}\rangle\langle\mathcal{M}|\right] = \sum_{\sigma,\tau} \mathcal{M}_\sigma \mathcal{M}^*_\tau \langle\sigma|\tau\rangle = \mathrm{Tr}[\mathcal{M}S] \ . \tag{3.26}$$

A notationally alternative way to define a completeness relation for the non-orthogonal colour-flow basis vectors would be to make use of the definition of the scalar product matrix in the form of the first part of equation (3.24) and to reformulate this relation to obtain

$$\sum_{\sigma,\tau} S^{-1}_{\tau\sigma} |\tau\rangle \langle\sigma| = \mathbb{1} \ , \tag{3.27}$$

as well as

$$|\lambda\rangle = \sum_{\tau,\sigma} S^{-1}_{\tau\sigma} S_{\sigma\lambda} |\tau\rangle \ . \tag{3.28}$$

A general operator $\mathbf{A}$ acting on a basis vector can then be cast into the form

$$\mathbf{A}|\sigma\rangle = \sum_{\rho,\lambda} S^{-1}_{\rho\lambda} |\rho\rangle \langle\lambda|\mathbf{A}|\sigma\rangle = \sum_{\rho,\lambda,\tau} S^{-1}_{\rho\lambda} S_{\lambda\tau} \mathcal{A}_{\tau\sigma} |\rho\rangle = \sum_{\tau} \mathcal{A}_{\tau\sigma} |\tau\rangle \ . \tag{3.29}$$

In this way of writing one does not introduce the dual basis vectors described above.
It is noteworthy that, since the colour-flow basis is not orthogonal/orthonormal, it is not a basis but rather a spanning-set. It is overcomplete for every finite number of colours N, only for the limit $N \to \infty$ it would be strictly speaking a proper basis. In the latter case, in a physical picture, one would have an infinite number of colour charges and thus all partons can be distinguished.

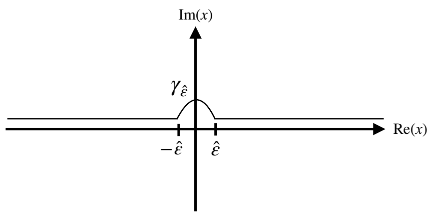

Figure 6: Contour used for the derivation of the Sokhotski-Plemelj identity.

3.3 Feynman's tree theorem

The Feynman tree theorem (FTT) allows one to rewrite loop integrals in the form of phase-space type integrals, such that the process of combining virtual loop graphs with real emission diagrams in order to cancel infrared divergences at the integrand level can be efficiently performed.

To start with, an important ingredient needed to formulate the Feynman tree theorem is the Sokhotski-Plemelj identity (see e.g. [13])

$$\frac{1}{x \pm i0} = \mathcal{P}\left(\frac{1}{x}\right) \mp i\pi\delta(x) \ , \tag{3.30}$$

where $\mathcal{P}$ denotes the principal value prescription. One way to prove this relation proceeds through integration in the complex plane with a test function $f(x)$ which has the property $f(x) \to 0$ for $x \to \pm\infty$ such that the integrand is well-defined when integrating over the real axis. For the contour γ depicted in Figure 6 one finds

$$\int_\gamma \mathrm{d}x\, \frac{f(x)}{x} = \lim_{\hat\varepsilon\to 0}\left[\int_{-\infty}^{-\hat\varepsilon} \mathrm{d}x\, \frac{f(x)}{x} + \int_{\hat\varepsilon}^{\infty} \mathrm{d}x\, \frac{f(x)}{x}\right] + \lim_{\hat\varepsilon\to 0}\int_{\gamma_{\hat\varepsilon}} \mathrm{d}x\, \frac{f(x)}{x} \ , \tag{3.31}$$

where the first two integrals give the principal value prescription and $\gamma_{\hat\varepsilon}$ describes the infinitesimal semi-circle contour around the pole, where one parameterises $x(\varphi) = \hat\varepsilon e^{i\varphi}$ for $0 \leq \varphi \leq \pi$ such that

$$\lim_{\hat\varepsilon\to 0}\int_{\gamma_{\hat\varepsilon}} \mathrm{d}x\, \frac{f(x)}{x} = -\lim_{\hat\varepsilon\to 0}\int_0^\pi \mathrm{d}\varphi \frac{i\hat\varepsilon e^{i\varphi}}{\hat\varepsilon e^{i\varphi}} f(\hat\varepsilon e^{i\varphi}) = -i\pi f(0) \ . \tag{3.32}$$

Since one can deform the integration contour into a slightly imaginary direction $i\varepsilon$ and make an expansion of the test-function $f(x + i\varepsilon) \approx f(x)$, one can conclude that the integral over the contour in equation (3.31) equals to the desired integral of $\int_{-\infty}^{\infty} dx\, f(x)/(x + i\varepsilon)$. Thus, when combining the result of equation (3.31) with (3.32) and removing the test-function one finds the Sokhotski-Plemelj identity.

Note that if one of the integral boundaries lies at a pole of the propagator, the Sokhotski-Plemelj identity has to be slightly adjusted. For instance, for an integral of the form $\int_{-1}^{1} \mathrm{d}x\, 1/[1 - x \pm i0]$ one finds an additional factor of $1/2$ since the contour around the pole has to be integrated within the boundaries $[0, \pi/2]$

$$\frac{1}{1 - x \pm i0} = \mathcal{P}\left(\frac{1}{1-x}\right) \mp \frac{i\pi}{2}\delta(1 - x) \ . \tag{3.33}$$

Subtracting the Sokhotski-Plemelj identity in equation (3.30) of different signs from each other and replacing x by k^2 in order to match the notation for the propagator of a loop momentum k, leads to

$$\frac{1}{k^2 - i0} = \frac{1}{k^2 + i0} + 2\pi i\, \delta(k^2) \ . \tag{3.34}$$

If one wants to pay special attention to the $i0$-prescription, one can reformulate equation (3.34). Assuming that the "0" of the prescription is dimensionless, one can introduce another factor of k^2 in order to have matching dimensions of energy for the propagator. In particular, one can write

$$\frac{1}{k^2 - i0(T\cdot k)^2} = \frac{1}{k^2 + i0(T\cdot k)^2} + 2\pi i\, \delta(k^2) \ , \tag{3.35}$$

where T^μ is a timelike vector, which one can choose without restriction of generality to be equal to $(T^\mu) = (\sqrt{2}, \vec{0})$. Thus, this implies that $T\cdot k = \sqrt{2}k^0$. In fact, the first expression on the right hand side of equation (3.35) corresponds to the usual Feynman propagator, since one can observe that

$$\begin{aligned}\frac{1}{k^2 + i0(T\cdot k)^2} &= \frac{1}{(k^0)^2 - \vec{k}^2 + 2i0(k^0)^2} = \frac{1}{\left[k^0 - |\vec{k}| + i0k^0\right]\left[k^0 + |\vec{k}| + i0k^0\right]} \\ &= \frac{1}{2|\vec{k}|}\left[\frac{1}{k^0 - |\vec{k}| + i0k^0} - \frac{1}{k^0 + |\vec{k}| + i0k^0}\right] \ ,\end{aligned} \tag{3.36}$$

holds and thus the poles are located at $k^0 = |\vec{k}| - i0$ and $k^0 = -|\vec{k}| + i0$ in the complex plane of k^0 for the first and second part of the last line, respectively.
An implication of equation (3.35) is

$$\frac{1}{k^2 - i0|T\cdot k|(T\cdot k)} = \frac{1}{k^2 + i0(T\cdot k)^2} + 2\pi i\, \delta(k^2)\theta(T\cdot k) \ , \tag{3.37}$$

where the first expression on the left hand side can be identified with the advanced propagator, having its poles in the upper half-plane of k^0. Hence,

$$G_A(k) = \frac{1}{k^2 - i0|T\cdot k|(T\cdot k)} \ , \tag{3.38}$$

is the advanced propagator, while

$$G(k) = \frac{1}{k^2 + i0(T\cdot k)^2} \ , \tag{3.39}$$

is the Feynman propagator and equation (3.37) shows how they relate to each other, i.e. in particular one finds [7, 8]

$$G_A(k) = G(k) + 2\pi i\, \delta(k^2)\theta(T\cdot k) \ . \tag{3.40}$$

The reformulation of the $i0$-prescription is used in this work whenever special attention has to be paid to the imaginary part. However, in order to avoid clutter, the momentum factors in the $i0$-prescription will be neglected otherwise. Still, one can easily reinstate them if needed by considering the definitions in the equations above.
In Figure 7 a general depiction of the location of the poles of an advanced, a Feynman and an eikonal propagator is provided. Mind however, that the single pole of the eikonal propagator

can be located in either of the four quadrants, depending on whether the propagator is of the form $[p_i \cdot k + i0]^{-1}$ or $[-p_i \cdot k + i0]^{-1}$ and whether the cosine of the angle between the momentum $\vec{k}$ and $\vec{p_i}$ is positive or negative.

Consider a process at one-loop with a number of n massless, external lines, which have momenta labelled by $p_1, ..., p_n$. The momenta of the (massless) internal propagators are given by $k_m = k + \sum_{l=1}^{m} p_l$ with k being the loop momentum. If the integrand only consists of advanced propagators, the loop integral will evaluate to zero, since all of the poles lie on the same half-plane, i.e. [7, 8]

$$L_A^{(n)}(p_1, ..., p_n) = -i \int \frac{đ^d k}{i\pi^{d/2}} \prod_{m=1}^{n} G_A(k_m) = 0 \;, \tag{3.41}$$

where for the normalisation of the integral measure the following convention is adopted

$$\frac{\mathrm{d}^d k}{(2\pi)^d} = i \frac{(4\pi)^{(4-d)/2}}{(4\pi)^2} \frac{\mathrm{d}^d k}{i\pi^{d/2}} = \frac{đ^d k}{i\pi^{d/2}} \;. \tag{3.42}$$

At this point attention has to be drawn to the fact that the statement of equation (3.41) is only true, if, when performing the contour integration, the contribution of the arc of the half-circle in the complex plane vanishes for the limit of its radius $R \to \infty$. In general, for an amplitude one will have a numerator structure which possibly depends on a loop momentum k, call it $f(k)$, and a propagator, a different polynomial in k, $h(k)$. Now, by parameterising the contribution of the arc and taking the limit $R \to \infty$, one finds that in order for this contribution to vanish it is necessary that the relation $\deg(h(k)) \geq \deg(f(k)) + 2$ is satisfied. Hence, this has to be carefully considered for eikonal propagators, or in particular, when using an axial-type gauge, such as light-cone gauge. For the Feynman diagrams considered throughout this work the relation is satisfied, the FTT can be applied.

Assuming that equation (3.41) is satisfied and using equation (3.37) allows one to reformulate the integral to obtain [7, 8]

$$\begin{aligned} L_A^{(n)}(p_1, ..., p_n) &= -i \int \frac{đ^d k}{i\pi^{d/2}} \prod_{m=1}^{n} \left[G(k_m) + 2\pi i \, \tilde{\delta}(k) \right] \\ &= L^{(n)}(p_1, ..., p_n) + L^{(n)}_{\text{1-cut}}(p_1, ..., p_n) + ... + L^{(n)}_{\text{n-cut}}(p_1, ..., p_n) \;, \end{aligned} \tag{3.43}$$

where $L^{(n)}(p_1, ..., p_n)$ describes the loop integral with Feynman propagators only and the "cut"-contributions (setting the cut momentum on-shell) correspond to [7, 8]

$$L^{(n)}_{\text{r-cut}} = -i \int \frac{đ^d k}{i\pi^{d/2}} \left[(2\pi i)^r \tilde{\delta}(k_1) ... \tilde{\delta}(k_r) G(k_{r+1}) ... G(k_n) + \text{unequal permutations} \right] \;. \tag{3.44}$$

Here, the convenient short-hand notation $\tilde{\delta}(k) = \delta(k^2)\theta(T \cdot k)$ has been used.

Since $L_A^{(n)}(p_1, ..., p_n) = 0$ it follows that [7, 8]

$$L^{(n)}(p_1, ..., p_n) = -\left[L^{(n)}_{\text{1-cut}}(p_1, ..., p_n) + ... + L^{(n)}_{\text{n-cut}}(p_1, ..., p_n) \right] \;. \tag{3.45}$$

The Feynman tree theorem thus instructs one to determine all the different possible cut-contributions (single and multiple cuts) in order to rewrite the loop integral in the form of

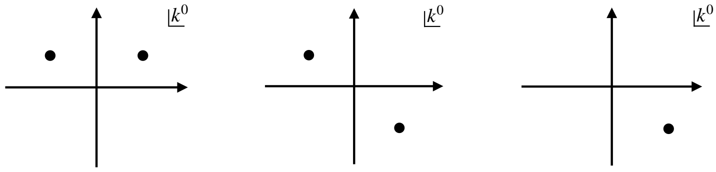

(a) (b) (c)

Figure 7: General pole structure of (a) an advanced, (b)a Feynman and (c) an eikonal propagator in the k^0-plane of the momentum.

a phase-space integral.

In this work the focus lies on processes with soft gluons, accordingly the aim is to apply the FTT not only to the "full" Feynman propagators but in particular to eikonal propagators as well. In the eikonal limit one encounters the case that the pole of certain eikonal propagators lies already in the upper half-plane of the zeroth component of the loop momentum and thus such propagators are not cut in the procedure of the FTT.

In order to illustrate this, consider the one-loop diagram with a soft gluon exchange, where the momenta of the hard lines i and j are both outgoing. In the eikonal limit the amplitude of this process is described by

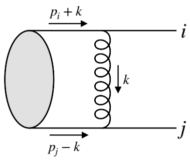

$$= ig^2(-\mathbf{T}_i \cdot \mathbf{T}_j) \int \frac{đ^d k}{i\pi^{d/2}} \frac{\mu^{2\varepsilon}\, 4(p_i \cdot p_j)}{[k^2 + 2i0(k^0)^2][2p_i \cdot k + 2i0(p_i^0)^2][-2p_j \cdot k + 2i0(p_j^0)^2]} \ , \tag{3.46}$$

where the amplitude of the hard, short distance process is not explicitly written, it is understood to be included in the "blob" of the diagram. Focusing on the loop integral and following the procedure of the FTT, one can first write the loop integral with advanced propagators only (cf. equation (3.41))

$$0 = \mu^{2\varepsilon} \int \frac{đ^d k}{i\pi^{d/2}} G_A(k) \frac{1}{[2p_i \cdot k - 2i0(p_i^0)^2]} \frac{1}{[-2p_j \cdot k + 2i0(p_j^0)^2]} \ . \tag{3.47}$$

One observes that the eikonal propagator of line j already has its pole in the upper half-plane. In some sense, for this momentum convention, the eikonal propagator can be identified with the advanced propagator. Hence, if one rewrites the advanced propagators using equation (3.40) in the next step, this procedure does not have to be applied to the eikonal propagator with momentum $(-p_j \cdot k)$. Therefore one obtains

$$\begin{aligned} 0 = \mu^{2\varepsilon} \int \frac{đ^d k}{i\pi^{d/2}} &\left(\frac{1}{[k^2 + 2i0(k^0)^2]} + (2\pi i)\delta(k^2)\theta(k^0) \right) \frac{1}{[-2p_j \cdot k + 2i0(p_j^0)^2]} \\ &\left(\frac{1}{[2p_i \cdot k + 2i0(p_i^0)^2]} + (2\pi i)\delta(2p_i \cdot k) \right) \ . \end{aligned} \tag{3.48}$$

Multiplying out, one can express the desired integral as the sum over three cut-contributions (two single cuts and one double cut), the propagator with momentum $(-p_j \cdot k)$ is left untouched,

$$\begin{aligned}
&\mu^{2\varepsilon} \int \frac{\text{đ}^d k}{i\pi^{d/2}} \frac{1}{[k^2 + 2i0(k^0)^2][2p_i \cdot k + 2i0(p_i^0)^2][-2p_j \cdot k + 2i0(p_j^0)^2]} \\
&= -\mu^{2\varepsilon} \int \frac{\text{đ}^d k}{i\pi^{d/2}} \Bigg\{ \frac{(2\pi i)\delta(k^2)\theta(k^0)}{[2p_i \cdot k + 2i0(p_i^0)^2][-2p_j \cdot k + 2i0(p_j^0)^2]} \\
&\qquad + \frac{(2\pi i)\delta(2p_i \cdot k)}{[k^2 + 2i0(k^0)^2][-2p_j \cdot k + 2i0(p_j^0)^2]} + \frac{(2\pi i)^2 \delta(k^2)\theta(k^0)\delta(2p_i \cdot k)}{[-2p_j \cdot k + 2i0(p_j^0)^2]} \Bigg\} .
\end{aligned} \tag{3.49}$$

It is noteworthy that if a different momentum flow is adopted, i.e. one momentum of the hard lines is outgoing while the other one is incoming, all different cuts have to be taken into account since there is no propagator with momentum $(-p_{i,j} \cdot k)$ (see section 4.4).
In sections 4.3 and 4.2 the one-loop soft gluon exchange diagram is further evaluated in terms of its kinematical contribution as well as its colour factor. The application of the FTT at two-loop order is described in section 5.3.

3.4 Soft gluon evolution equations

The soft gluon evolution algorithm aims to provide an iterative solution to the soft gluon RGE in order to achieve soft gluon resummation for general observables. In particular, it is also valid for the resummation of leading logarithms in non-global observables.

Soft gluon evolution is concerned with "dressing" a hard, short-distance process with a number of soft gluons in the form of real emissions and virtual exchanges. The standard way of determining the soft anomalous dimension is to specify the observable of interest, perform the loop-integration (using e.g. rapidity regulators) as well as the phase-space integrals of the real emission. The result is then expanded, a part of the poles in ε will cancel, the ones that remain have to be removed by renormalisation.
However, in this case a different approach is taken. The aim is to cancel infrared divergences at the integrand level. Therefore the anomalous dimension is determined at the integrand level which gives a more detailed control over a whole class of observables, since one does not have to impose restrictions concerning angles or rapidity within the real emission. There is a virtual evolution for a whole class of observables where one only has to specify how the observable factorises and to provide information on the ordering parameter (e.g. energy or transverse momentum).

In the end, when explicitly choosing an observable one will obtain the same result for the soft anomalous dimension with this procedure as one will find by using the standard approach. Still, with the method presented in the following it is also possible to look at the difference between a representative, ideal observable and a real, experimentally accessible one and to integrate this difference numerically.

A general cross-section can be written in the following way [2]

$$\sigma = \sum_{n\geq 0} \int \mathrm{Tr}[\mathbf{U}_n(p_n)] u(p_n)\, \mathrm{d}\Pi(p_n) \ , \tag{3.50}$$

where the $\mathrm{d}\Pi(p_n)$ denotes the phase-space integration measure concerning the n soft gluon momenta $p_n = \{q_1, ..., q_n\}$; there are also a number of m hard momenta, which are not explicitly written. The cross-section is formulated for the observable $u(p_n)$ which is a function of the soft momenta $q_1, ..., q_n$. This measurement function is considered here to be trivial in colour space and in the described case the evolution proceeds only with soft gluons (a more general treatment including collinear emissions can be found in [3]). Hence, the phase-space factorisation is given by

$$\mathrm{d}\Pi(p_n) = \frac{\mathrm{d}^d q_n}{(2\pi)^{d-1}} \tilde{\delta}(q_n)\, \mathrm{d}\Pi(p_{n-1}) \ . \tag{3.51}$$

In the following, a derivation of the soft gluon evolution algorithm is presented [9].
The operator $\mathbf{U}_n$ of the n-parton colour space can be regarded as a density operator in the sense that $\mathbf{U}_n = |\mathcal{M}_n\rangle \langle\mathcal{M}_n|$ holds. The quantity $\mathbf{U}_n(p_n)$ is the bare, unrenormalised operator in colour space for which the following recursion relation holds

$$\mathbf{U}_n(p_n) = \alpha^{\mathrm{bare}} \left[\mathbf{V}_n(p_n)\mathbf{U}_n(p_n) + \mathbf{U}_n(p_n)\mathbf{V}_n^{\dagger}(p_n) - \mathbf{D}_n(p_n)\mathbf{U}_{n-1}(p_{n-1})\mathbf{D}_n^{\dagger}(p_n)\right] \ . \tag{3.52}$$

This suggests a diagrammatic interpretation. The operator $\mathbf{V}_n(p_n)$ implements a virtual soft gluon exchange; the first two terms in equation (3.52) thus refer to the amplitude dressed with a virtual exchange and a tree-level conjugated amplitude and the other way around. The third term in equation (3.52) represents the real emission contribution. The operator $\mathbf{D}_n(p_n)$ is the soft emission operator, for the soft momentum q_n it is defined as

$$\mathbf{D}_n^{\alpha}(q_n) = \sum_i \mathbf{T}_i \frac{p_i^{\alpha}}{p_i \cdot q_n} \ , \tag{3.53}$$

where the sum is over hard momentum lines. It holds that $\mathbf{U}_{-1} = 0$, such that for $\mathbf{U}_0$ only the tree-level diagram/the hard process remains. The diagrammatic recursion relation in equation (3.52) gives the leading contributions to the observable and lies at the basis of the soft evolution procedure.

The cross-section in equation (3.50) is formulated in a general way, therefore it allows to also include a class of observables which are "non-global". Whilst global observables resolve radiation across the entirety of phase space, non-global observables have regions which put no constraint (for example regarding its energy) on radiation.
Accordingly, the measurement function for a non-global observable can be split up into an "in"-region, where the energies of the emitted gluons are restricted to lie below the soft scale μ_s (the resolution scale), and an "out"-region where there is no such constraint on the radiated gluons (see Figure 8 for an exemplary illustration of the described regions). For a non-global observable defined in this way the cancellation of IR divergences is still ensured. However, while for a global observable resummation of large logarithms has to be performed for energies

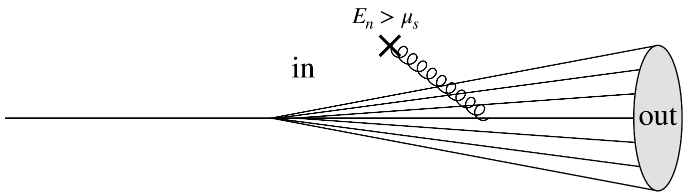

Figure 8: Schematic depiction of an example for a non-global observable, in the "in"-region the energies of the radiated gluons are restricted to lie below the soft scale μ_s, while there is no such restriction on the energy in the "out"-region.

$E_n < \mu_s$, for the non-global case, there is also an unobserved part with energy $E_n > \mu_s$ in the out-region. Such an out-region can occur due to an experimental setup with parts not covered by the detector. Splitting up the measurement function into the in-region ($\Theta(q_n \in \Omega_{\text{in}})$) and the out-region ($\Theta(q_n \in \Omega_{\text{out}})$) and considering only one soft emission of momentum q_n results in

$$\begin{aligned} u(p_n) = u(p_{n-1}) \, [&\Theta(q_n \in \Omega_{\text{in}})\theta(\mu_s - \kappa(q_n)) \\ &+\Theta(q_n \in \Omega_{\text{out}})\theta(\mu_s - \kappa(q_n)) + \Theta(q_n \in \Omega_{\text{out}})\theta(\kappa(q_n) - \mu_s)] \ , \end{aligned} \tag{3.54}$$

where the $\kappa(q_n)$ is a general notation that allows one to formulate the measurement function with respect to different ordering variables. For instance, in a simple case, the $\kappa(q_n)$ can refer to the energy of the emitted gluon or to its transverse momentum. The contribution in the first line in equation (3.54) can be combined with the first one in the second line to give the global part, the observable is fully inclusive in the chosen variable, for example for emissions with energies $E_n < \mu_s$. However, there is an additional non-global part, namely the second contribution in the second line.

It is now desirable to find an IR-finite expression for the $\mathbf{U}_n$ operator. To achieve this, first focus on the measurement function, which can be rewritten as

$$\begin{aligned} u(p_n) &= u(p_n) - \theta(\mu_s - \kappa(q_n))u(p_{n-1}) + \theta(\mu_s - \kappa(q_n))u(p_{n-1}) \\ &= \Theta(q_n \in \Omega_{\text{out}})\theta(\kappa(q_n) - \mu_s)u(p_{n-1}) + \theta(\mu_s - \kappa(q_n))u(p_{n-1}) \ . \end{aligned} \tag{3.55}$$

In the first line the global contribution of a soft emission with its characteristic variable lying below the soft scale μ_s has been added and subtracted. Plugging in the expression of equation (3.54) for $u(p_n)$ one observes that the contributions which remain are the emission in the out-region above the soft scale and a global part with the characteristic emission variable below the soft scale. The latter can be combined with the virtual exchanges in order to achieve cancellation of IR divergences in the following way.

Consider the part of the cross-section for a soft emission of momentum q_{n+1} with its characterising variable smaller than the soft scale

$$\begin{aligned} &\text{Tr}\left[\mathbf{D}_{n+1}\mathbf{U}_n\mathbf{D}^\dagger_{n+1}\right]\theta(\mu_s - \kappa(q_{n+1}))u(p_n)\,\mathrm{d}\Pi(p_{n+1}) \\ &= \frac{1}{2}\text{Tr}\left[\left(\mathbf{D}^\dagger_{n+1}\mathbf{D}_{n+1} - i\mathbf{C}^{(1)}_n\right)\mathbf{U}_n\right]\theta(\mu_s - \kappa(q_{n+1}))\frac{\tilde{\delta}(q_{n+1})}{(2\pi)^{d-1}}\,\mathrm{d}^d q_{n+1}\,\mathrm{d}\Pi(p_n) \\ &+ \frac{1}{2}\text{Tr}\left[\mathbf{U}_n\left(\mathbf{D}^\dagger_{n+1}\mathbf{D}_{n+1} + i\mathbf{C}^{(1)}_n\right)\right]\theta(\mu_s - \kappa(q_{n+1}))\frac{\tilde{\delta}(q_{n+1})}{(2\pi)^{d-1}}\,\mathrm{d}^d q_{n+1}\,\mathrm{d}\Pi(p_n) \ , \end{aligned} \tag{3.56}$$

where the cyclicity of the trace was used and the imaginary part has been introduced (added and subtracted) for later convenience. The only constraint on $\mathbf{C}_n^{(1)}$ is its hermiticity. Combining this contribution with the virtual exchanges leads to an operator $\mathbf{\Omega}_n$ which is free of infrared divergences,

$$\mathbf{\Omega}_n = \mathbf{V}_n + \frac{i}{2}\mathbf{C}_n^{(1)} - \frac{1}{2}\int \frac{\mathrm{d}q_{n+1}}{(2\pi)^{d-1}}\tilde{\delta}(q_{n+1})\, \mathbf{D}_{n+1}^{\dagger}\mathbf{D}_{n+1}\theta(\mu_s - \kappa(q_{n+1}))\ . \tag{3.57}$$

In this way, the operator $\mathbf{C}_n^{(1)}$ can be used to subtract the infrared divergences of the imaginary part of $\mathbf{V}_n$ at one-loop order. With the operator $\mathbf{\Omega}_n$ one can therefore rewrite the recursion of equation (3.52) in an IR-finite form

$$\mathbf{U}_n = \alpha^{\mathrm{bare}}\left[\mathbf{\Omega}_n\mathbf{U}_n + \mathbf{U}_n\mathbf{\Omega}_n^{\dagger} - \mathbf{D}_n\mathbf{U}_{n-1}\mathbf{D}_n^{\dagger}\,\theta(\kappa(q_n) - \mu_s)\Theta(q_n \in \Omega_{\mathrm{out}})\right]\ . \tag{3.58}$$

Note that the emission contribution now only involves the soft emission in the out-region with $\kappa(q_n) > \mu_s$, since the global part of the emission with $\mu_s > \kappa(q_n)$ has already been combined with the virtual exchange.
Still, a UV divergence remains for the operator $\mathbf{\Omega}_n$. The renormalisation procedure for $\mathbf{U}_n$ absorbs the momentum modes above a scale μ_F into the renormalisation factor $\mathbf{Z}_n$, which can be regarded as an operator in colour space. The coupling gets renormalised at a scale μ_R in the way described in section 2.2, equation (2.20). Defining the renormalised quantity by $\mathbf{U}_n^{\mathrm{ren}} \equiv \mathbf{A}_n$, this leads one to

$$\begin{aligned}\mathbf{U}_n(\mu) = {}& \mathbf{Z}_n(\mu,\mu_R,\mu_F)\mathbf{A}_n(\mu_R,\mu_F)\mathbf{Z}_n^{\dagger}(\mu,\mu_R,\mu_F) \\ & - \alpha_s(\mu_R)\,\mathbf{D}_n\mathbf{A}_{n-1}(\mu_R,\mu_F)\mathbf{D}_n^{\dagger}\,\theta(\kappa(q_n) - \mu_F)\,\Theta(q_n \in \Omega_{\mathrm{out}})\ ,\end{aligned} \tag{3.59}$$

where one can observe that for only one emission in an expansion one has to take into account the renormalised coupling $\alpha_s(\mu_R)$, the renormalisation factors sandwiching the $\mathbf{A}_{n-1}$ operator are simply unity. The emission and the virtual contribution are now cut off above the scale μ_F. Furthermore, one can expand the first line in equation (3.59) to first order in the renormalised coupling to find

$$\begin{aligned}\mathbf{U}_n(\mu) &= \mathbf{A}_n + \alpha_s(\mu_R)\,\mathbf{Z}_n^{(1)}\mathbf{A}_n + \alpha_s(\mu_R)\,\mathbf{A}_n(\mathbf{Z}_n^{(1)})^{\dagger} \\ &\qquad - \alpha_s(\mu_R)\,\mathbf{D}_n\mathbf{A}_{n-1}\mathbf{D}_n^{\dagger}\,\theta(\kappa(q_n) - \mu_F)\Theta(q_n \in \Omega_{\mathrm{out}}) + \mathcal{O}(\alpha_s^2) \\ &= \alpha_s(\mu_R)\left[\mathbf{\Omega}_n\mathbf{A}_n + \mathbf{A}_n\mathbf{\Omega}_n^{\dagger} - \mathbf{D}_n\mathbf{A}_{n-1}\mathbf{D}_n^{\dagger}\theta(\kappa(q_n) - \mu_s)\Theta(q_n \in \Omega_{\mathrm{out}})\right] + \mathcal{O}(\alpha_s^2)\ .\end{aligned} \tag{3.60}$$

This allows one to determine $\mathbf{Z}_n$ by identifying the divergent part in $\mathbf{\Omega}_n$ and therefore one gets a UV-finite contribution at the order considered so far, i.e. at $\mathcal{O}(\alpha_s)$

$$\begin{aligned}0 = {}& \mathbf{A}_n - \alpha_s(\mu_R)\left(\mathbf{\Omega}_n - \mathbf{Z}_n^{(1)}\right)\mathbf{A}_n - \alpha_s(\mu_R)\,\mathbf{A}_n\left(\mathbf{\Omega}_n - \mathbf{Z}_n^{(1)}\right)^{\dagger} \\ & + \alpha_s(\mu_R)\,\mathbf{D}_n\mathbf{A}_{n-1}\mathbf{D}_n^{\dagger}\,\theta(\mu_F - \kappa(q_n))\,\theta(\kappa(q_n) - \mu_s)\Theta(q_n \in \Omega_{\mathrm{out}}) + \mathcal{O}(\alpha_s^2)\ .\end{aligned} \tag{3.61}$$

One can now formulate an evolution equation in μ_F

$$\begin{aligned}\mu_F\frac{\partial \mathbf{A}_n}{\partial \mu_F} =& \alpha_s(\mu_R)\mathbf{\Gamma}_n\mathbf{A}_n + \alpha_s(\mu_R)\mathbf{A}_n\mathbf{\Gamma}_n^\dagger \\ &- \alpha_s(\mu_R)\,\mathbf{D}_n\mathbf{A}_{n-1}\mathbf{D}_n^\dagger\,\mu_F\,\delta(\mu_F-\kappa(q_n))\,\theta(\mu_F-\mu_s)\,\Theta(q_n\in\Omega_{\text{out}}) + \mathcal{O}(\alpha_s^2)\ ,\end{aligned} \tag{3.62}$$

where, at this order, the soft anomalous dimension matrix $\mathbf{\Gamma}_n$ is defined as

$$\mathbf{\Gamma}_n \equiv -\mu_F\,\frac{\partial}{\partial\mu_F}\mathbf{Z}_n^{(1)}\ . \tag{3.63}$$

Therefore, by requiring that the expression $\left(\mathbf{\Omega}_n - \mathbf{Z}_n^{(1)}\right)$ has to be finite, one determines the form of $\mathbf{Z}_n^{(1)}$ as well as the one of $\mathbf{C}_n^{(1)}$.
One can write down the soft evolution of the cross-section for the radiation of n soft gluons in terms of the renormalised density operators $\mathbf{A}_n$, which satisfy the iterative equation (3.61), in the following way [2]

$$\begin{aligned}\sigma_0 &= \mathrm{Tr}\left[\tilde{\mathbf{V}}_0(\mu_s,Q)\mathbf{H}(Q)\tilde{\mathbf{V}}_0^\dagger(\mu_s,Q)\right] \equiv \mathrm{Tr}[\mathbf{A}_0(\mu_s)] \\ \mathrm{d}\sigma_1 &= \mathrm{Tr}\left[\tilde{\mathbf{V}}_1(\mu_s,E_1)\mathbf{D}_1^\alpha\tilde{\mathbf{V}}_0(E_1,Q)\mathbf{H}(Q)\tilde{\mathbf{V}}_0^\dagger(E_1,Q)\mathbf{D}_{1\alpha}^\dagger\tilde{\mathbf{V}}_1^\dagger(\mu_s,E_1)\right]\mathrm{d}\Pi_1 \\ &\equiv \mathrm{Tr}[\mathbf{A}_1(\mu_s)]\,\mathrm{d}\Pi_1 \\ \mathrm{d}\sigma_2 &= \mathrm{Tr}\Big[\tilde{\mathbf{V}}_2(\mu_s,E_2)\mathbf{D}_2^\beta\tilde{\mathbf{V}}_1(E_2,E_1)\mathbf{D}_1^\alpha\tilde{\mathbf{V}}_0(E_1,Q)\mathbf{H}(Q) \\ &\qquad \tilde{\mathbf{V}}_0^\dagger(E_1,Q)\mathbf{D}_{1\alpha}^\dagger\tilde{\mathbf{V}}_1^\dagger(E_2,E_1)\mathbf{D}_{2\beta}^\dagger\tilde{\mathbf{V}}_2^\dagger(\mu_s,E_2)\Big]\,\mathrm{d}\Pi_1\mathrm{d}\Pi_2 \equiv \mathrm{Tr}[\mathbf{A}_2(\mu_s)]\,\mathrm{d}\Pi_1\mathrm{d}\Pi_2\ ,\end{aligned} \tag{3.64}$$

where this pattern can be continued to n emissions. In equation (3.64) the energy is chosen as the ordering variable. The operator $\tilde{\mathbf{V}}_n(a,b)$, the Sudakov operator, is now the solution of global part of the evolution equation (3.62), it sums the virtual exchanges to all orders between two scales a, b. It has the form [2]

$$\tilde{\mathbf{V}}_n(a,b) = \mathcal{P}\left\{\exp\left[-\int_a^b \frac{\mathrm{d}k}{k}\mathbf{\Gamma}_n(k)\right]\right\}\ , \tag{3.65}$$

where $\mathcal{P}$ denotes the path-ordering with respect to the chosen scale variable, in this case the energy.

In Figure 9 a graphic representation of the evolution is given. It shows the soft gluon evolution of the cross-section from the hard scale Q down to an emission energy E_1 which is larger than the soft scale μ_s. The insertion of the Sudakov operator sums the virtual exchanges to all orders between the two scales Q and E_1. At the scale E_1 an emission occurs, implemented via the emission operator $\mathbf{D}_1$. The same procedure can be repeated until the next emission scale is reached, as long as it is larger than the soft scale. In this way the evolution down to μ_s is performed, at this point the evolution stops.

The necessary ingredients for this algorithm are the knowledge of the Sudakov operators at a given loop-order. The first step towards their determination is to find an expression for the soft

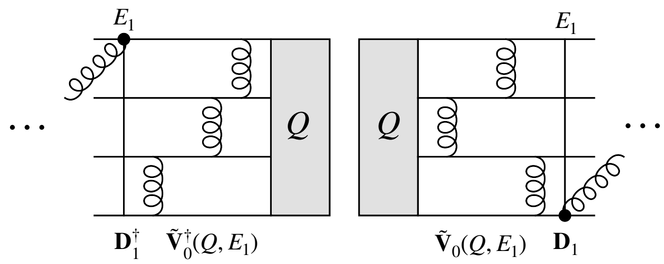

Figure 9: Illustration of the iterative solution of the non-global evolution equation. The right hand side depicts the evolution of the amplitude, whilst the left hand side the complex conjugated amplitude.

anomalous dimension at a given loop-order, which subsequently has to be exponentiated.
In order to determine the soft anomalous dimension matrix in the colour-flow basis at a given loop-order the kinematic part has to be evaluated for both virtual and emission contributions and the colour structure needs to be expressed as a matrix element of the colour-correlators in the colour-flow basis.
An example for a non-global observable is the di-jet veto. In this case all of the collinear contributions will cancel and therefore, due to the presence of soft divergences only, single logarithms remain.

4 Leading order soft evolution

In this section the soft anomalous dimension at one-loop order is reviewed. In the first part the focus lies on the colour structure and on finding an expression for the one-loop soft anomalous dimension as a matrix element in the colour-flow basis. In the second part the Feynman tree theorem is applied to the one-loop integral and the cut contributions are written in the form of a phase-space integral. The radiative cut contribution is then compared to the real emission diagram at the level of a cross-section. In the last part of this section the effect of the momentum flow of the hard lines on the imaginary part is discussed.

4.1 Soft anomalous dimension at leading order basis-independently

The soft anomalous dimension matrix at one-loop, in a basis-independent form, can be expressed as [6]

$$\mathbf{\Gamma}^{(1)} = \frac{1}{2}\sum_{i\neq j}(-\mathbf{T}_i \cdot \mathbf{T}_j)\, I_{ij}^{(1)} \ , \tag{4.1}$$

where $I_{ij}^{(1)}$ are the one-loop coefficients, i.e. the one-loop integral, which is already renormalised and the infrared divergences have been subtracted by taking into account the squared single emission contribution. When analysing the loop integral in section 4.3 the quantity which is calculated will be denoted by $\mathbf{V}^{(1)}$ (compare equation (3.52)), since the loop integral still contains an infrared and an artificial (due to the eikonal approximation) ultraviolet divergence at this point (and it is therefore not equal to $I_{ij}^{(1)}$ in equation (4.1)). At variance with the virtual exchange operator in equation (3.52) the superscript denoting leading order is added here explicitly. At the end of section 4.3 one can observe the cancellation of the infrared divergence when taking into account the squared single soft emission diagram. The UV divergence has to be taken care of by the renormalisation program as described in the previous section.
The Feynman diagram corresponding to the virtual correction $\mathbf{V}^{(1)}$ is simply given by the one-loop soft gluon exchange. Note that in the soft limit in Feynman gauge and at leading order in α_s the self-energy diagram involving a single line does not contribute for on-shell external lines. Since the colour structure of the soft anomalous dimension in the colour-flow basis is discussed separately from the loop integral, the symbol $\mathbf{\Gamma}^{(1)}$ is used.

4.2 The soft anomalous dimension in the colour-flow basis

In equation (4.1) the soft anomalous dimension is considered in a basis-independent way, here the task is to express it as a matrix element in the colour-flow basis. In general, for the expansion in the t'Hooft coupling ($\alpha_s N$) of the soft anomalous dimension in the colour-flow basis, one can write

$$[\tau|\mathbf{\Gamma}|\sigma\rangle = (\alpha_s N)\, [\tau|\mathbf{\Gamma}^{(1)}|\sigma\rangle + (\alpha_s N)^2\, [\tau|\mathbf{\Gamma}^{(2)}|\sigma\rangle + \dots \ . \tag{4.2}$$

In this section the focus lies on the leading order coefficient. In the following, the result for the matrix element of the colour-correlator $\mathbf{T}_i \cdot \mathbf{T}_j$ will be determined in the colour-flow basis, afterwards the kinematic dependence will be considered.

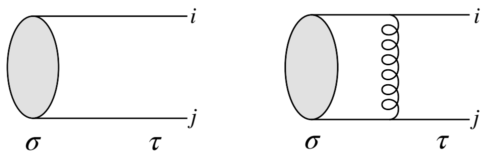

Figure 10: On the left hand side the tree-level amplitude is depicted, on the right hand side the one-loop amplitude. The σ describes the basis permutation pertaining to the hard process, the τ corresponds to basis permutation after the exchange of the gluon. Accordingly, the two permutations match for the tree-level process.

It holds that $[\tau|\sigma\rangle = \delta_{\sigma\tau}$ for two basis tensors $|\tau\rangle$ and $|\sigma\rangle$; this matches the matrix element of the tree-level diagram (see Figure 10). For the one-loop gluon exchange between two lines i and j the object of interest is $[\tau|(\mathbf{T}_i \cdot \mathbf{T}_j)|\sigma\rangle$. One needs to consider this quantity for all the different combinations of parton lines and combine these expressions into a single one.

For two hard quark lines i and j one finds a colour structure of

$$(t^a)^{\alpha_{c_i}}{}_{\beta_{c_i'}} (t^a)^{\alpha_{c_j}}{}_{\beta_{c_j'}} = T_R \left[\delta^{\alpha_{c_i}}_{\beta_{c_j'}} \delta^{\alpha_{c_j}}_{\beta_{c_i'}} - \frac{1}{N} \delta^{\alpha_{c_i}}_{\beta_{c_i'}} \delta^{\alpha_{c_j}}_{\beta_{c_j'}} \right] \tag{4.3}$$

$$= \lambda_i \lambda_j$$

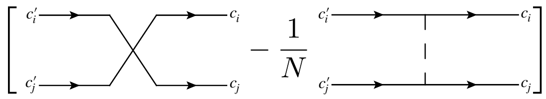

where in the first line the Fierz identity is used. In the second line the colour-line diagrams which correspond to the colour-flow Kronecker deltas are depicted and the factor of T_R is rewritten as $\lambda_i \lambda_j$ according to the conventions described previously.
When instead considering a quark line i and an anti-quark line j, one obtains

$$-(t^a)^{\alpha_{c_i}}{}_{\beta_{c_i'}} (t^a)^{\alpha_{\bar{c}_j'}}{}_{\beta_{\bar{c}_j}} = -T_R \left[\delta^{\alpha_{c_i}}_{\beta_{\bar{c}_j}} \delta^{\alpha_{\bar{c}_j'}}_{\beta_{c_i'}} - \frac{1}{N} \delta^{\alpha_{c_i}}_{\beta_{c_i'}} \delta^{\alpha_{\bar{c}_j'}}_{\beta_{\bar{c}_j}} \right] \tag{4.4}$$

$$= -\lambda_i \bar{\lambda}_j$$

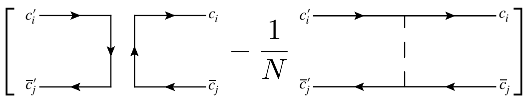

The other combinations of partons work analogously; for gluon lines, one rewrites the structure constants as a trace of fundamental generators, for which the Fierz identity can be used again. Now, if a gluon is exchanged one can ask how the basis permutation τ will change with respect to σ, the basis permutation determined by the hard process. This means that, for the matrix element of interest, one has $[\tau|(\mathbf{T}_i \cdot \mathbf{T}_j)\,|\sigma\rangle = [\tau|\tilde{\sigma}\rangle = \delta_{\tau\tilde{\sigma}}$, where $(\mathbf{T}_i \cdot \mathbf{T}_j)\,|\sigma\rangle \equiv |\tilde{\sigma}\rangle$. The task is to reformulate the $\tilde{\sigma}$ permutation (which is equal to the τ-permutation) in terms of the "original" one, σ, and to relate it to τ. In order to see this change of permutations one rewrites the Kronecker deltas of the permutations such that the change (if there is any) between the permutations τ and σ is immediately evident. This rewriting can be done in the following way:

For two quark lines i and j the basis permutation σ connects the colour indices of the quarks to any other two anti-colour indices (labelled by $\bar{c}_k'$ and $\bar{c}_m'$) which pertain to the hard process and are thus part of the permutation σ,

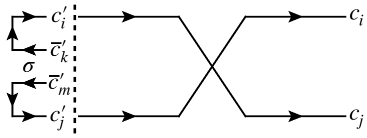

$$= \left(\delta^{\alpha_{c_i}}_{\beta_{\bar{c}'_k}}\,\delta^{\alpha_{c'_j}}_{\beta_{\bar{c}_m}}\right)\left(\delta^{\alpha_{c_j}}_{\beta_{c'_i}}\,\delta^{\beta_{c'_i}}_{\alpha_{c'_i}}\,\delta^{\alpha_{c_i}}_{\beta_{c'_j}}\,\delta^{\beta_{c'_j}}_{\alpha_{c'_j}}\right) = \delta^{\alpha_{c_i}}_{\beta_{\bar{c}'_m}}\,\delta^{\alpha_{c_j}}_{\beta_{\bar{c}'_k}} \tag{4.5}$$

$$\to \delta_{\tau_{(a,b)}\sigma}\delta_{(a,b)(c_i,c_j)} \ .$$

The colour-flow Kronecker deltas obtained in the first line of equation (4.5) are an expression for the quantity $\langle c|\tilde{\sigma}\rangle$, which now has to be compared to $\langle c|\sigma\rangle$ which equals to the first expression in brackets in the upper equation. One can observe that, in order to make the two permutations σ and τ match, one has to swap the colour indices c_i and c_j in the τ-permutation. The action of swapping the colour indices and then comparing to τ is described by the expression of $\delta_{\tau_{(a,b)}\sigma}\delta_{(a,b)(c_i,c_j)}$ - the two elements (a, b) have to be swapped such that the permutations τ and σ match and in this case the elements (a, b) are given by (c_i, c_j).

For the case of a quark line i and an anti-quark line j it is necessary to distinguish two different cases for the basis permutation σ. In addition to the case described above where the colour indices are connected to any other anti-colour indices of the permutation σ, one now has to explicitly consider a colour-connection between the lines i and j, i.e. between the colour/anti-colour indices of c'_i and $\bar{c}'_j$. These two possibilities lead to

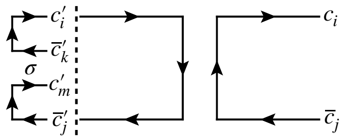

$$= \left(\delta^{\alpha_{c'_i}}_{\beta_{\bar{c}'_k}}\,\delta^{\alpha_{c'_m}}_{\beta_{\bar{c}'_j}}\right)\left(\delta^{\beta_{\bar{c}'_j}}_{\alpha_{\bar{c}'_j}}\,\delta^{\alpha_{\bar{c}'_j}}_{\beta_{c'_i}}\,\delta^{\beta_{c'_i}}_{\alpha_{c'_i}}\,\delta^{\alpha_{c_i}}_{\beta_{\bar{c}_j}}\right) = \delta^{\alpha_{c'_m}}_{\beta_{\bar{c}'_k}}\,\delta^{\alpha_{c_i}}_{\beta_{\bar{c}_j}} \tag{4.6}$$

$$\to \delta_{\tau_{(a,b)}\sigma}\delta_{(a,b)(c_i,\sigma^{-1}(\bar{c}_j))} \ ,$$

where in this case the elements c_i and $\sigma^{-1}(\bar{c}_j) = c'_m$ have to be swapped such that the permutations τ and σ match.
However, for the second possibility of the basis permutation σ no swap is necessary, instead one obtains

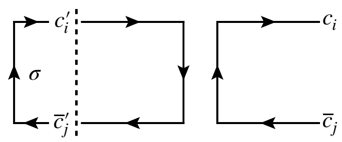

$$= \left(\delta^{\alpha_{c'_i}}_{\beta_{\bar{c}'_j}}\right)\left(\delta^{\alpha_{c_i}}_{\beta_{\bar{c}_j}}\,\delta^{\beta_{\bar{c}'_j}}_{\alpha_{c'_j}}\,\delta^{\alpha_{c'_j}}_{\beta_{c'_i}}\,\delta^{\beta_{c'_i}}_{\alpha_{c'_i}}\right) = N\delta^{\alpha_{c_i}}_{\beta_{\bar{c}_j}} \tag{4.7}$$

$$\to N\delta_{\sigma\tau}\delta_{c_i\sigma^{-1}(\bar{c}_j)} \ .$$

In the case of a colour-connection between the lines i and j one finds that the permutations σ and τ match ($\delta_{\sigma\tau}$), the $\delta_{c_i\sigma^{-1}(\bar{c}_j)}$ specifies the colour-connection of the basis. Further, there is a factor of N, due to the "colour-loop".

In the same way the cases of two anti-quark lines i, j and of an anti-quark line i and a quark line j can be treated. When considering gluon lines there are no additional contributions specific to gluon lines at one-loop level, i.e. they can be built from the combined quark/anti-quark cases

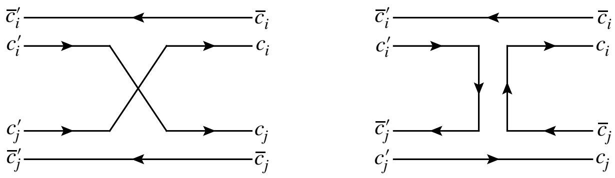

Figure 11: Illustration of two colour-line diagrams for gluon lines i and j. At one-loop level all of the colour-line diagrams for hard gluon lines can be built from those of the different combinations of hard quark and anti-quark lines.

(see Figure 11).

Analysing all of the different combinations of hard lines and the corresponding colour flow due to the gluon exchange leads to the following result for the matrix element of the colour-correlator $\mathbf{T}_i \cdot \mathbf{T}_j$ [2]

$$\begin{aligned}
[\tau|(\mathbf{T}_i \cdot \mathbf{T}_j)\,|\sigma\rangle = & -N\delta_{\tau\sigma}\left[\lambda_i\bar{\lambda}_j\delta_{c_i\sigma^{-1}(\bar{c}_j)} + \bar{\lambda}_i\lambda_j\delta_{c_j\sigma^{-1}(\bar{c}_i)} + \frac{1}{N^2}(\lambda_i - \bar{\lambda}_i)(\lambda_j - \bar{\lambda}_j)\right] \\
& + \sum_{(a,b)} \delta_{\tau_{(a,b)}\sigma}\Big(\lambda_i\lambda_j\delta_{(a,b)(c_i,c_j)} + \bar{\lambda}_i\bar{\lambda}_j\delta_{(a,b)(\sigma^{-1}(\bar{c}_i),\sigma^{-1}(\bar{c}_j))} \\
& \qquad - \lambda_i\bar{\lambda}_j\delta_{(a,b)(c_i,\sigma^{-1}(\bar{c}_j))} - \bar{\lambda}_i\lambda_j\delta_{(a,b)(c_j,\sigma^{-1}(\bar{c}_i))}\Big) \; .
\end{aligned} \tag{4.8}$$

In a matrix representation the contributions of the first line of equation (4.8) determine the diagonal elements, the terms with the "swaps" are off-diagonal elements. It is worth noticing that at one-loop the swap-terms are only single swaps of (anti-)colour indices. At higher order this will not be the case anymore.
With the result in equation (4.8) one can deduce the structure of the one-loop soft anomalous dimension matrix element in the colour-flow basis to be [2, 6]

$$(\alpha_s N)[\tau|\mathbf{\Gamma}^{(1)}|\sigma\rangle = (\alpha_s N)\left[\left(\Gamma_\sigma^{(1)} + \frac{1}{N^2}\rho^{(1)}\right)\delta_{\sigma\tau} + \frac{1}{N}\Sigma_{\sigma\tau}^{(1)}\right] \; . \tag{4.9}$$

As an expansion parameter $\alpha_s N$, the t' Hooft coupling, has been used. This allows for efficiently performing the large-N limit of QCD. The structure $\Gamma_\sigma^{(1)}$ denotes the leading colour-diagonal elements, for the colour part of the soft anomalous dimension this corresponds to the first two terms in equation (4.8). The $\rho^{(1)}$ coefficient stands for colour-diagonal elements suppressed in the number of colours, it is given by the third term of equation (4.8). The off-diagonal elements $\Sigma_{\sigma\tau}^{(1)}$ pertain to the colour-swap terms concerning the colour part of the soft anomalous dimension.
With equation (4.9) one can immediately determine the leading (in the large N-limit) colour-diagonal part and the off-diagonal elements of the soft anomalous dimension matrix.
It turns out, however, that it might be desirable to consider an expansion in the whole colour-diagonal part, instead of taking into account only the $\Gamma_\sigma^{(1)}$ coefficients in the large-N limit. On the one hand the reason for this is provided by the fact that the structure $\rho^{(1)}$ can give large contributions due to the sum over pairs of colour-partners, so-called dipoles, which has to be

performed. This can effectively compensate the $1/N$ suppression. On the other hand, when one takes into account collinear contributions, the quark splitting function has a colour factor of $C_F = \frac{N^2-1}{2N}$, performing the large-N limit would now lead to a replacement of C_F by $\frac{C_A}{2}$. This is, however, not done in the collinear sector.

4.3 Kinematic part of the loop-diagram

Concerning the kinematic part it is convenient to rewrite the loop integral as a phase-space type integral using the Feynman tree theorem such that it is possible to combine it with the single emission diagram in order to be able to explicitly observe the cancellation of IR divergences. Using Feynman rules, one obtains for the one-loop diagram in Feynman gauge

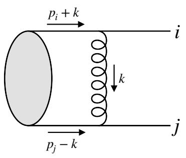

$$= (-\mathbf{T}_i \cdot \mathbf{T}_j) \int \frac{\mathrm{d}^d k}{i\pi^{d/2}} \frac{\mu^{2\varepsilon}\,(ig^2)\,4(p_i \cdot p_j)}{[2p_i \cdot k + 2i0(p_i^0)^2][-2p_j \cdot k + 2i0(p_j^0)^2][k^2 + 2i0(k^0)^2]}$$

$$= (-\mathbf{T}_i \cdot \mathbf{T}_j)\,\Omega_{ij}^{(1)} \;, \tag{4.10}$$

where the external momenta are assumed to be both outgoing. In the case that there are additional hard lines, a sum has to be introduced, such that soft gluon exchanges are are taken into account between all the possible hard lines, the sum then runs from $i, j = 1, ..., n$ with $i \neq j$ where n is the total number of hard lines.
In the following calculation it is convenient to use a Sudakov decomposition for the loop momentum,

$$k^\mu = \alpha p_i^\mu + \beta p_j^\mu + k_\perp^\mu \;. \tag{4.11}$$

The forward and backward components can be chosen to be

$$p_i = \sqrt{\frac{p_i \cdot p_j}{2}} \left(1, \vec{0}_\perp^{(d-2)}, 1\right) \;,$$

$$p_j = \sqrt{\frac{p_i \cdot p_j}{2}} \left(1, \vec{0}_\perp^{(d-2)}, -1\right) \;,$$

where $p_i \cdot p_j > 0$. With this choice, the transverse part is then uniquely determined as $k_\perp = p_\perp(0, \vec{n}_\perp^{(d-2)}, 0)$ with $\vec{n}_\perp^2 = 1$. In terms of these variables the measure translates to

$$\mu^{2\varepsilon}\mathrm{d}^d k = \mathrm{d}p_\perp p_\perp \theta(p_\perp)\; (p_i \cdot p_j) \left(\frac{\mu}{p_\perp}\right)^{2\varepsilon} \mathrm{d}\alpha\, \mathrm{d}\beta\, \mathrm{d}\Omega^{(d-3)} \;, \tag{4.12}$$

see appendix A for the details on the Jacobian determinant in this case.
The Feynman tree theorem now instructs one to evaluate the cut diagrams - in the presence of eikonal propagators one finds a radiative cut, an absorptive cut in the eikonal momentum $(p_i \cdot k)$ and the combined double cut (cf. equation (3.49)). Schematically, the required cuts if both hard

momenta are taken to be outgoing, correspond to

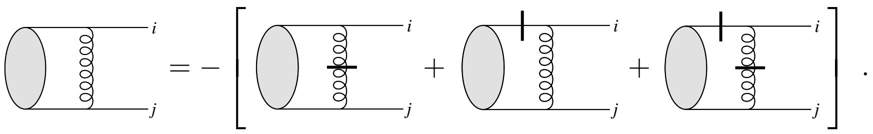

(4.13)

The radiative cut, which leads to the real part of the one-loop integral, can be expressed as

$$\begin{aligned}\Omega^{(1)}_{ij,\text{rad.cut}} &= -i\frac{\alpha_s}{\pi}\frac{(2\pi)^{2\varepsilon}\mu^{2\varepsilon}}{(2\pi)^2}\int \mathrm{d}^d k\,(2\pi i)\tilde{\delta}(k)\,\frac{p_i\cdot p_j}{[p_i\cdot k+i0][-p_j\cdot k+i0]}\\ &= \frac{\alpha_s}{\pi}\frac{(2\pi)^{2\varepsilon}}{2\pi}\int_{-\infty}^{\infty}\mathrm{d}\alpha\int_{-\infty}^{\infty}\mathrm{d}\beta\int_0^{\infty}\mathrm{d}p_\perp p_\perp\theta(p_\perp)\left(\frac{\mu}{p_\perp}\right)^{2\varepsilon}\int \mathrm{d}\Omega^{(d-3)}\\ &\quad\frac{\delta(2\alpha\beta(p_i\cdot p_j)-p_\perp^2)\theta(\alpha+\beta)}{[\beta+i0][-\alpha+i0]}\ ,\end{aligned}\tag{4.14}$$

where, due to the choice of variables, the factor $(p_i \cdot p_j)$ is positive and thus can be dropped in front of the $i0$-prescription. When evaluating the α-integration with the delta function, one finds an additional restriction for the α, β variables, namely $\theta(\alpha\beta)$. Together with the $\theta(\alpha+\beta)$ restriction from the cut, this leads to a $\theta(\alpha)\theta(\beta)$. As a result, one obtains

$$\Omega^{(1)}_{ij,\text{rad.cut}} = -\frac{\alpha_s}{\pi}\frac{(2\pi)^{2\varepsilon}}{2\pi}\int_0^{\infty}\mathrm{d}\beta\frac{1}{\beta+i0}\int_0^{\infty}\frac{\mathrm{d}p_\perp}{p_\perp}\left(\frac{\mu}{p_\perp}\right)^{2\varepsilon}\int \mathrm{d}\Omega^{(d-3)}\ ,\tag{4.15}$$

with a logarithmic divergence in β, the integration in β can be rewritten in terms of the angle θ

$$\Omega^{(1)}_{ij,\text{rad.cut}} = -\frac{\alpha_s}{\pi}\frac{(2\pi)^{2\varepsilon}}{2\pi}\int_{-1}^{1}\frac{\mathrm{d}\cos\theta}{(1-\cos\theta)(1+\cos\theta)}\int_0^{\infty}\frac{\mathrm{d}p_\perp}{p_\perp}\left(\frac{\mu}{p_\perp}\right)^{2\varepsilon}\int \mathrm{d}\Omega^{(d-3)}\ ,\tag{4.16}$$

such that the collinear divergences still contained in $\Omega^{(1)}_{ij,\text{rad.cut}}$ become apparent. Because of this, the soft anomalous dimension is formally divergent, however, the divergences are of collinear origin only. One can choose an observable for which the collinear divergences cancel.

As an alternative choice of variables one can express the radiative cut of the one-loop integral in terms of rapidity η [18]

$$\Omega^{(1)}_{ij,\text{rad.cut}} = -\frac{\alpha_s}{\pi}\frac{(2\pi)^{2\varepsilon}}{2\pi}\int_0^{\infty}\frac{\mathrm{d}p_\perp}{p_\perp}\left(\frac{\mu}{p_\perp}\right)^{2\varepsilon}\int \mathrm{d}\eta\,\mathrm{d}\Omega^{(d-3)}\,\omega_{ij}^{(p_\perp)}\ ,\tag{4.17}$$

where

$$\omega_{ij}^{(p_\perp)} = \frac{p_\perp^2}{2}\frac{p_i\cdot p_j}{(p_i\cdot k)(p_j\cdot k)}\ .\tag{4.18}$$

The variables of transverse momentum and (pseudo-)rapidity are preferably used to describe processes of hadron-hadron collisions or lepton-hadron collisions [19]. Consult appendix A for the Jacobian determinant in order to translate to rapidity and to find the variable definitions. Yet another possible choice of variables is energy instead of transverse momentum. In e^+-e^- collisions energy and solid angle are oftentimes the variables of choice. In terms of energy-ordering the radiative cut of the one-loop integral reads [2]

$$
\begin{aligned}
\Omega^{(1)}_{ij,\text{rad.cut}} &= -\frac{\alpha_s}{\pi}\frac{(2\pi)^{2\varepsilon}}{2\pi}\int_{-1}^{1}\mathrm{d}\cos\theta\,\frac{(1-\cos^2\theta)^{-\varepsilon}}{(1-\cos\theta)(1+\cos\theta)}\int_0^\infty\frac{\mathrm{d}E}{E}\left(\frac{\mu}{E}\right)^{2\varepsilon}\mathrm{d}\Omega^{(d-3)} \\
&= -\frac{\alpha_s}{\pi}(2\pi)^{2\varepsilon}\int_0^\infty\frac{\mathrm{d}E}{E}\left(\frac{\mu}{E}\right)^{2\varepsilon}\int\frac{\mathrm{d}\hat{\Omega}^{(d-2)}}{4\pi}\frac{n_i\cdot n_j}{(n\cdot n_i)(n\cdot n_j)} \\
&= -\frac{\alpha_s}{\pi}(2\pi)^{2\varepsilon}\int_0^\infty\frac{\mathrm{d}E}{E}\left(\frac{\mu}{E}\right)^{2\varepsilon}\int\frac{\mathrm{d}\hat{\Omega}^{(d-2)}}{2\pi}\,\omega^{(E)}_{ij}\ ,
\end{aligned}
\tag{4.19}
$$

where it is used that $p^\mu_{i,j} = \sqrt{\frac{p_i\cdot p_j}{2}}\,n^\mu_{i,j}$ and $k^\mu = En^\mu$ for on-shell loop momentum. Further, for the angular integration the following notation is introduced

$$
\int\mathrm{d}\hat{\Omega}^{(d-2)} = \int_{-1}^{1}\mathrm{d}\cos\theta\,(1-\cos^2\theta)^{-\varepsilon}\int\mathrm{d}\Omega^{(d-3)}\ . \tag{4.20}
$$

The absorptive part of the one-loop diagram gives a purely imaginary contribution. The diagram with the cut of the eikonal propagator of momentum $(p_i\cdot k)$ evaluates to (using again the Sudakov decomposition for the loop momentum)

$$
\begin{aligned}
\Omega^{(1)}_{ij,\,\text{absorp.cut}} &= -i\frac{\alpha_s}{\pi}\frac{(2\pi)^{\varepsilon}\mu^{2\varepsilon}}{(2\pi)^2}\int\mathrm{d}^dk\,(2\pi i)\delta(p_i\cdot k)\,\frac{p_i\cdot p_j}{[k^2+i0][-p_j\cdot k+i0]} \\
&= \frac{\alpha_s}{\pi}\frac{(2\pi)^{\varepsilon}}{2\pi}\int_{-\infty}^{\infty}\mathrm{d}\alpha\int_0^\infty\mathrm{d}p_\perp p_\perp\theta(p_\perp)\left(\frac{\mu}{p_\perp}\right)^{2\varepsilon}\mathrm{d}\Omega^{(d-3)}\frac{1}{[-p_\perp^2+i0][-\alpha+i0]}\ ,
\end{aligned}
\tag{4.21}
$$

where the integration in the variable β has already been performed using the delta function. In order to evaluate the integration in α one can make use of the Sokhotski-Plemelj identity in the following way

$$
\begin{aligned}
-\int_{-\infty}^{\infty}\frac{\mathrm{d}\alpha}{[\alpha-i0]} &= -\int_{-\infty}^{\infty}\mathrm{d}\alpha\left[\frac{1}{[\alpha+i0]}+2\pi i\delta(\alpha)\right] \\
&= -2\pi i-\int_{-\infty}^{\infty}\mathrm{d}\alpha\,\frac{1}{2}\left[\frac{1}{[\alpha+i0]}-\frac{1}{[\alpha-i0]}\right] = -i\pi\ .
\end{aligned}
\tag{4.22}
$$

Equivalently, one obtains this result by noticing that the principal value of this integral vanishes, the imaginary part remains. Therefore, one finds for the absorptive cut

$$
\Omega^{(1)}_{ij,\,\text{absorp.cut}} = \frac{\alpha_s}{\pi}(2\pi)^{2\varepsilon}\int_0^\infty\frac{\mathrm{d}p_\perp}{p_\perp}\left(\frac{\mu}{p_\perp}\right)^{2\varepsilon}\int\frac{\mathrm{d}\Omega^{(d-3)}}{2\pi}\,(i\pi)\ . \tag{4.23}
$$

The last contribution which needs to be evaluated for the one-loop diagram is the double-cut diagram. However, it turns out that it vanishes, since

$$
\begin{aligned}
\Omega^{(1)}_{ij,\text{double-cut}} &= -i\frac{\alpha_s}{\pi}\frac{(2\pi)^{2\varepsilon}\mu^{2\varepsilon}}{(2\pi)^2}\int \mathrm{d}^d k\,(2\pi i)^2\delta(\hat{p}_i\cdot k)\tilde{\delta}(k)\,\frac{p_i\cdot p_j}{[-p_j\cdot k+i0]} \\
&= i\frac{\alpha_s}{\pi}(2\pi)^{2\varepsilon}\int_{-\infty}^{\infty}\mathrm{d}\alpha\int_{-\infty}^{\infty}\mathrm{d}\beta\int_0^{\infty}\mathrm{d}p_\perp p_\perp\left(\frac{\mu}{p_\perp}\right)^{2\varepsilon}\int \mathrm{d}\Omega^{(d-3)} \\
&\quad \frac{\delta(\beta)\delta(2\alpha\beta(p_i\cdot p_j)-p_\perp^2)\theta(\alpha+\beta)}{[-\alpha+i0]} \\
&= i\frac{\alpha_s}{\pi}(2\pi)^{2\varepsilon}\int_{-\infty}^{\infty}\mathrm{d}\alpha\,\frac{1}{2}\int_0^{\infty}\mathrm{d}p_\perp^2\left(\frac{\mu}{p_\perp}\right)^{2\varepsilon}\frac{\delta(p_\perp^2)}{[-\alpha+i0]}\int \mathrm{d}\Omega^{(d-3)} \\
&= 0\;.
\end{aligned}
\tag{4.24}
$$

In the $p_\perp$ variable the integral above only shows an IR singularity and no divergence of UV origin, since one can cut off the upper boundary due to $\delta(p_\perp^2)$. Hence, $\varepsilon < 0$ holds for $(\mu/p_\perp)^{2\varepsilon}$.

Finally, combining the cut-contributions one finds

$$
\Omega^{(1)}_{ij} = -\frac{\alpha_s}{\pi}(2\pi)^{2\varepsilon}\int\frac{\mathrm{d}p_\perp}{p_\perp}\,\theta(p_\perp)\left(\frac{\mu}{p_\perp}\right)^{2\varepsilon}\int\frac{\mathrm{d}\Omega^{(d-3)}}{2\pi}\left\{\int \mathrm{d}\eta\;\omega_{ij}^{(p_\perp)} - i\pi\right\}\;. \tag{4.25}
$$

Reformulating in terms of energy-ordering and taking into account the colour structure one obtains

$$
\begin{aligned}
\mathbf{V}^{(1)} &= -\left(-\mathbf{T}_i\cdot\mathbf{T}_j\right)\frac{\alpha_s}{\pi}(2\pi)^{2\varepsilon}\int\frac{\mathrm{d}E}{E}\,\theta(E)\left(\frac{\mu}{E}\right)^{2\varepsilon} \\
&\qquad\times\left\{\int\frac{\mathrm{d}\Omega^{(d-2)}}{4\pi}\frac{n_i\cdot n_j}{(n_i\cdot n)(n_j\cdot n)} - \frac{\mathrm{d}\Omega^{(d-3)}}{2\pi}\,(i\pi)\right\}\;,
\end{aligned}
\tag{4.26}
$$

which is of the same form as the result of the soft anomalous dimension at one-loop level given in [2]. Mind however, that as opposed to the result in [2] the integration boundaries of the energy integral still range from zero to infinity in this case. For this reason the result in equation (4.26) is labeled by $\mathbf{V}^{(1)}$ rather than $\mathbf{\Gamma}^{(1)}$.
The eikonal factor $\omega_{ij}^{(n)}$, i.e. the first term of equation (4.26) in the second line still contains collinear divergences for $n\cdot n_i \to 0$ or $n\cdot n_j \to 0$. These have to be subtracted, for instance with a prescription [20]

$$
\omega_{ij}^{(n)} - \frac{1}{n\cdot n_i} - \frac{1}{n\cdot n_j}\;, \tag{4.27}
$$

which leaves behind an integrable singularity. The subtractions can then be combined with collinear/hard-collinear contributions, since one can use colour conservation to rewrite them in a colour-diagonal form. Alternatively, one can also use a different subtraction which has the form [20]

$$
\tilde{\omega}_{ij}^{(n)} = \omega_{ij}^{(n)} - s_{ij} - s_{ji}\;, \tag{4.28}
$$

with a subtraction term s_{ij} defined as [20]

$$s_{ij} = \frac{1}{n_i \cdot n} - \frac{n_j \cdot n - n_i \cdot n_j}{(n_i \cdot n_j)(n_i \cdot n)} \ . \tag{4.29}$$

This type of subtraction will leave behind a finite result concerning the collinear singularities. The imaginary part of the result in equation (4.26) is commonly referred to as Coulomb or Glauber contribution. It should be stressed that although at this order it does not have an influence on the result when squaring the amplitude, the Coulomb contribution does alter the result if at least four hard lines are involved in a process where one does not only consider the large-N limit and it is connected to the occurrence of super-leading logarithms for non-global observables [21].
Furthermore, the result in equation (4.26) only exhibits an imaginary part if the momentum flow of both hard momenta is chosen to be outgoing (or equivalently incoming), i.e. if it defines a physical final state. In section 4.4 the case of one incoming and one outgoing hard momentum is considered and the vanishing of the imaginary part can be correctly observed when using the FTT.

In order to obtain the virtual exchange at leading order at a cross-sectional level one takes the interference between the one-loop amplitude and the Born process in the sense that

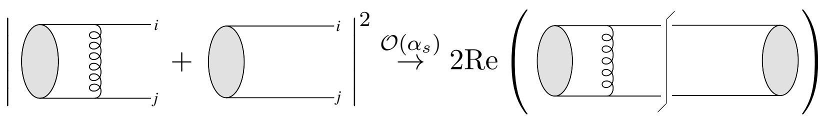

, (4.30)

where the $\mathcal{O}(\alpha_s)$ indicates that one is only interested in the leading order contribution, i.e. the interference diagram, at this point. Hence one gets twice the real part of equation (4.26) for the absolute value squared of the amplitude. Note that if one introduces an unordered colour sum of the hard lines for the one-loop amplitude one has to take into account an additional factor of 1/2 in order to compensate for the double counting of the diagram under the exchange of the hard lines (cf. equation (4.1)).

The amplitude of the single soft emission diagram with n external lines leads to an expression for the tree-level soft current [5]

$$\mathbf{J}^{\mu}(k) = \sum_{l=1}^{n} \mathbf{T}_l \frac{p_l^{\mu}}{p_l \cdot k} \ . \tag{4.31}$$

The conservation of the soft current follows from the property of colour conservation in equation (3.6), since [5]

$$k_{\mu}\mathbf{J}^{\mu}(k) = \sum_{l=1}^{n} \mathbf{T}_l \ , \tag{4.32}$$

and hence, together with the tree-level amplitude $\mathcal{M}(p_1, ...p_n)$ of external momenta $p_1, ..., p_n$ one finds [5]

$$k_\mu \mathbf{J}^\mu(k)\,|\mathcal{M}(p_1, ...p_n)\rangle = \sum_{l=1}^{n} \mathbf{T}_l\,|\mathcal{M}(p_1, ...p_n)\rangle = 0\ . \tag{4.33}$$

It turns out that the square of the single emission diagram gives exactly minus the radiative cut contribution of the one-loop diagram (except for the integration boundaries), which makes the cancellation of the infrared divergences explicit. In a diagrammatic language the absolute value squared of the single emission diagrams can be schematically illustrated as

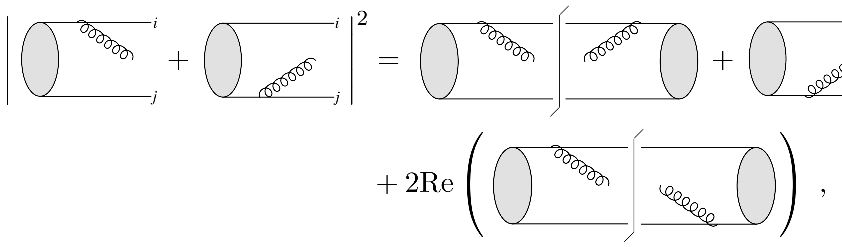

(4.34)

where the first and the second diagram do not give a contribution in the soft limit in Feynman gauge due to the on-shellness of the external lines, whereas the third one gives

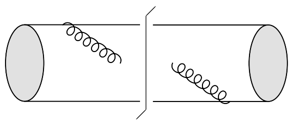

$$= -g^2\,(-\mathbf{T}_i\cdot\mathbf{T}_j)\,\mu^{2\varepsilon}\int_0^{\mu_s} \mathrm{d}\Pi_k\,\frac{p_i\cdot p_j}{[p_i\cdot k][-p_j\cdot k]}$$
$$= \frac{\alpha_s}{\pi}(2\pi)^{2\varepsilon}(-\mathbf{T}_i\cdot\mathbf{T}_j)\int_0^{\mu_s}\frac{\mathrm{d}E}{E}\left(\frac{\mu}{E}\right)^{2\varepsilon}\int\frac{\mathrm{d}\Omega^{(d-2)}}{4\pi}\frac{n_i\cdot n_j}{(n_i\cdot n)(n_j\cdot n)}\ . \tag{4.35}$$

The phase-space integral is given by $\mathrm{d}\Pi_k = \frac{\mathrm{d}^d k}{(2\pi)^{d-1}}\delta(k^2)\theta(k^0)$ and the upper integration boundary is taken to be the soft scale μ_s. Consequently, the radiative part of the virtual diagram squared is exactly minus the real emission diagram; the infrared divergences cancel.
Note again that if an unordered colour sum is introduced one has to include a factor of 1/2 for the single emission contribution as well.

4.4 Different momentum flow

If one takes the external momentum p_i to be outgoing and p_j incoming, the one-loop integral now reads

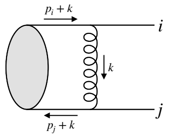

$$= (-\mathbf{T}_i \cdot \mathbf{T}_j) \int \frac{đ^d k}{i\pi^{d/2}} \frac{\mu^{2\varepsilon}\,(ig^2)\,4(p_i \cdot p_j)}{[2p_i \cdot k + 2i0(p_i^0)^2][2p_j \cdot k + 2i0(p_j^0)^2][k^2 + 2i0(k^0)^2]}\ , \quad (4.36)$$

which leads to the conclusion that when using the FTT in this case, due to the sign structure of the propagators, all lines have to be cut. Diagrammatically, this gives

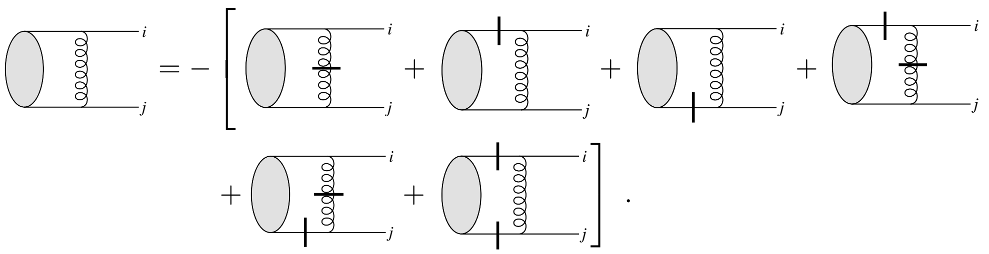

(4.37)

It turns out that the single eikonal cut of momentum $(p_i \cdot k)$ gives the same result as already determined in equation (4.23) and due to the symmetry in i and j the cut of momentum $(p_j \cdot k)$ does so as well. In accordance with the previous consideration of the double cuts in one eikonal line and the soft gluon, these diagrams vanish, hence all that remains is to evaluate the contribution of the eikonal double cut. As expected, it introduces a contribution of the form

$$\begin{aligned}\Omega_{ij,\,\mathrm{double-eikonal}} &= -i\frac{\alpha_s}{\pi}\frac{(2\pi)^{2\varepsilon}\mu^{2\varepsilon}}{(2\pi)^2}\int \mathrm{d}^d k\,(2\pi i)^2 \delta(p_i \cdot k)\delta(p_j \cdot k)\frac{p_i \cdot p_j}{[k^2 + i0]} \\ &= -i\frac{\alpha_s}{\pi}(2\pi)^{2\varepsilon}\int \frac{\mathrm{d}p_\perp}{p_\perp}\theta(p_\perp)\left(\frac{\mu}{p_\perp}\right)^{2\varepsilon}\int \frac{\mathrm{d}\Omega^{(d-3)}}{\pi}\,(i\pi)\ ,\end{aligned} \quad (4.38)$$

which exactly cancels the result of both of the single eikonal cuts leaving only the real part, i.e. the radiative cut, as it must.

For the case of two outgoing or equivalently two incoming hard partons discussed in the previous section one can use colour conservation to rewrite the imaginary part as $\sum_{i,j}(\mathbf{T}_i \cdot \mathbf{T}_j)(i\pi) \propto \sum_i \mathbf{T}_i^2(i\pi)$, which equals to a Casimir invariant. When evolving the amplitude, the imaginary part then simply leads to a phase which subsequently cancels, since one finds a structure $e^{A\,i\pi}\mathcal{M}\,e^{-A\,i\pi}$, where A is some evolution coefficient. However, if the amplitude with an incoming and outgoing hard parton would lead to an imaginary part, the above argument does not hold due to the non-trivial colour structure which remains since one cannot exploit colour conservation. In this case one would instead have a structure of the form $e^{i\pi}\mathcal{M}\,e^{-X\,i\pi}$ for the evolution, where X stands for the non-trivial colour structure. This type of mechanism generating a non-vanishing imaginary part lies at the basis of QCD coherence breaking, see [22].

5 Ingredients for a next-to-leading order/next-to-leading colour evolution

5.1 Soft anomalous dimension at next-to-leading order

In the previous section the results for the soft anomalous dimension matrix at one-loop order have been presented. In the following, the analysis done at one-loop will be extended by deriving ingredients which are necessary for a next-to-leading order soft gluon evolution. In particular, one needs to investigate the structure of the matrix elements of the soft anomalous dimension in the colour-flow basis at next-to-leading order/next-to-leading colour. This involves analysing the colour structures which appear for the Feynman diagrams at one-loop/one-emission and two-loop level, if they contribute in the soft limit.

As already mentioned in the previous section, the integrals described here correspond to the virtual correction $\mathbf{V}^{(1,1)}$ which still contains infrared and ultraviolet divergences. In order to find an expression for $\mathbf{\Gamma}^{(1,1)}$ (cf. equation (3.62)) from $\mathbf{V}^{(1,1)}$ the singularities have to be subtracted/treated with the renormalisation procedure and at one-loop/one-emission level the tree-level eikonal current has to be subtracted in order to avoid overcounting. When focussing only on the colour structure the symbol $\mathbf{\Gamma}^{(1,1)}$ is used.

5.1.1 One-loop/one-emission order

In this section the colour structures of the one-loop/one-emission diagrams are analysed in the soft limit. In order to find the amplitude squared, the one-loop/one-emission diagrams have to be brought together with the single emission contribution.

The one-loop/one-emission Feynman diagrams which involve only one external line are depicted in Figure 12. However, in the soft limit and in Feynman gauge, only diagrams 12(a) and (e) contribute. The diagrams 12(b) and (c) vanish in the soft limit for an on-shell external line, since the numerator involves a p_i^2. Furthermore, diagram 12(d) can also be neglected in the soft limit as

$$\mathcal{M}_{12(\mathrm{d})} = -ig^3 C_r \mathbf{T}_i^a \frac{\lambda^d}{\lambda^4}\mu^{2\varepsilon} \int \frac{\text{đ}^d k}{i\pi^{d/2}} \frac{p_i^\mu \varepsilon_\mu^*(q)}{[k^2+i0][-p_i\cdot k+i0][p_i\cdot q+i0]} , \tag{5.1}$$

and letting $d \to 4$ one observes that the amplitude is of $\mathcal{O}(\lambda^0)$. The one-emission diagram however, with which this amplitude is interfered with when calculating the amplitude squared, is of $\mathcal{O}(\lambda)$. As a result, for $\lambda \to 0$, the diagram of Figure 12(d) can be neglected. For the one-loop/one-emission diagrams to contribute in the soft limit they thus have to give a leading singular contribution in λ, i.e. they have to be of $\mathcal{O}(\frac{1}{\lambda})$.

Taking the emission momentum q to be outgoing, one finds for the amplitude of diagram (a) in

Figure 12 in the soft limit

$$
\begin{aligned}
\mathcal{M}_{12(\mathrm{a})} &= g^3 f_{abc}\mathbf{T}_i^b\mathbf{T}_i^a\,\frac{\lambda^d}{\lambda^5}\,\mu^{2\varepsilon}\int\frac{\mathrm{đ}^dk}{i\pi^{d/2}}\,\frac{p_{i\alpha}p_{i\beta}[(q-k)^\alpha g^{\mu\beta}-(2q+k)^\beta g^{\mu\alpha}+(2k+q)^\mu g^{\alpha\beta}]}{[k^2+i0][(k+q)^2+i0][-p_i\cdot k+i0](p_i\cdot q)}\,\varepsilon^*_\mu(q)\\
&= ig^3\frac{C_A}{2}\mathbf{T}_i^c\,\frac{\lambda^d}{\lambda^5}\,\mu^{2\varepsilon}\int\frac{\mathrm{đ}^dk}{i\pi^{d/2}}\left\{\frac{1}{[k^2+i0][(k+q)^2+i0][-p_i\cdot k+i0]}\right.\\
&\qquad\left.-\frac{2}{[k^2+i0][(k+q)^2+i0](p_i\cdot q)}\right\}(p_i\cdot\varepsilon^*(q))\\
&= T_R\mathbf{T}_i^c\,\Omega^{(1,1)}_{i,\mathrm{vertex-corr.}}\ ,
\end{aligned}
\tag{5.2}
$$

with the loop integrand $\Omega^{(1,1)}_{i,\mathrm{vertex-corr.}}$. For the colour structure it has been used that $if_{abc}\mathbf{T}_i^b\mathbf{T}_i^a = if_{abc}\,\frac{1}{2}[\mathbf{T}_i^b,\mathbf{T}_i^a] = \frac{C_A}{2}\mathbf{T}_i^c$. Hence, for this diagram one does not find a new (i.e. not yet treated) colour structure.

Note that the Feynman diagram with the self-energy "bubble" in Figure 12(e) does contribute in the soft limit as well. Due to the fact that the amplitude of the bubble-diagram contains a propagator raised to second power, a modified treatment is needed when applying the Feynman tree theorem. Therefore, the bubble-diagram at one-loop/one-emission and two-loop level will be analysed separately, their treatment can be found in section 5.5.
The one-loop/one-emission Feynman diagrams involving two or three hard lines i, j and l are depicted in Figure 13. The corresponding amplitudes in Feynman gauge are

$$
\begin{aligned}
\mathcal{M}_{13(\mathrm{a})} &= -ig^3\,\mathbf{T}_i^a(\mathbf{T}_i\cdot\mathbf{T}_j)\frac{\lambda^d}{\lambda^5}\,\mu^{2\varepsilon}\int\frac{\mathrm{đ}^dk}{i\pi^{d/2}}\frac{(p_i\cdot p_j)(p_i\cdot\varepsilon^*(q))}{[p_i\cdot(k+q)+i0][k^2+i0][-p_j\cdot k+i0](p_i\cdot q)}\\
&= \mathbf{T}_i^a(\mathbf{T}_i\cdot\mathbf{T}_j)\,\Omega^{(1,1)}_{ij}\ ,
\end{aligned}
\tag{5.3}
$$

for the diagram with a soft gluon emission after the virtual exchange, and for the emission prior to the exchange one obtains

$$
\begin{aligned}
\mathcal{M}_{13(\mathrm{b})} &= -ig^3\,(\mathbf{T}_i\cdot\mathbf{T}_j)\mathbf{T}_i^a\frac{\lambda^d}{\lambda^5}\,\mu^{2\varepsilon}\int\frac{\mathrm{đ}^dk}{i\pi^{d/2}}\frac{(p_i\cdot p_j)(p_i\cdot\varepsilon^*(q))}{[p_i\cdot(k+q)+i0][k^2+i0][-p_j\cdot k+i0][p_i\cdot k+i0]}\\
&= (\mathbf{T}_i\cdot\mathbf{T}_j)\mathbf{T}_i^a\,\tilde{\Omega}^{(1,1)}_{ij}\ .
\end{aligned}
\tag{5.4}
$$

The amplitude of the one-loop/one-emission diagram of Figure 13(c) can be written as

$$
\begin{aligned}
\mathcal{M}_{13(\mathrm{c})} &= ig^3(if_{abc})\mathbf{T}_i^a\mathbf{T}_j^b\,\frac{\lambda^{d+1}}{\lambda^6}\,\mu^{2\varepsilon}\int\frac{\mathrm{đ}^dk}{i\pi^{d/2}}\\
&\qquad\frac{p_j\cdot(2q+k)(p_i\cdot\varepsilon^*(q))+p_i\cdot(k-q)(p_j\cdot\varepsilon^*(q))-2(p_i\cdot p_j)(k\cdot\varepsilon^*(q))}{[p_i\cdot(k+q)+i0][(k+q)^2+i0][k^2+i0][-p_j\cdot k+i0]}\\
&\qquad= (if_{abc})\mathbf{T}_i^a\mathbf{T}_j^b\,\hat{\Omega}^{(1,1)}_{ij}\ .
\end{aligned}
\tag{5.5}
$$

In this case it is convenient to perform a Passarino-Veltman reduction, this leads one to

$$
\begin{aligned}
\mathcal{M}_{13(\mathrm{c})} &= 2ig^3(if_{abc})\mathbf{T}_i^a\mathbf{T}_j^b\,\mu^{2\varepsilon}\,\varepsilon^*_\mu(q) \\
&\Bigg\{(p_j\cdot q)p_i^\mu\int\frac{đ^dk}{i\pi^{d/2}}\frac{1}{[k^2+i0][(k+q)^2+i0][p_i\cdot(k+q)+i0][-p_j\cdot k+i0]} \\
&-\frac{p_i\cdot q}{p_j\cdot q}p_j^\mu\int\frac{đ^dk}{i\pi^{d/2}}\frac{1}{[k^2+i0][(k+q)^2+i0][-p_i\cdot k+i0]} \\
&-\frac{p_i\cdot p_j}{2}\left(\frac{p_i^\mu}{p_i\cdot q}+\frac{p_j^\mu}{p_j\cdot q}\right)\int\frac{đ^dk}{i\pi^{d/2}}\frac{1}{[k^2+i0][p_i\cdot(k+q)+i0][-p_j\cdot k+i0]}\Bigg\}\;.
\end{aligned}
\tag{5.6}
$$

Finally, the amplitude of the diagram with three hard lines i, j and l gives

$$
\begin{aligned}
\mathcal{M}_{13(\mathrm{d})} &= -ig^3\,(\mathbf{T}_i\cdot\mathbf{T}_j)\mathbf{T}_l^a\frac{\lambda^d}{\lambda^5}\,\mu^{2\varepsilon}\int\frac{đ^dk}{i\pi^{d/2}}\frac{(p_i\cdot p_j)(p_l\cdot\varepsilon^*(q))}{[p_i\cdot k+i0][-p_j\cdot k+i0][k^2+i0](p_l\cdot q)} \\
&= (\mathbf{T}_i\cdot\mathbf{T}_j)\mathbf{T}_l^a\,\Omega_{ijl}^{(1,1)}\;.
\end{aligned}
\tag{5.7}
$$

Thus, in a basis-independent way, one can write the soft correction at one-loop/one-emission level as

$$
\begin{aligned}
\mathbf{V}^{(1,1)} &= \sum_{i\neq j}\left[\mathbf{T}_i^a(\mathbf{T}_i\cdot\mathbf{T}_j)\,\Omega_{ij}^{(1,1)}+(\mathbf{T}_i\cdot\mathbf{T}_j)\mathbf{T}_i^a\,\tilde{\Omega}_{ij}^{(1,1)}+\frac{1}{2}f^{abc}\mathbf{T}_i^b\mathbf{T}_j^c\,\hat{\Omega}_{ij}^{(1,1)}\right] \\
&\quad+\sum_{i\neq j\neq l}\frac{1}{2}\mathbf{T}_l^a(\mathbf{T}_i\cdot\mathbf{T}_j)\,\Omega_{ijl}^{(1,1)}+\sum_i T_R\mathbf{T}_i^a\left[\Omega_{i,\mathrm{self-en.}}^{(1,1)}+\Omega_{i,\mathrm{vertex-corr.}}^{(1,1)}\right]\;,
\end{aligned}
\tag{5.8}
$$

where the coefficients $\Omega^{(1,1)}$ stand for the loop integrands of the different diagrams, they are defined in the previous equations. Note that unordered colour sums have been introduced in equation (5.8), they are only taken over distinct hard parton lines, i.e. it holds that $i\neq j$ and $i\neq j\neq l$. As a result of performing an unordered colour sum one needs to introduce factors of $1/2$ for some of the diagrams in order to avoid overcounting.
The colour structure for the self-energy diagrams and the vertex-correction have been written as a $T_R\,\mathbf{T}_i^a$. The Casimir invariant C_A of the one-loop/one-emission gluon-bubble and the vertex-correction is understood to be absorbed into the kinematical factors of the diagrams. Equivalently, the factor of the number of flavours n_f which is present for the fermion-bubble can be absorbed into the kinematical part. Furthermore, since the colour structure of the gluon-bubble and the vertex-correction is $\frac{C_A}{2}\mathbf{T}_i^a$, one can use that the normalisation is $T_R=1/2$ and in this way one can write a global colour factor for the gluon-/fermion-bubble diagrams and the vertex-correction.

Now, one can find expressions for the colour structures of the one-loop/one-emission diagrams involving two or three hard lines in the colour-flow basis. This proceeds in analogy to the one-loop case. The detailed results for the individual matrix elements in the colour-flow basis can be found in appendix E.
With these results one obtains the following building blocks for the soft anomalous dimension

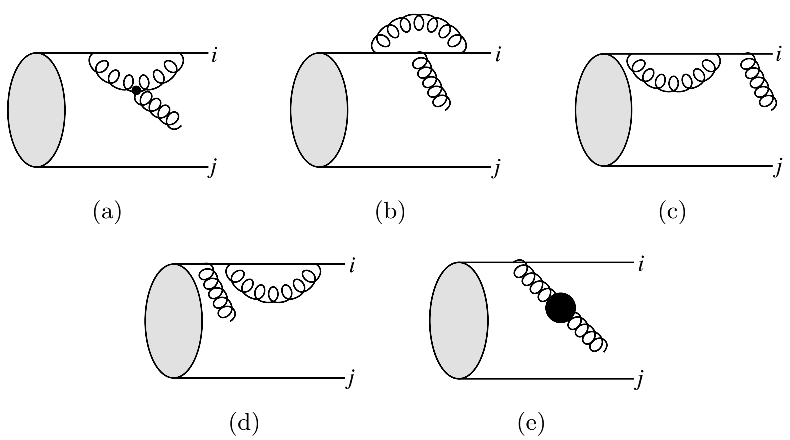

Figure 12: One-loop/one-emission diagrams involving a single hard line.

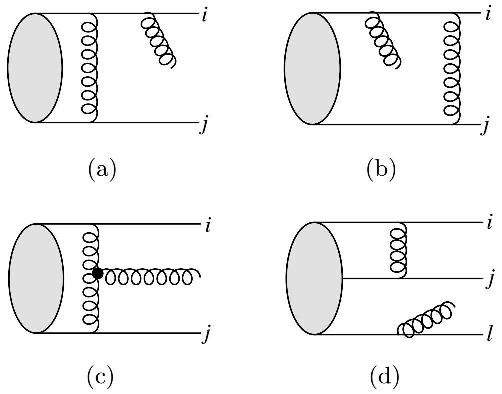

Figure 13: One-loop/one-emission diagrams involving two and three hard lines.

matrix elements in the colour-flow basis

$$(\alpha_s N)^2[\tau|\mathbf{V}^{(1,1)}|\sigma\rangle = (\alpha_s N)^2 \Bigg[\left(\frac{1}{N^2}\rho_{\sigma\tau} + \frac{1}{N^4}\rho_\tau \right) \delta_{\sigma\tau\setminus n} \\ + \frac{1}{N}\hat{\Sigma}^{(1,1)}_{\sigma\tau} + \frac{1}{N^3}\left(\tilde{\Sigma}^{(1,1)}_{\sigma\tau} + \hat{\tilde{\Sigma}}_{\sigma\tau} \right) + \frac{1}{N^2}\left(\Sigma'^{(1,1)}_{\sigma\tau} + \Sigma''^{(1,1)}_{\sigma\tau} \right) \Bigg] \;, \tag{5.9}$$

where all of the Σ-terms originate from colour-line diagrams for which swaps of (anti-)colour indices have to be performed and the ρ-structures from those without swaps. In appendix E, table 2 contains the information on which Feynman diagrams contribute to which coefficients of equation (5.9).

The action of emission operator $\mathbf{T}_i^a$ corresponds to going from a lower to a higher dimension in colour space, as the emission of a soft gluon introduces another pair of (anti-)colour labels. Therefore, the soft anomalous dimension matrix element for the one-loop/one-emission amplitudes does not contain a $\delta_{\sigma\tau}$, but a $\delta_{\sigma\tau\setminus n}$, which should indicate that the permutations σ and τ are equal after merging and removing the pair of the colour labels of the emitted gluon. As opposed to the one-loop case there are not only single swaps in the colour labels but also double-swap structures $\Sigma'^{(1,1)}_{\sigma\tau}$ which introduce swaps of the colour labels of the form $(a,b)(b,c)$. Furthermore one finds contributions with two single swaps of different colour labels of the form

$(a,b)(c,d)$, these are encoded in the coefficient $\Sigma''^{(1,1)}_{\sigma\tau}$.
As an illustration of the form of the contributions to $\Sigma'^{(1,1)}_{\sigma\tau}$ consider the following colour-line diagram originating from the Feynman diagram in Figure 13(c) for a hard quark line i and anti-quark line j

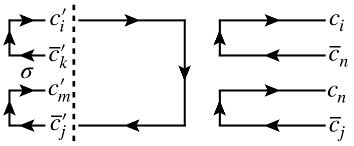

$$= \delta^{\alpha_{c'_m}}_{\beta_{\bar{c}'_k}} \delta^{\alpha_{c_i}}_{\beta_{\bar{c}_n}} \delta^{\alpha_{c_n}}_{\beta_{\bar{c}_j}} \to \delta_{\sigma\tau_{(a,b)(b,c)}\backslash n}\delta_{(a,b)(c_n,c_i)}\delta_{(b,c)(c_i,\sigma^{-1}(\bar{c}_j))} \ . \tag{5.10}$$

The first swap of the colour labels is performed such that the labels of the emitted gluon, c_n and $\bar{c}_n$, are being merged. This requires one to swap the colour labels c_n and c_i. After this swap however, the permutations σ and τ are still not equal, a second swap has to be carried out, namely between c_i and $c'_m = \sigma^{-1}(\bar{c}_j)$. These two consecutive swaps ensure that, after removing the colour labels of the emitted gluon, the permutations σ and τ match.
The $\Sigma''^{(1,1)}_{\sigma\tau}$ is built from terms for which two independent swaps have to be made. A contribution to this structure comes for example from the diagram with three hard lines (see Figure 13(d))

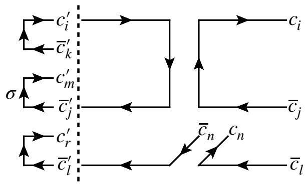

$$= \delta^{\alpha_{c'_m}}_{\beta_{\bar{c}'_k}} \delta^{\alpha_{c'_r}}_{\beta_{\bar{c}_n}} \delta^{\alpha_{c_n}}_{\beta_{\bar{c}_l}} \delta^{\alpha_{c_i}}_{\beta_{\bar{c}_j}} \to \delta_{\sigma\tau_{(a,b)(c,d)}\backslash n}\delta_{(a,b)(\sigma^{-1}(\bar{c}_l),c_n)}\delta_{(c,d)(c_i\sigma^{-1}(\bar{c}_j))} \ , \tag{5.11}$$

where in this case the first swap again merges the labels c_n and $\bar{c}_n$, a second swap, now of labels which are not involved in the first swap, is required to make the permutations σ and τ match.
The structure $\hat{\Sigma}^{(1,1)}_{\sigma\tau}$ describes terms with single swaps and a colour-connection in σ, which also does not occur in this combination at one-loop order. The diagram in Figure 13(a) provides an example for this structure for a quark line i and an anti-quark line j, where one swap is necessary to merge the labels of the emitted gluon and the colour-connection of the basis permutation σ leads to a factor of N

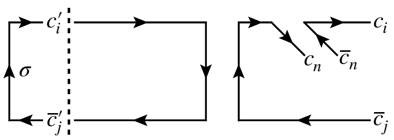

$$= N\delta^{\alpha_{c_n}}_{\beta_{\bar{c}_j}} \delta^{\alpha_{c_i}}_{\beta_{\bar{c}_n}} \to N\delta_{\sigma\tau_{(a,b)}\backslash n}\delta_{c_i\sigma^{-1}(\bar{c}_j)}\delta_{(a,b)(c_i,c_n)} \ . \tag{5.12}$$

All contributions including a single swap and a factor of $1/N$ without colour-connected external lines make up the $\tilde{\Sigma}^{(1,1)}_{\sigma\tau}$-coefficient and all those terms for which the emitted gluon is additionally colour-connected to itself are assigned to the coefficient $\hat{\tilde{\Sigma}}_{\sigma\tau}$ in equation (5.9). Take diagram (b) from Figure 13 as an example for both of these structures. The following colour-flow diagram contributes to $\tilde{\Sigma}^{(1,1)}_{\sigma\tau}$

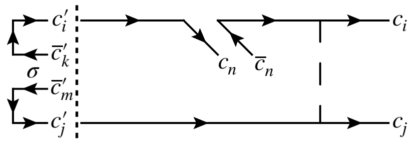

$$= \frac{1}{N}\delta^{\alpha_{c_n}}_{\beta_{\overline{c}_k'}}\delta^{\alpha_{c_j}}_{\beta_{\overline{c}_m'}}\delta^{\alpha_{c_i}}_{\beta_{\overline{c}_n}} \to \frac{1}{N}\delta_{\sigma\tau_{(a,b)}\backslash n}\delta_{(a,b)(c_i,c_n)}\ , \tag{5.13}$$

while

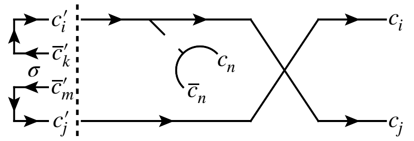

$$= \frac{1}{N}\delta^{\alpha_{c_n}}_{\beta_{\overline{c}_n}}\delta^{\alpha_{c_j}}_{\beta_{\overline{c}_k'}}\delta^{\alpha_{c_i}}_{\beta'_{\overline{c}_m}} \to \frac{1}{N}\delta_{c_n\tau^{-1}(\overline{c}_n)}\delta_{\sigma\tau_{(a,b)}\backslash n}\delta_{(a,b)(c_i,c_j)}\ , \tag{5.14}$$

gives a contribution to $\hat{\tilde{\Sigma}}^{(1,1)}_{\sigma\tau}$. At this point it should be remarked that both of these structures cannot occur for a hard gluon line i, this information is encoded by a factor of $(\lambda_i - \bar{\lambda}_i)$ when writing down the whole matrix element of the colour structure in the colour-flow basis (cf. Appendix E).

The contribution $\rho_{\sigma\tau}$, which are terms with a colour-connection between the external lines and without swaps, can be exemplified by a colour-flow diagram relating to the diagram (c) from Figure 13

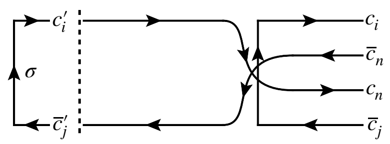

$$= \delta^{\alpha_{c_n}}_{\beta_{\overline{c}_n}}\delta^{\alpha_{c_i}}_{\beta_{\overline{c}_j}} \to \delta_{\sigma\tau\backslash n}\delta_{c_n\tau^{-1}(\overline{c}_n)}\delta_{c_i\sigma^{-1}(\overline{c}_j)}\ . \tag{5.15}$$

The ρ_τ-coefficient denotes terms with a $1/N^2$ suppression in the number of colours, thus the only source of contribution can be diagrams with two U(1)-gluons involved. For instance, consider the diagram (d) in Figure 13. In this case the colour-line diagram is drawn without the "colour-flow arrows" and labels in order to indicate that one finds this contribution for all combinations of quark and anti-quark lines (however not for gluons)

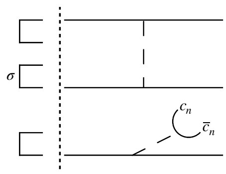

$$\to \frac{1}{N^2}\delta_{\sigma\tau\backslash n}\delta_{c_n\tau^{-1}(\overline{c}_n)}\ . \tag{5.16}$$

Turning to the kinematical factors, one can use the Feynman tree theorem to rewrite the loop-integration in k analogously to the one-loop case. The integrals of the distinct diagrams are kept separate, due to the fact that already the colour structures are treated separately. Additionally, the subtraction of the tree-level current is not taken into account at this point.

The distinct one-loop integrals of the one-loop/one-emission diagrams of the equations (5.2)-(5.7) are listed (neglecting any constant prefactors at this point) below in order to provide an overview of the relevant integrals

$$
\begin{aligned}
&\text{(i)} \quad \mu^{2\varepsilon} \int \frac{đ^d k}{i\pi^{d/2}} \frac{1}{[k^2+i0][(k+q)^2+i0][p_i\cdot(k+q)+i0][-p_j\cdot k+i0]} \\
&\text{(ii)} \quad \mu^{2\varepsilon} \int \frac{đ^d k}{i\pi^{d/2}} \frac{1}{[k^2+i0][(k+q)^2+i0][-p_i\cdot k+i0]} \\
&\text{(iii)} \quad \mu^{2\varepsilon} \int \frac{đ^d k}{i\pi^{d/2}} \frac{1}{[k^2+i0][(k+q)^2+i0]} \\
&\text{(iv)} \quad \mu^{2\varepsilon} \int \frac{đ^d k}{i\pi^{d/2}} \frac{1}{[k^2+i0][p_i\cdot(k+q)+i0][p_i\cdot k+i0][-p_j\cdot k+i0]} \\
&\text{(v)} \quad \mu^{2\varepsilon} \int \frac{đ^d k}{i\pi^{d/2}} \frac{1}{[k^2+i0][p_i\cdot(k+q)+i0][-p_j\cdot k+i0]} \\
&\text{(vi)} \quad \mu^{2\varepsilon} \int \frac{đ^d k}{i\pi^{d/2}} \frac{1}{[k^2+i0][p_i\cdot k+i0][-p_j\cdot k+i0]} \ .
\end{aligned}
\tag{5.17}
$$

For each of these one-loop integrals of equation (5.17)(i)-(v) the FTT is applied (the integral (vi) is the one-loop case which has been analysed in the previous section), and shifts in the loop momentum are performed to simplify the delta functions. Further, multiple cut-contributions where the delta functions/Heaviside functions are not compatible have already been set to zero. In appendix F a list of such cut-contributions evaluating to zero can be found. Attention has to be paid once again to cutting eikonal propagators, these have to be cut only if the pole is not already in the upper half-plane. The integral (iii) is scaleless, when applying the FTT to it and using the Sokhotski-Plemelj identity one finds that it vanishes exactly for $p_i^0 > 0$ and on-shell external lines.

Working through the FTT procedure for the integrals (i), (ii),(iv) and (v) results in the following:

$$
\begin{aligned}
\text{(i)} = -\mu^{2\varepsilon} \int \frac{đ^d k}{i\pi^{d/2}} \Bigg\{ & \frac{(2\pi i)\tilde{\delta}(k)}{[(k+q)^2+i0][p_i\cdot(k+q)+i0][-p_j\cdot k+i0]} \\
&+ \frac{(2\pi i)\tilde{\delta}(k)}{[(k-q)^2+i0][p_i\cdot k+i0][p_j\cdot(q-k)+i0]} \\
&+ \frac{(2\pi i)\delta(p_i\cdot k)}{[(k-q)^2+i0][k^2+i0][p_j\cdot(q-k)+i0]} \\
&+ \frac{(2\pi i)^2\tilde{\delta}(k)\tilde{\delta}(k+q)}{[p_i\cdot(k+q)+i0][-p_j\cdot k+i0]} + \frac{(2\pi i)^2\tilde{\delta}(k)\delta(p_i\cdot k)}{[(k-q)^2+i0][p_j\cdot(q-k)+i0]} \Bigg\} \ ,
\end{aligned}
\tag{5.18}
$$

$$
\begin{aligned}
\text{(ii)} = -\mu^{2\varepsilon} \int \frac{đ^d k}{i\pi^{d/2}} \Bigg\{ & \frac{(2\pi i)\tilde{\delta}(k)}{[(k+q)^2+i0][-p_i\cdot k+i0]} + \frac{(2\pi i)\tilde{\delta}(k)}{[(k-q)^2+i0][p_i\cdot(q-k)+i0]} \\
&+ \frac{(2\pi i)\tilde{\delta}(k)\tilde{\delta}(k+q)}{[-p_i\cdot k+i0]} \Bigg\} \ ,
\end{aligned}
\tag{5.19}
$$

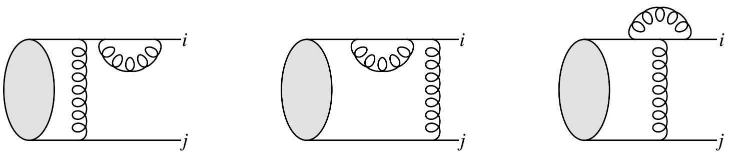

Figure 14: Two-loop Feynman diagrams involving two external lines, whose amplitudes do not contribute in the soft limit.

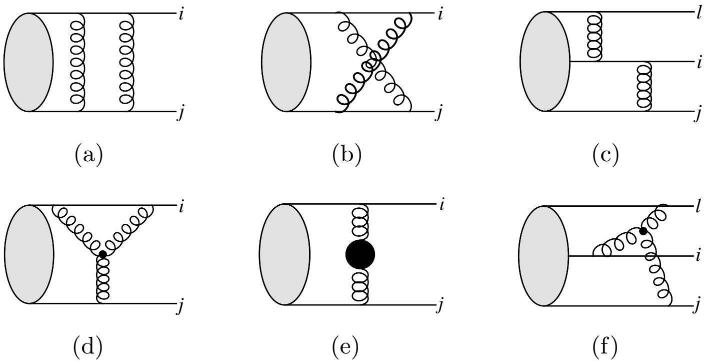

Figure 15: Two-loop diagrams for two and three hard, external lines, which contribute in the soft limit.

$$\begin{aligned}(\mathrm{iv}) = -\mu^{2\varepsilon} \int \frac{đ^d k}{i\pi^{d/2}} \Bigg\{ & \frac{(2\pi i)\tilde{\delta}(k)}{[p_i \cdot (k+q) + i0][p_i \cdot k + i0][-p_j \cdot k + i0]} \\ & + \frac{(2\pi i)\delta(p_i \cdot k)}{[k^2 + i0][p_i \cdot (k+q) + i0][-p_j \cdot k + i0]} + \frac{(2\pi i)^2 \tilde{\delta}(k)\delta(p_i \cdot k)}{[p_i \cdot (k+q) + i0][-p_j \cdot k]} \\ & + \frac{(2\pi i)\delta(p_i \cdot k)}{[(k-q)^2 + i0][p_i \cdot (k-q) + i0][p_j \cdot (q-k) + i0]} \Bigg\} , \end{aligned} \tag{5.20}$$

$$(\mathrm{v}) = -\mu^{2\varepsilon} \int \frac{đ^d k}{i\pi^{d/2}} \left\{ \frac{(2\pi i)\tilde{\delta}(k)}{[p_i \cdot (k+q) + i0][-p_j \cdot k + i0]} + \frac{(2\pi i)\delta(p_i \cdot k)}{[(k-q)^2 + i0][p_j \cdot (q-k) + i0]} \right\} . \tag{5.21}$$

5.1.2 Two-loop order

The same procedure which has been carried out at one-loop/one-emission level in the previous section can also be performed at two-loop level. In this case, however, there are no contributions in the soft limit in Feynman gauge from Feynman diagrams which involve only a single hard, external line. Additionally, the diagrams in Figure 14 vanish in the soft limit in Feynman gauge. The two-loop diagrams which lead to a non-vanishing contribution in the soft limit are depicted in Figure 15. The amplitudes corresponding to these diagrams are given in Feynman gauge in the following.

The amplitude for the soft gluon double exchange in Figure 15(a) can be written as

$$\begin{aligned}\mathcal{M}_{15(\mathrm{a})} =& - g^4(\mathbf{T}_i\cdot\mathbf{T}_j)(\mathbf{T}_i\cdot\mathbf{T}_j)\frac{\lambda^{2d}}{\lambda^8}\,\mu^{4\varepsilon}\int\frac{đ^d q}{i\pi^{d/2}}\frac{đ^d k}{i\pi^{d/2}} \\ & \frac{(p_i\cdot p_j)(p_i\cdot p_j)}{[p_i\cdot(k+q)+i0][-p_j\cdot(k+q)+i0][k^2+i0][q^2+i0][p_i\cdot q+i0][-p_j\cdot q+i0]} \\ =& (\mathbf{T}_i\cdot\mathbf{T}_j)(\mathbf{T}_i\cdot\mathbf{T}_j)\,\Omega^{(2)}_{ij}\ ,\end{aligned}\tag{5.22}$$

while the crossed double gluon exchange in Figure 15(b) leads to

$$\begin{aligned}\mathcal{M}_{15(\mathrm{b})} =& - g^4\mathbf{T}_i^a\mathbf{T}_i^b\mathbf{T}_j^b\mathbf{T}_j^a\frac{\lambda^{2d}}{\lambda^8}\,\mu^{4\varepsilon}\int\frac{đ^d q}{i\pi^{d/2}}\frac{đ^d k}{i\pi^{d/2}} \\ & \frac{(p_i\cdot p_j)(p_i\cdot p_j)}{[p_i\cdot(k+q)+i0][-p_j\cdot(k+q)+i0][k^2+i0][q^2+i0][p_i\cdot q+i0][-p_j\cdot k+i0]} \\ =& \mathbf{T}_i^a\mathbf{T}_i^b\mathbf{T}_j^b\mathbf{T}_j^a\,\tilde{\Omega}^{(2)}_{ij}\ .\end{aligned}\tag{5.23}$$

For the double exchange between three hard lines, illustrated in Figure 15(c) one obtains

$$\begin{aligned}\mathcal{M}_{15(\mathrm{c})} =& - g^4(\mathbf{T}_i\cdot\mathbf{T}_l)(\mathbf{T}_i\cdot\mathbf{T}_j)\frac{\lambda^{2d}}{\lambda^8}\,\mu^{4\varepsilon}\int\frac{đ^d q}{i\pi^{d/2}}\frac{đ^d k}{i\pi^{d/2}} \\ & \frac{(p_i\cdot p_j)(p_i\cdot p_l)}{[p_i\cdot(q-k)+i0][k^2+i0][q^2+i0][p_i\cdot q+i0][-p_j\cdot q+i0][p_l\cdot k+i0]} \\ =& (\mathbf{T}_i\cdot\mathbf{T}_l)(\mathbf{T}_i\cdot\mathbf{T}_j)\,\Omega^{(2)}_{ijl}\ .\end{aligned}\tag{5.24}$$

The diagram of the type of a vertex-correction in Figure 15(d) gives

$$\begin{aligned}\mathcal{M}_{15(\mathrm{d})} =& - g^4\frac{C_A}{2}(\mathbf{T}_i\cdot\mathbf{T}_j)\frac{\lambda^{2d+1}}{\lambda^9}\,\mu^{4\varepsilon}\int\frac{đ^d q}{i\pi^{d/2}}\frac{đ^d k}{i\pi^{d/2}} \\ & \frac{(p_i\cdot p_j)(p_i\cdot k-p_i\cdot q)}{[p_i\cdot(k+q)+i0][-p_j\cdot(k+q)+i0][k^2+i0][q^2+i0][(k+q)^2+i0][p_i\cdot k+i0]} \\ =& -g^4\frac{C_A}{2}(\mathbf{T}_i\cdot\mathbf{T}_j)\frac{\lambda^{2d+1}}{\lambda^9}\,\mu^{4\varepsilon}\int\frac{đ^d q}{i\pi^{d/2}}\frac{đ^d k}{i\pi^{d/2}}(p_i\cdot p_j) \\ & \left\{\frac{2}{[p_i\cdot(k+q)+i0][-p_j\cdot(k+q)+i0][q^2+i0][k^2+i0][(k+q)^2+i0]}\right. \\ & \left.-\frac{1}{[-p_j\cdot(k+q)+i0][k^2+i0][q^2+i0][(k+q)^2+i0][p_i\cdot k+i0]}\right\} \\ =& T_R(\mathbf{T}_i\cdot\mathbf{T}_j)\,\Omega^{(2)}_{ij,\mathrm{vertex-corr.}}\ ,\end{aligned}\tag{5.25}$$

and finally, suspending the analysis of the bubble-diagram until section 5.5, for the irreducible diagram with the triple-gluon vertex between three hard partons one gets

$$
\begin{aligned}
\mathcal{M}_{15(\mathrm{f})} =& g^4 i f_{abc} \mathbf{T}_i^a \mathbf{T}_j^b \mathbf{T}_l^c \, \frac{\lambda^{2d+1}}{\lambda^9} \, \mu^{4\varepsilon} \int \frac{đ^d q}{i\pi^{d/2}} \frac{đ^d k}{i\pi^{d/2}} \\
& \frac{p_i \cdot (2k+q)(p_j \cdot p_l) + p_l \cdot (q-k)(p_i \cdot p_j) - p_j \cdot (2q+k)(p_i \cdot p_l)}{[p_l \cdot (k+q) + i0][k^2 + i0][q^2 + i0][(k+q)^2 + i0][-p_i \cdot q + i0][-p_j \cdot k + i0]} \\
=& g^4 i f_{abc} \mathbf{T}_i^a \mathbf{T}_j^b \mathbf{T}_l^c \, \frac{\lambda^{2d+1}}{\lambda^9} \, \mu^{4\varepsilon} \int \frac{đ^d q}{i\pi^{d/2}} \frac{đ^d k}{i\pi^{d/2}} \\
& \frac{2\left[(p_j \cdot p_l)(p_i \cdot k) - (p_i \cdot p_j)(p_l \cdot k) - (p_i \cdot p_l)(p_j \cdot q)\right]}{[p_l \cdot (k+q) + i0][k^2 + i0][q^2 + i0][(k+q)^2 + i0][-p_i \cdot q + i0][-p_j \cdot k + i0]} \\
=& i f_{abc} \mathbf{T}_i^a \mathbf{T}_j^b \mathbf{T}_l^c \, \hat{\Omega}^{(2)}_{ijl} \ ,
\end{aligned}
\tag{5.26}
$$

where, in order to find the result after the second equal sign, the property of colour conservation is used.

With these results one thus finds the following for the soft two-loop correction written in a basis-independent way

$$
\begin{aligned}
\mathbf{V}^{(2)} =& \frac{1}{2} \sum_{i \neq j} \left[(\mathbf{T}_i \cdot \mathbf{T}_j)(\mathbf{T}_i \cdot \mathbf{T}_j) \, \Omega^{(2)}_{ij} + \mathbf{T}_i^a \mathbf{T}_i^b \mathbf{T}_j^b \mathbf{T}_j^a \, \tilde{\Omega}^{(2)}_{ij} \right] \\
& + \sum_{i \neq j \neq l} \left[(\mathbf{T}_i \cdot \mathbf{T}_j)(\mathbf{T}_i \cdot \mathbf{T}_l) \, \Omega^{(2)}_{ijl} + \frac{1}{2} f^{abc} \mathbf{T}_i^a \mathbf{T}_j^b \mathbf{T}_l^c \, \hat{\Omega}^{(2)}_{ijl} \right] \\
& + \sum_{i \neq j} T_R (\mathbf{T}_i \cdot \mathbf{T}_j) \left[\frac{1}{2} \Omega^{(2)}_{ij,\mathrm{self-en.}} + \Omega^{(2)}_{ij,\mathrm{vertex-corr.}} \right] \ .
\end{aligned}
\tag{5.27}
$$

Note that the same convention concerning the colour structure of the self-energy and the vertex-correction introduced for the one-loop/one-emission soft correction holds here. Furthermore, the unordered colour sums again imply that one needs to introduce factors of 1/2 for some of the diagrams. The colour sums are taken over distinct hard lines, the cases $i = j$ and $i = j = l$ are excluded.
Using the commutation relations for the colour charge operators one can rewrite equation (5.27) to obtain

$$
\begin{aligned}
\mathbf{V}^{(2)} =& \frac{1}{2} \sum_{i \neq j} (\mathbf{T}_i \cdot \mathbf{T}_j)(\mathbf{T}_i \cdot \mathbf{T}_j) \left[\Omega^{(2)}_{ij} + \tilde{\Omega}^{(2)}_{ij} \right] \\
& + \sum_{i \neq j \neq l} \left[(\mathbf{T}_i \cdot \mathbf{T}_j)(\mathbf{T}_i \cdot \mathbf{T}_l) \, \Omega^{(2)}_{ijl} + \frac{1}{2} f^{abc} \mathbf{T}_i^a \mathbf{T}_j^b \mathbf{T}_l^c \, \hat{\Omega}^{(2)}_{ijl} \right] \\
& + \sum_{i \neq j} T_R \, (\mathbf{T}_i \cdot \mathbf{T}_j) \left[\frac{1}{2} \Omega^{(2)}_{ij,\,\mathrm{self-en.}} + \Omega^{(2)}_{ij,\,\mathrm{vertex-corr.}} + \frac{1}{2} \tilde{\Omega}^{(2)}_{ij} \right] \ .
\end{aligned}
\tag{5.28}
$$

Taking care of the UV divergences contained in the loop integrals by performing renormalisation and subtracting the IR divergences by combining the virtual contributions with the emission, one finds the corresponding expression for the soft anomalous dimension at two-loop level and when translating to the colour-flow basis one obtains

$$\begin{aligned}(\alpha_s N)^2[\tau|\mathbf{\Gamma}^{(2)}|\sigma\rangle =& (\alpha_s N)^2\left[\left(\Gamma^{(2)}_\sigma + \frac{1}{N^2}\left(\rho_\sigma + \tilde{\rho}\right) + \frac{1}{N^4}\rho^{(2)}\right)\delta_{\sigma\tau}\right.\\ &\left. + \frac{1}{N}\left(\Sigma^{(2)}_{\sigma\tau} + \hat{\Sigma}^{(2)}_{\sigma\tau}\right) + \frac{1}{N^3}\tilde{\Sigma}^{(2)}_{\sigma\tau} + \frac{1}{N^2}\left(\Sigma'^{(2)}_{\sigma\tau} + \Sigma''^{(2)}_{\sigma\tau}\right)\right] \ .\end{aligned} \tag{5.29}$$

As in the one-loop case, there are two main parts, the diagonal structure for which the permutations σ and τ are equal and the off-diagonal elements, which contain the "swap"-terms. Most interestingly, at two-loop order there are, compared to one-loop order, additional diagonal terms $\tilde{\rho}$ and ρ_σ. These structures are of special importance since the sum over two-parton correlations, so-called "dipoles", has to be extended to include three-parton correlations as well. As an example of a three-parton correlation, which is part of the ρ_σ-contribution, consider the following colour-flow diagram corresponding to diagram (f) in Figure 15

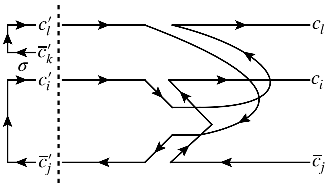

$$\rightarrow \lambda_i \bar{\lambda}_j \lambda_l \delta_{\sigma\tau}\delta_{c_i \sigma^{-1}(\bar{c}_j)} \ . \tag{5.30}$$

Due to the sum over dipoles and three-parton correlations, the ρ-terms can compensate the $1/N$ suppression. Therefore it might be desirable to make an expansion in the whole diagonal part of the soft anomalous dimension in order to account for the enhanced ρ-terms, instead of considering the large-N limit only.

Examples for each of the coefficients appearing in equation (5.29) are given in the following. Consider diagram (a) of Figure 15 for an illustration of the diagonal $\Gamma^{(2)}_\sigma$ contributions. For a colour-connection in the basis σ between the external lines one finds a colour flow with a N^2 enhancement,

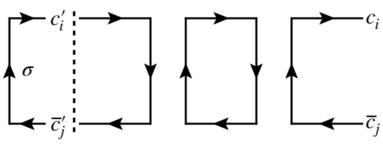

$$\rightarrow N^2 \delta_{\sigma\tau}\delta_{c_i \sigma^{-1}(\bar{c}_j)} \ . \tag{5.31}$$

If the basis permutation in the upper diagram is chosen such that the external lines i and j are not connected in colour, one instead finds a contribution to $\Sigma^{(2)}_{\sigma\tau}$, i.e. a single-swap term with a factor of N but without a colour-connection of the external lines.

The diagonal $\tilde{\rho}$ building block contains colour flows which are the same before and after the two-loop gluon exchanges. For instance, such a behaviour can be observed for the crossed gluon exchange in Figure 15(b), one finds a colour flow of

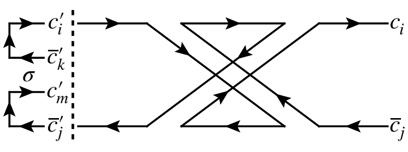

$$\rightarrow \delta_{\sigma\tau} \ . \tag{5.32}$$

The last of the diagonal structures in equation (5.29), $\rho^{(2)}$, contains all of the colour flows with double U(1)-gluon exchanges. For instance, the double exchange diagram with three external lines leads one to

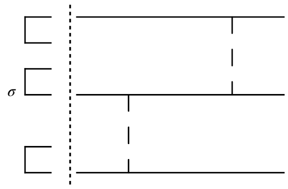

$$\to \frac{1}{N^4}\delta_{\sigma\tau} \;, \tag{5.33}$$

where this colour-line diagram can be drawn for all of the different combinations of quark and anti-quark lines.
The $\hat{\Sigma}^{(2)}_{\sigma\tau}$-coefficient describes colour flows with single swaps in the (anti-)colour labels and a colour-connection between the external lines. Such terms appear for all Feynman diagrams in Figure 15, for instance for diagram 15(f) one finds

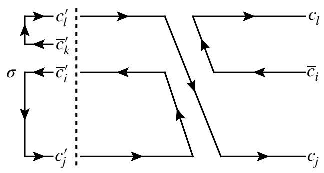

$$= N\delta^{\alpha_{c_j}}_{\beta_{\bar{c}'_k}}\delta^{\alpha_{c_l}}_{\beta_{\bar{c}_i}} \to N\delta_{c_j\sigma^{-1}(\bar{c}_i)}\delta_{\sigma\tau_{(a,b)}}\delta_{(a,b)(c_j,c_l)} \;. \tag{5.34}$$

In contrast to the "swap"-structure just described, the $\tilde{\Sigma}^{(2)}_{\sigma\tau}$-coefficient incorporates colour flows with single swaps but with a $1/N$ suppression in the number of colours. This suppression comes from terms with a single U(1)-gluon contribution such as

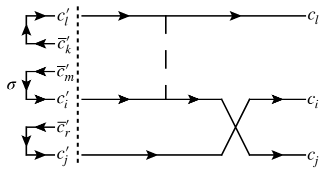

$$= \frac{1}{N}\delta^{\alpha_{c_l}}_{\beta_{\bar{c}'_k}}\delta^{\alpha_{c_i}}_{\beta_{\bar{c}'_r}}\delta^{\alpha_{c_j}}_{\beta_{\bar{c}'_m}} \to \frac{1}{N}\delta_{\sigma\tau_{(a,b)}}\delta_{(a,b)(c_i,c_j)} \;. \tag{5.35}$$

As already encountered in the one-loop/one-emission case, there are "double-swap" structures at two-loop order as well, where a colour index is swapped twice, for instance the double gluon exchange between three external lines gives a colour flow of

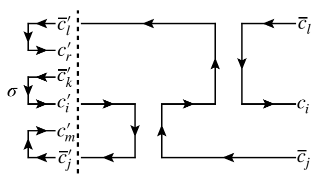

$$= \delta^{\alpha_{c'_m}}_{\beta_{\bar{c}'_k}}\delta^{\alpha_{c'_r}}_{\beta_{\bar{c}_j}}\delta^{\alpha_{c_i}}_{\beta_{\bar{c}_l}} \to \delta_{\sigma\tau_{(a,b)(b,c)}}\delta_{(a,b)(c_i,\sigma^{-1}(\bar{c}_j))}\delta_{(b,c)(\sigma^{-1}(\bar{c}_j),\sigma^{-1}(\bar{c}_l))} \;, \tag{5.36}$$

and thus it contributes to the coefficient $\Sigma'^{(2)}_{\sigma\tau}$. Finally, one again finds for external gluon lines colour flows for which two consecutive swaps of different (anti-)colour labels have to be performed in order to get matching permutations σ and τ. A contribution to the structure $\Sigma''^{(2)}_{\sigma\tau}$ can be

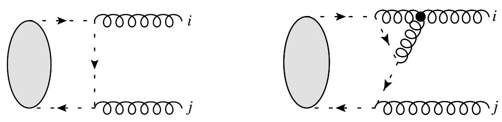

(a) (b)

Figure 16: Example of diagrams with hard ghost lines. Their amplitudes give subleading contributions in the soft limit.

found from diagram (a) of Figure 15 for two gluon lines i and j

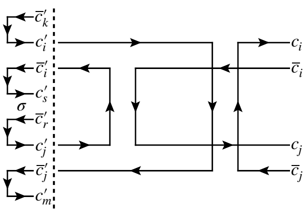

$$= \delta^{\alpha_{c'_s}}_{\beta_{\bar{c}'_k}} \delta^{\alpha_{c'_m}}_{\beta_{\bar{c}'_r}} \delta^{\alpha_{c_j}}_{\beta_{\bar{c}_i}} \delta^{\alpha_{c_i}}_{\beta_{\bar{c}_j}} \to \delta_{\sigma\tau_{(a,b)(c,d)}} \delta_{(a,b)(c_i,\sigma^{-1}(\bar{c}_j))} \delta_{(c,d)(c_j,\sigma^{-1}(\bar{c}_i))} \,. \tag{5.37}$$

The explicit results for all of the relevant two-loop matrix elements of the colour structures in the colour-flow basis can be found in appendix E.2.
Notice that the only relevant contribution which includes ghosts comes from the bubble-diagram (see Figure 15(f)). The diagrams with hard ghost lines (see Figure 16) are subleading in the soft limit. For instance, diagram (b) of Figure 16 has a loop integrand $I_{16(\mathrm{b})}$ of the form

$$\begin{aligned} I_{16(\mathrm{b})} = \int \frac{\text{đ}^d q}{i\pi^{d/2}} \int \frac{\text{đ}^d k}{i\pi^{d/2}} & \frac{[(2p_i + q - k)^\tau g^{\mu\nu} + (k - p_i - q)^\mu g^{\nu\tau} + (2k - 2q - p_i)^\nu g^{\mu\tau}]}{[(p_i + q + k)^2 + i0][(q-k)^2 + i0]} \\ & \cdot \frac{k_\mu q_\tau (q - p_j)^\rho \varepsilon^*_\nu(p_i) \varepsilon^*_\rho(p_j)}{[k^2 + i0][(p_i + q)^2 + i0][(p_j - q)^2 + i0][q^2 + i0]} \,, \end{aligned} \tag{5.38}$$

and when taking $q \to \lambda q$ as well as $k \to \lambda k$ and consecutively $\lambda \to 0$ one finds that the amplitude is of order λ, thus it gives a subleading contribution.

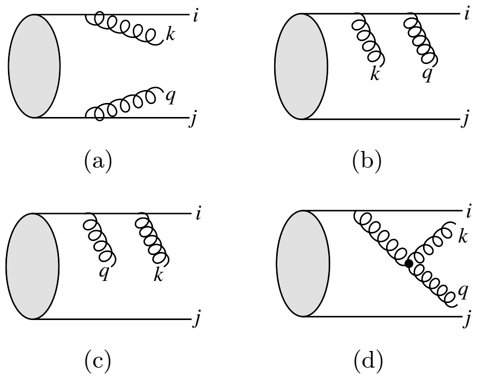

Figure 17: Double soft gluon emission diagrams with gluon momenta k and q.

5.2 Double emission diagrams and the two-gluon current

With the aim of cancelling the infrared divergences of the radiative cuts of the squared two-loop amplitudes one has to combine them with the double emission diagrams. The latter are reviewed in this section and the soft current for double emission is derived.

In order to find an expression for the double soft gluon current one has to combine the following amplitudes, their corresponding Feynman diagrams are depicted in Figure 17

$$
\begin{aligned}
\mathcal{M}_{17(\mathrm{a})} &= g^2 \mathbf{T}_i^c \mathbf{T}_j^b \, \frac{p_i^\mu p_j^\nu}{(p_i \cdot k)(p_j \cdot q)} \ , \\
\mathcal{M}_{17(\mathrm{b})} &= g^2 \mathbf{T}_i^b \mathbf{T}_i^c \, \frac{p_i^\mu p_i^\nu}{(p_i \cdot q)(p_i \cdot (q+k))} \ , \\
\mathcal{M}_{17(\mathrm{c})} &= g^2 \mathbf{T}_i^c \mathbf{T}_i^b \frac{p_i^\mu p_i^\nu}{(p_i \cdot k)(p_i \cdot (q+k))} \ , \\
\mathcal{M}_{17(\mathrm{d})} &= g^2 (-i f^{abc}) \mathbf{T}_i^a \frac{2k^\nu p_i^\mu + p_i \cdot (q-k) g^{\mu\nu} - 2q^\mu p_i^\nu}{2(k \cdot q)(p_i \cdot (q+k))} \ ,
\end{aligned}
\tag{5.39}
$$

where, for $\mathcal{M}_{17(\mathrm{d})}$ the unphysical terms have been neglected, since $k \cdot \varepsilon^*(k) = 0$ and $q \cdot \varepsilon^*(q) = 0$. Combining the amplitudes with the different orderings in the soft emission from line i, i.e. $\mathcal{M}_{17(\mathrm{b})}$ and $\mathcal{M}_{17(\mathrm{c})}$ one finds

$$
\begin{aligned}
\mathcal{M}_{17(\mathrm{b})+(\mathrm{c})} &= \frac{p_i^\mu p_i^\nu}{p_i \cdot (q+k)} \left[\frac{\mathbf{T}_i^c \mathbf{T}_i^b}{p_i \cdot k} + \frac{\mathbf{T}_i^b \mathbf{T}_i^c}{p_i \cdot q} \right] \\
&= \frac{1}{2} \frac{p_i^\mu p_i^\nu}{(p_i \cdot q)(p_i \cdot k)} \left(\mathbf{T}_i^c \mathbf{T}_i^b + \mathbf{T}_i^b \mathbf{T}_i^c \right) + \frac{1}{2} (i f^{abc}) \mathbf{T}_i^a \frac{p_i^\mu p_i^\nu}{p_i \cdot (q+k)} \left(\frac{1}{p_i \cdot q} - \frac{1}{p_i \cdot k} \right) \ .
\end{aligned}
\tag{5.40}
$$

Of course, by swapping the indices i and j one can include the emissions from line j. Using equations (5.39) and (5.40) one finds the soft two-gluon current [10]

$$\begin{aligned}\mathbf{J}^{\mu\nu}_{bc}(q,k) &= \frac{1}{2}\{\mathbf{J}^{\mu}_{b}(q), \mathbf{J}^{\nu}_{c}(k)\} \\ &+ i f_{abc} \sum_{l} \mathbf{T}^{a}_{l} \left\{ \frac{p_i^\nu q^\mu - p_i^\mu k^\nu}{(k\cdot q)(p_i\cdot(q+k))} - \frac{p_i\cdot(q-k)}{2(p_i\cdot(q+k))}\left[\frac{p_i^\mu p_i^\nu}{(p_i\cdot q)(p_i\cdot k)} + \frac{g^{\mu\nu}}{k\cdot q}\right]\right\} ,\end{aligned} \tag{5.41}$$

where the anti-commutator of the soft gluon current $\mathbf{J}^{\mu}_{b}$ (cf. equation (4.31)) contains the first term in the second line in equation (5.40), as well as $\mathcal{M}_{17(\mathrm{a})}$. The sum over l includes all of the external lines of the amplitude. Hence, for the diagrams depicted in Figure 17, it involves two of them and thus stands for $(\sum_{l=i,j} ...)$, but one may as well generalise to a number of n external lines, such that $(\sum_{l=1}^{n} ...)$.
In Feynman gauge the square of the two-loop current leads to [10]

$$(\mathbf{J}^{ab}_{\mu\tau}(k,q))^\dagger(-g^{\mu\nu})(-g^{\tau\lambda})\mathbf{J}^{ab}_{\nu\lambda}(k,q) = \frac{1}{2}\left\{\mathbf{J}^2(q), \mathbf{J}^2(k)\right\} + C_A \sum_{i,j} (\mathbf{T}_i\cdot\mathbf{T}_j) S_{ij}(q,k) , \tag{5.42}$$

where the function S_{ij} is defined as [10]

$$\begin{aligned}S_{ij}(k,q) = &\frac{(p_i\cdot p_j)^2}{2(p_i\cdot q)(p_i\cdot k)(p_j\cdot q)(p_j\cdot k)}\left[2 - \frac{(p_i\cdot q)(p_j\cdot k)+(p_i\cdot k)(p_j\cdot q)}{p_i\cdot(k+q)\,p_j\cdot(k+q)}\right] \\ &- \frac{(1-\varepsilon)}{(k\cdot q)^2}\frac{(p_i\cdot q)(p_j\cdot k)+(p_i\cdot k)(p_j\cdot q)}{p_i\cdot(k+q)\,p_j\cdot(k+q)} \\ &- \frac{p_i\cdot p_j}{2(k\cdot q)}\left[\frac{2}{(p_i\cdot q)(p_j\cdot k)} + \frac{2}{(p_i\cdot k)(p_j\cdot q)}\right. \\ &\left. - \frac{1}{p_i\cdot(k+q)\,p_j\cdot(k+q)}\left(4 + \frac{((p_i\cdot q)(p_j\cdot k)+(p_i\cdot k)(p_j\cdot q))^2}{(p_i\cdot q)(p_i\cdot k)(p_j\cdot q)(p_j\cdot k)}\right)\right] .\end{aligned} \tag{5.43}$$

For the detailed calculation of the two-loop current squared consult appendix D.

5.3 Handling the kinematic part: The Feynman tree theorem at two-loop level

In this section the Feynman tree theorem for diagrams of two-loop order is described and applied to the relevant two-loop integrals described in section 5.1.2. In this way a set of cut-contributions for the two-loop integrals is obtained which can be attributed to the different two-loop Feynman diagrams.

When applying the FTT at two-loop level one can choose one of the loop momenta, say k, and work through the cutting procedure in the usual manner as described for the one-loop case in section 3.3. As a next step one has to shift the loop momenta such that the cuts are all expressed in terms of the cut momentum k only. After this shift it is possible to further apply the FTT to the other loop momentum q. Each of the cut-diagrams in k are then subject to further (i.e. single and multiple) cuts in q. However, if after the first application of the FTT a shift in the loop momentum can not achieve that only one loop-momentum is constrained or equivalently, that the cuts are only expressed in terms of one loop-momentum, then the cutting procedure has to be terminated. In such a case one has to be careful with signs: Using the FTT introduces a global negative sign, therefore diagrams which are in fact cut only in one momentum and cannot be shifted further receive only one negative sign, while the other contributions, for which the FTT is used for both loop momenta, have an overall positive sign.

In order to illustrate this workflow, the FTT cutting procedure is diagrammatically illustrated in Figure 18 for the example of the virtual double exchange of soft gluons with momenta k and q. On the top of the figure the Feynman diagram is drawn with the momenta of the propagators in the soft approximation explicitly written. As a first step the momentum k is cut according to the one-loop FTT procedure. This introduces three contributions, two single cuts and one double cut. The second step is the shift of the loop momentum in order to express the delta function only in terms of k. One observes that for the double cut such a shift is not possible. For this diagram the cutting procedure ends at this point, the two delta functions can be used to solve the k^0 and the q^0 integration.
For the second single cut contribution a shift is performed, $k \to (k-q)$, which ensures that the delta function pertaining to the cut in k is only dependent on k. The first single cut does not require any shifts. The third step consists of cutting the first two diagrams in q. In this way one obtains double, triple and quartic cuts. Now, it has to be checked if the cuts are actually kinematically possible. In this case two of the cut-diagrams vanish due to being overconstrained by the delta functions/Heaviside functions of the cuts. Furthermore, when using light-cone coordinates for both k and q it turns out that three additional cut-diagrams vanish due to same reason as encountered in the one-loop case for the double-cut contribution (cf. equation (4.24)). The cut-integrals which correspond to such cases are not written in the results which are listed below. In appendix F a list of the kinematically impossible/vanishing cuts of each of the two-loop diagrams is given.

The two-loop integrals pertaining to the diagrams with two hard lines (cf. Figure 15(a), (b)

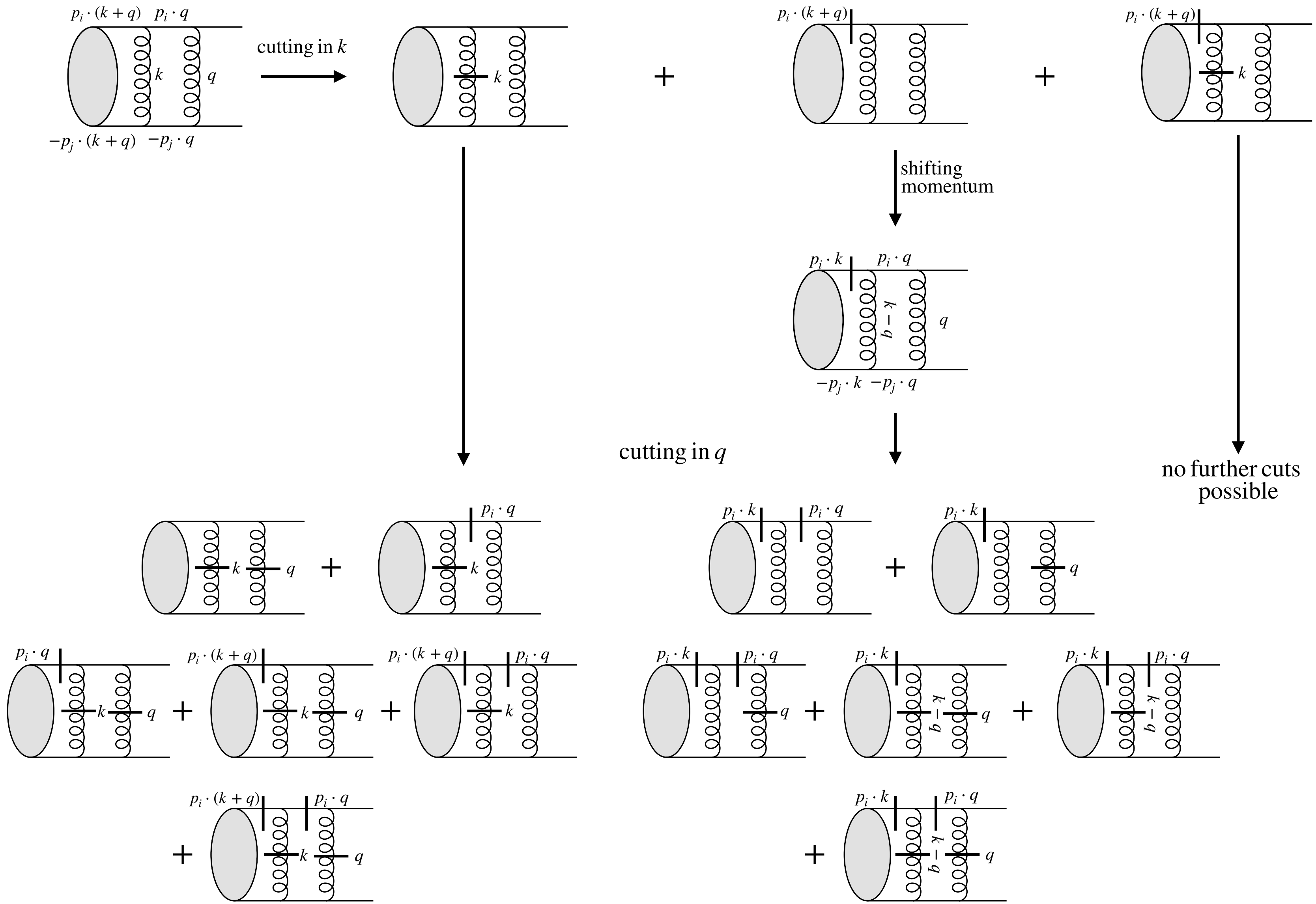

Figure 18: Example of the cutting procedure according to the Feynman tree theorem at two-loop level.

and (d)) are the following

$$
\begin{aligned}
&\text{(i) } \mu^{4\varepsilon}\int \frac{đ^d k}{i\pi^{d/2}}\frac{đ^d q}{i\pi^{d/2}}\frac{1}{[p_i\cdot(k+q)+i0][-p_j\cdot(k+q)+i0][k^2+i0][q^2+i0][p_i\cdot q+i0][-p_j\cdot q+i0]}\\
&\text{(ii) } \mu^{4\varepsilon}\int \frac{đ^d k}{i\pi^{d/2}}\frac{đ^d q}{i\pi^{d/2}}\frac{1}{[p_i\cdot(k+q)+i0][-p_j\cdot(k+q)+i0][k^2+i0][q^2+i0][p_i\cdot q+i0][-p_j\cdot k+i0]}\\
&\text{(iii) } \mu^{4\varepsilon}\int \frac{đ^d k}{i\pi^{d/2}}\frac{đ^d q}{i\pi^{d/2}}\frac{1}{[p_i\cdot k+i0][-p_j\cdot k+i0][k^2+i0][q^2+i0][(q-k)^2+i0]}\\
&\text{(iv) } \mu^{4\varepsilon}\int \frac{đ^d k}{i\pi^{d/2}}\frac{đ^d q}{i\pi^{d/2}}\frac{1}{[p_i\cdot k+i0][-p_j\cdot(k+q)+i0][k^2+i0][q^2+i0][(k+q)^2+i0]}\;.
\end{aligned}
\tag{5.44}
$$

Applying the FTT to the two-loop integrals (i)-(iv) of equation (5.44) and neglecting cuts which are kinematically impossible, one finds

$$
\begin{aligned}
\text{(i)} = \mu^{4\varepsilon}\int \frac{đ^d k}{i\pi^{d/2}}\frac{đ^d q}{i\pi^{d/2}}\Bigg\{&\frac{(2\pi i)^2\tilde{\delta}(q)\tilde{\delta}(k)}{[p_i\cdot(k+q)+i0][-p_j\cdot(k+q)+i0][p_i\cdot q+i0][-p_j\cdot q+i0]}\\
&+\frac{(2\pi i)^2\tilde{\delta}(k)\delta(p_i\cdot q)}{[p_i\cdot(k+q)+i0][-p_j\cdot(k+q)+i0][q^2+i0][-p_j\cdot q+i0]}\\
&+\frac{(2\pi i)^2\delta(p_i\cdot k)\delta(p_i\cdot q)}{[-p_j\cdot k+i0][q^2+i0][(k-q)^2+i0][-p_j\cdot q+i0]}\\
&+\frac{(2\pi i)^2\tilde{\delta}(q)\delta(p_i\cdot k)}{[p_i\cdot q+i0][-p_j\cdot k+i0][(k-q)^2+i0][-p_j\cdot q+i0]}\\
&-\frac{(2\pi i)^2\tilde{\delta}(k)\delta(p_i\cdot q)}{[p_i\cdot(q-k)+i0][-p_j\cdot q+i0][(q-k)^2+i0][-p_j\cdot(q-k)+i0]}\\
&+\frac{(2\pi i)^3\tilde{\delta}(q)\tilde{\delta}(k-q)\delta(p_i\cdot k)}{[p_i\cdot q+i0][-p_j\cdot k+i0][-p_j\cdot q+i0]}\\
&+\frac{(2\pi i)^3\tilde{\delta}(k-q)\delta(p_i\cdot k)\delta(p_i\cdot q)}{[q^2+i0][-p_j\cdot k+i0][-p_j\cdot q+i0]}\Bigg\}\;,
\end{aligned}
\tag{5.45}
$$

$$
\begin{aligned}
\text{(ii)} = \mu^{4\varepsilon} \int \frac{đ^d k}{i\pi^{d/2}} \frac{đ^d q}{i\pi^{d/2}} \Bigg\{ & \frac{(2\pi i)^2 \tilde{\delta}(k) \tilde{\delta}(q)}{[p_i \cdot (k+q) + i0][p_i \cdot q + i0][-p_j \cdot (k+q) + i0][-p_j \cdot k + i0]} \\
& + \frac{(2\pi i)^2 \tilde{\delta}(k) \delta(p_i \cdot q)}{[p_i \cdot (k+q) + i0][q^2 + i0][-p_j \cdot (k+q) + i0][-p_j \cdot k + i0]} \\
& + \frac{(2\pi i)^2\, \delta(p_i \cdot k) \delta(p_i \cdot q)}{[(k-q)^2 + i0][q^2 + i0][p_j \cdot (q-k) + i0][-p_j \cdot k + i0]} \\
& + \frac{(2\pi i)^2 \tilde{\delta}(q) \delta(p_i \cdot k)}{[p_i \cdot q + i0][(k-q)^2 + i0][p_j \cdot (q-k) + i0][-p_j \cdot k + i0]} \\
& + \frac{(2\pi i)^2\, \delta(p_i \cdot k) \delta(p_j \cdot q)}{[p_i \cdot (k+q) + i0][(k+q)^2 + i0][q^2 + i0][-p_j \cdot k + i0]} \\
& - \frac{(2\pi i)^2 \tilde{\delta}(k) \delta(p_i \cdot q)}{[p_i \cdot (q-k) + i0][(q-k)^2 + i0][-p_j \cdot q + i0][-p_j \cdot k + i0]} \\
& + \frac{(2\pi i)^3\, \delta(p_i \cdot k) \delta(p_i \cdot q) \delta(p_j \cdot (q-k))}{[(k-q)^2 + i0][q^2 + i0][-p_j \cdot k + i0]} \\
& + \frac{(2\pi i)^3\, \tilde{\delta}(q) \delta(p_i \cdot k) \delta(p_j \cdot (q-k))}{[p_i \cdot q + i0][(k-q)^2 + i0][-p_j \cdot k + i0]} \\
& + \frac{(2\pi i)^3 \tilde{\delta}(k-q) \delta(p_i \cdot k) \delta(p_i \cdot q)}{[q^2 + i0][p_j \cdot (q-k) + i0][-p_j \cdot k + i0]} \\
& + \frac{(2\pi i)^3 \tilde{\delta}(k-q) \delta(p_j \cdot (q-k)) \delta(p_i \cdot k)}{[p_i \cdot q + i0][q^2 + i0][-p_j \cdot k + i0]} \\
& + \frac{(2\pi i)^3 \tilde{\delta}(q) \tilde{\delta}(k-q) \delta(p_i \cdot k)}{[p_i \cdot q + i0][p_j \cdot (q-k) + i0][-p_j \cdot k + i0]} \\
& + \frac{(2\pi i)^4 \tilde{\delta}(k-q) \delta(p_i \cdot k) \delta(p_i \cdot q) \delta(p_j \cdot (q-k))}{[q^2 + i0][-p_j \cdot k + i0]} \Bigg\} ,
\end{aligned} \tag{5.46}
$$

$$
\begin{aligned}
\text{(iii)} = \mu^{4\varepsilon} \int \frac{đ^d k}{i\pi^{d/2}} \frac{đ^d q}{i\pi^{d/2}} \Bigg\{ & \frac{(2\pi i)^2 \tilde{\delta}(k) \tilde{\delta}(q)}{[p_i \cdot k + i0][(q-k)^2 + i0][-p_j \cdot k + i0]} \\
& + \frac{(2\pi i)^2 \tilde{\delta}(q) \delta(p_i \cdot k)}{[(q-k)^2 + i0][k^2 + i0][-p_j \cdot k + i0]} \\
& + \frac{(2\pi i)^2 \tilde{\delta}(q) \tilde{\delta}(k)}{[p_i \cdot k + i0][(k+q)^2 + i0][-p_j \cdot k + i0]} \\
& + \frac{(2\pi i)^2 \tilde{\delta}(q) \delta(p_i \cdot k)}{[(k+q)^2 + i0][k^2 + i0][-p_j \cdot k + i0]} \\
& - \frac{(2\pi i)^2 \tilde{\delta}(k) \tilde{\delta}(q)}{[p_i \cdot (q-k) + i0][(q-k)^2 + i0][-p_j \cdot (q-k) + i0]} \\
& + \frac{(2\pi i)^3 \tilde{\delta}(q) \tilde{\delta}(k) \tilde{\delta}(q-k)}{[p_i \cdot k + i0][-p_j \cdot k + i0]} \\
& + \frac{(2\pi i)^3 \tilde{\delta}(q) \tilde{\delta}(q-k) \delta(p_i \cdot k)}{[k^2 + i0][-p_j \cdot k + i0]} + \frac{(2\pi i)^3 \tilde{\delta}(q) \tilde{\delta}(k) \tilde{\delta}(k+q)}{[p_i \cdot k + i0][-p_j \cdot k + i0]} \\
& + \frac{(2\pi i)^3 \tilde{\delta}(q) \tilde{\delta}(k+q) \delta(p_i \cdot k)}{[k^2 + i0][-p_j \cdot k + i0]} \Bigg\} ,
\end{aligned} \tag{5.47}
$$

$$
\begin{aligned}
\text{(iv)} = \mu^{4\varepsilon} \int \frac{đ^d k}{i\pi^{d/2}} \frac{đ^d q}{i\pi^{d/2}} \Bigg\{ & \frac{(2\pi i)^2 \tilde{\delta}(k) \tilde{\delta}(q)}{[p_i \cdot k + i0][(k+q)^2 + i0][-p_j \cdot (k+q) + i0]} \\
& + \frac{(2\pi i)^2 \tilde{\delta}(q) \delta(p_i \cdot k)}{[k^2 + i0][(k+q)^2 + i0][-p_j \cdot (k+q) + i0]} \\
& + \frac{(2\pi i)^2 \tilde{\delta}(k) \tilde{\delta}(q)}{[p_i \cdot k + i0][(q-k)^2 + i0][-p_j \cdot q + i0]} \\
& + \frac{(2\pi i)^2 \tilde{\delta}(q) \delta(p_i \cdot k)}{[k^2 + i0][(q-k)^2 + i0][-p_j \cdot q + i0]} \\
& - \frac{(2\pi i)^2 \tilde{\delta}(q) \tilde{\delta}(k)}{[p_i \cdot (k-q) + i0][(k-q)^2 + i0][-p_j \cdot k + i0]} \\
& + \frac{(2\pi i)^3 \tilde{\delta}(k) \tilde{\delta}(q) \tilde{\delta}(k+q)}{[p_i \cdot k + i0][-p_j \cdot (k+q) + i0]} \\
& + \frac{(2\pi i)^3 \tilde{\delta}(q) \tilde{\delta}(k+q) \delta(p_i \cdot k)}{[k^2 + i0][-p_j \cdot (k+q) + i0]} + \frac{(2\pi i)^3 \tilde{\delta}(q) \tilde{\delta}(k) \tilde{\delta}(q-k)}{[p_i \cdot k + i0][-p_j \cdot q + i0]} \\
& + \frac{(2\pi i)^3 \tilde{\delta}(q-k) \tilde{\delta}(q) \delta(p_i \cdot k)}{[k^2 + i0][-p_j \cdot q + i0]} \Bigg\} \, .
\end{aligned} \tag{5.48}
$$

Writing down the cuts of the loop integrals in this way allows one to quickly identify the real radiative cut-contributions which can be compared to the contributions of the squared real emission diagrams. Furthermore, the eikonal cuts which lead to imaginary Coulomb-gluon contributions can be identified.

In section 5.4 the cancellation of IR divergences between the real emission diagrams and the radiative cuts with matching colour structures is shown.

For the remaining two-loop diagrams (cf. Figure 15(c) and (f)) with three hard parton lines one has to analyse the following loop integrals

$$
\begin{aligned}
\text{(v)} &= \mu^{4\varepsilon} \int \frac{đ^d k}{i\pi^{d/2}} \frac{đ^d q}{i\pi^{d/2}} \frac{1}{[p_i \cdot (k+q) + i0][p_i \cdot q + i0][k^2 + i0][q^2 + i0][-p_j \cdot k + i0][-p_l \cdot q + i0]} \\
\text{(vi)} &= \mu^{4\varepsilon} \int \frac{đ^d k}{i\pi^{d/2}} \frac{đ^d q}{i\pi^{d/2}} \frac{p_i \cdot k}{[-p_i \cdot q + i0][k^2 + i0][q^2 + i0][(k+q)^2 + i0][-p_j \cdot k + i0][p_l \cdot (k+q) + i0]} \\
\text{(vii)} &= \mu^{4\varepsilon} \int \frac{đ^d k}{i\pi^{d/2}} \frac{đ^d q}{i\pi^{d/2}} \frac{p_l \cdot k}{[-p_i \cdot q + i0][k^2 + i0][q^2 + i0][(k+q)^2 + i0][-p_j \cdot k + i0][p_l \cdot (k+q) + i0]} \\
\text{(viii)} &= \mu^{4\varepsilon} \int \frac{đ^d k}{i\pi^{d/2}} \frac{đ^d q}{i\pi^{d/2}} \frac{p_j \cdot q}{[-p_i \cdot q + i0][k^2 + i0][q^2 + i0][(k+q)^2 + i0][-p_j \cdot k + i0][p_l \cdot (k+q) + i0]}
\end{aligned} \tag{5.49}
$$

where number (v) corresponds to the loop integrand of the double soft gluon exchange in Figure 15(c) and the others to the irreducible triple gluon vertex diagram of Figure 15(f). It is noteworthy that the denominator structure for integrals (vi)-(viii) is identical, however, the numerators, which depend on a loop momentum, differ. Hence, when applying the FTT to the propagator structure, which includes shifts of the loop momenta, one has to ensure to shift the loop momentum of the numerator as well.

Applying the FTT at two-loop level leads to

$$
\begin{aligned}
(\mathrm{v}) = \mu^{4\varepsilon} \int \frac{\text{đ}^d k}{i\pi^{d/2}} \frac{\text{đ}^d q}{i\pi^{d/2}} \Bigg\{ & \frac{(2\pi i)^2 \tilde{\delta}(k) \tilde{\delta}(q)}{[p_i \cdot (k+q) + i0][p_i \cdot q + i0][-p_j \cdot k + i0][-p_l \cdot q + i0]} \\
& + \frac{(2\pi i)^2 \tilde{\delta}(k) \delta(p_i \cdot q)}{[p_i \cdot (k+q) + i0][q^2 + i0][-p_j \cdot k + i0][-p_l \cdot q + i0]} \\
& + \frac{(2\pi i)^2 \tilde{\delta}(q) \delta(p_i \cdot k)}{[p_i \cdot q + i0][(k-q)^2 + i0][p_j \cdot (q-k) + i0][-p_l \cdot q + i0]} \\
& + \frac{(2\pi i)^2 \delta(p_i \cdot k) \delta(p_j \cdot q)}{[p_i \cdot (k+q) + i0][(k+q)^2 + i0][p_j \cdot q + i0][-p_l \cdot (k+q) + i0]} \\
& + \frac{(2\pi i)^2 \delta(p_i \cdot k) \delta(p_i \cdot q)}{[q^2 + i0][(k-q)^2 + i0][p_j \cdot (q-k) + i0][-p_l \cdot q + i0]} \\
& - \frac{(2\pi i)^2 \delta(\tilde{k}) \delta(p_i \cdot q)}{[p_i \cdot (q-k) + i0][(q-k)^2 + i0][-p_j \cdot k + i0][p_l \cdot (k-q) + i0]} \\
& + \frac{(2\pi i)^3 \tilde{\delta}(k-q) \delta(p_i \cdot k) \delta(p_i \cdot q)}{[q^2 + i0][p_j \cdot (q-k) + i0][-p_l \cdot q + i0]} \\
& + \frac{(2\pi i)^3 \tilde{\delta}(k-q) \delta(p_i \cdot k) \delta(p_j \cdot (q-k))}{[p_i \cdot q + i0][q^2 + i0][-p_l \cdot q + i0]} \\
& + \frac{(2\pi i)^3 \tilde{\delta}(q) \delta(p_i \cdot k) \delta(p_j \cdot (q-k))}{[p_i \cdot q + i0][(k-q)^2 + i0][-p_l \cdot q + i0]} \\
& + \frac{(2\pi i)^3 \delta(p_i \cdot k) \delta(p_i \cdot q) \delta(p_j \cdot (q-k))}{[q^2 + i0][(k-q)^2 + i0][-p_l \cdot q + i0]} \\
& + \frac{(2\pi i)^3 \tilde{\delta}(q) \tilde{\delta}(k-q) \delta(p_i \cdot k)}{[p_i \cdot q + i0][p_j \cdot (q-k) + i0][-p_l \cdot q + i0]} \\
& + \frac{(2\pi i)^4 \tilde{\delta}(k-q) \delta(p_i \cdot q) \delta(p_i \cdot k) \delta(p_j \cdot (q-k))}{[q^2 + i0][-p_l \cdot q + i0]} \Bigg\} \, ,
\end{aligned}
\tag{5.50}
$$

$$
\begin{aligned}
\text{(vi)} = \mu^{4\varepsilon} \int \frac{\text{đ}^d k}{i\pi^{d/2}} \frac{\text{đ}^d q}{i\pi^{d/2}} \Bigg\{ & -\frac{(2\pi i)^2 (p_i \cdot k) \tilde{\delta}(q) \delta(p_l \cdot k)}{[-p_i \cdot q + i0][k^2 + i0][(k-q)^2 + i0][p_j \cdot (q-k) + i0]} \\
& - \frac{(2\pi i)^2 (p_i \cdot k) \tilde{\delta}(k) \tilde{\delta}(q)}{[-p_i \cdot q + i0][(k-q)^2 + i0][p_j \cdot (q-k) + i0][p_l \cdot k + i0]} \\
& + \frac{(2\pi i)^2 (p_i \cdot k) \tilde{\delta}(q) \tilde{\delta}(k)}{[-p_i \cdot q + i0][(k+q)^2 + i0][-p_j \cdot k + i0][p_l \cdot (k+q) + i0]} \\
& + \frac{(2\pi i)^2 (p_i \cdot k) \tilde{\delta}(q) \tilde{\delta}(k)}{[p_i \cdot (k-q) + i0][(q-k)^2 + i0][-p_j \cdot k + i0][p_l \cdot q + i0]} \\
& + \frac{(2\pi i)^2 (p_i \cdot q) \tilde{\delta}(q) \delta(p_i \cdot k)}{[k^2 + i0][(k+q)^2 + i0][-p_j \cdot (k+q) + i0][p_l \cdot q + i0]} \\
& + \frac{(2\pi i)^2 (p_i \cdot k) \tilde{\delta}(k) \delta(p_l \cdot q)}{[p_i \cdot (k-q) + i0][q^2 + i0][(q-k)^2 + i0][-p_j \cdot k + i0]} \\
& + \frac{(2\pi i)^2 (p_i \cdot q) \delta(p_i \cdot k) \delta(p_l \cdot q)}{[q^2 + i0][k^2 + i0][(k+q)^2 + i0][-p_j \cdot (k+q) + i0]} \\
& + \frac{(2\pi i)^3 (p_i \cdot k) \tilde{\delta}(q) \tilde{\delta}(k) \tilde{\delta}(k+q)}{[-p_i \cdot q + i0][-p_j \cdot k + i0][p_l \cdot (k+q) + i0]} \\
& + \frac{(2\pi i)^3 (p_i \cdot k) \tilde{\delta}(q) \tilde{\delta}(k) \delta(p_l \cdot (k+q))}{[-p_i \cdot q + i0][(k+q)^2 + i0][-p_j \cdot k + i0]} \\
& + \frac{(2\pi i)^3 (p_i \cdot k) \tilde{\delta}(q) \tilde{\delta}(k) \tilde{\delta}(q-k)}{[p_i \cdot (k-q) + i0][-p_j \cdot k + i0][p_l \cdot q + i0]} \\
& + \frac{(2\pi i)^3 (p_i \cdot k) \tilde{\delta}(k) \tilde{\delta}(q) \delta(p_i \cdot (k-q))}{[(q-k)^2 + i0][-p_j \cdot k + i0][p_l \cdot q + i0]} \\
& + \frac{(2\pi i)^3 (p_i \cdot k) \tilde{\delta}(q) \tilde{\delta}(q-k) \delta(p_i \cdot (k-q))}{[k^2 + i0][-p_j \cdot k + i0][p_l \cdot q + i0]} \\
& + \frac{(2\pi i)^3 (p_i \cdot k) \tilde{\delta}(q-k) \delta(p_l \cdot q) \delta(p_i \cdot (k-q))}{[q^2 + i0][k^2 + i0][-p_j \cdot k + i0]} \\
& + \frac{(2\pi i)^3 (p_i \cdot k) \tilde{\delta}(k) \delta(p_l \cdot q) \delta(p_i \cdot (k-q))}{[(q-k)^2 + i0][q^2 + i0][-p_j \cdot k + i0]} \\
& + \frac{(2\pi i)^3 (p_i \cdot k) \tilde{\delta}(k) \tilde{\delta}(q-k) \delta(p_l \cdot q)}{[p_i \cdot (k-q) + i0][q^2 + i0][-p_j \cdot k + i0]} \Bigg\} ,
\end{aligned}
\tag{5.51}
$$

$$
\begin{aligned}
(\mathrm{vii}) = \mu^{4\varepsilon} \int \frac{\text{đ}^d k}{i\pi^{d/2}} \frac{\text{đ}^d q}{i\pi^{d/2}} \Bigg\{ & \frac{(2\pi i)^2 (p_l \cdot q) \tilde{\delta}(q) \delta(p_l \cdot k)}{[-p_i \cdot q + i0][k^2 + i0][(k-q)^2 + i0][p_j \cdot (q-k) + i0]} \\
& + \frac{(2\pi i)^2 (p_l \cdot q) \tilde{\delta}(k) \tilde{\delta}(q)}{[-p_i \cdot q + i0][(k-q)^2 + i0][p_j \cdot (q-k) + i0][p_l \cdot k + i0]} \\
& + \frac{(2\pi i)^2 (p_l \cdot k) \tilde{\delta}(q) \tilde{\delta}(k)}{[-p_i \cdot q + i0][(k+q)^2 + i0][-p_j \cdot k + i0][p_l \cdot (k+q) + i0]} \\
& + \frac{(2\pi i)^2 (p_l \cdot k) \tilde{\delta}(q) \tilde{\delta}(k)}{[p_i \cdot (k-q) + i0][(q-k)^2 + i0][-p_j \cdot k + i0][p_l \cdot q + i0]} \\
& + \frac{(2\pi i)^2 (p_l \cdot k) \tilde{\delta}(q) \delta(p_i \cdot k)}{[k^2 + i0][(k+q)^2 + i0][-p_j \cdot (k+q) + i0][p_l \cdot q + i0]} \\
& + \frac{(2\pi i)^2 (p_l \cdot k) \tilde{\delta}(k) \delta(p_l \cdot q)}{[p_i \cdot (k-q) + i0][q^2 + i0][(q-k)^2 + i0][-p_j \cdot k + i0]} \\
& + \frac{(2\pi i)^2 (p_l \cdot k) \delta(p_i \cdot k) \delta(p_l \cdot q)}{[q^2 + i0][k^2 + i0][(k+q)^2 + i0][-p_j \cdot (k+q) + i0]} \\
& + \frac{(2\pi i)^3 (p_l \cdot k) \tilde{\delta}(q) \tilde{\delta}(k) \tilde{\delta}(k+q)}{[-p_i \cdot q + i0][-p_j \cdot k + i0][p_l \cdot (k+q) + i0]} \\
& + \frac{(2\pi i)^3 (p_l \cdot k) \tilde{\delta}(q) \tilde{\delta}(k) \delta(p_l \cdot (k+q))}{[-p_i \cdot q + i0][(k+q)^2 + i0][-p_j \cdot k + i0]} \\
& + \frac{(2\pi i)^3 (p_l \cdot k) \tilde{\delta}(q) \tilde{\delta}(k) \tilde{\delta}(q-k)}{[p_i \cdot (k-q) + i0][-p_j \cdot k + i0][p_l \cdot q + i0]} \\
& + \frac{(2\pi i)^3 (p_l \cdot k) \tilde{\delta}(k) \tilde{\delta}(q) \delta(p_i \cdot (k-q))}{[(q-k)^2 + i0][-p_j \cdot k + i0][p_l \cdot q + i0]} \\
& + \frac{(2\pi i)^3 (p_l \cdot k) \tilde{\delta}(q) \tilde{\delta}(q-k) \delta(p_i \cdot (k-q))}{[k^2 + i0][-p_j \cdot k + i0][p_l \cdot q + i0]} \\
& + \frac{(2\pi i)^3 (p_l \cdot k) \tilde{\delta}(q-k) \delta(p_l \cdot q) \delta(p_i \cdot (k-q))}{[q^2 + i0][k^2 + i0][-p_j \cdot k + i0]} \\
& + \frac{(2\pi i)^3 (p_l \cdot k) \tilde{\delta}(k) \delta(p_l \cdot q) \delta(p_i \cdot (k-q))}{[(q-k)^2 + i0][q^2 + i0][-p_j \cdot k + i0]} \\
& + \frac{(2\pi i)^3 (p_l \cdot k) \tilde{\delta}(k) \tilde{\delta}(q-k) \delta(p_l \cdot q)}{[p_i \cdot (k-q) + i0][q^2 + i0][-p_j \cdot k + i0]} \Bigg\} ,
\end{aligned}
\tag{5.52}
$$

$$
\begin{aligned}
(\text{viii}) = \mu^{4\varepsilon} \int \frac{đ^d k}{i\pi^{d/2}} \frac{đ^d q}{i\pi^{d/2}} \Bigg\{ & -\frac{(2\pi i)^2 (p_j \cdot q) \tilde{\delta}(q) \delta(p_l \cdot k)}{[-p_i \cdot q + i0][k^2 + i0][(k-q)^2 + i0][p_j \cdot (q-k) + i0]} \\
& - \frac{(2\pi i)^2 (p_j \cdot q) \tilde{\delta}(k) \tilde{\delta}(q)}{[-p_i \cdot q + i0][(k-q)^2 + i0][p_j \cdot (q-k) + i0][p_l \cdot k + i0]} \\
& + \frac{(2\pi i)^2 (p_j \cdot q) \tilde{\delta}(q) \tilde{\delta}(k)}{[-p_i \cdot q + i0][(k+q)^2 + i0][-p_j \cdot k + i0][p_l \cdot (k+q) + i0]} \\
& + \frac{(2\pi i)^2 (p_j \cdot q) \tilde{\delta}(q) \tilde{\delta}(k)}{[p_i \cdot (k-q) + i0][(q-k)^2 + i0][-p_j \cdot k + i0][p_l \cdot q + i0]} \\
& - \frac{(2\pi i)^2 (p_j \cdot k) \tilde{\delta}(q) \delta(p_i \cdot k)}{[k^2 + i0][(k+q)^2 + i0][-p_j \cdot (k+q) + i0][p_l \cdot q + i0]} \\
& + \frac{(2\pi i)^2 (p_j \cdot q) \tilde{\delta}(k) \delta(p_l \cdot q)}{[p_i \cdot (k-q) + i0][q^2 + i0][(q-k)^2 + i0][-p_j \cdot k + i0]} \\
& - \frac{(2\pi i)^2 (p_j \cdot k) \delta(p_i \cdot k) \delta(p_l \cdot q)}{[q^2 + i0][k^2 + i0][(k+q)^2 + i0][-p_j \cdot (k+q) + i0]} \\
& + \frac{(2\pi i)^3 (p_j \cdot q) \tilde{\delta}(q) \tilde{\delta}(k) \tilde{\delta}(k+q)}{[-p_i \cdot q + i0][-p_j \cdot k + i0][p_l \cdot (k+q) + i0]} \\
& + \frac{(2\pi i)^3 (p_j \cdot q) \tilde{\delta}(q) \tilde{\delta}(k) \delta(p_l \cdot (k+q))}{[-p_i \cdot q + i0][(k+q)^2 + i0][-p_j \cdot k + i0]} \\
& + \frac{(2\pi i)^3 (p_j \cdot q) \tilde{\delta}(q) \tilde{\delta}(k) \tilde{\delta}(q-k)}{[p_i \cdot (k-q) + i0][-p_j \cdot k + i0][p_l \cdot q + i0]} \\
& + \frac{(2\pi i)^3 (p_j \cdot q) \tilde{\delta}(k) \tilde{\delta}(q) \delta(p_i \cdot (k-q))}{[(q-k)^2 + i0][-p_j \cdot k + i0][p_l \cdot q + i0]} \\
& + \frac{(2\pi i)^3 (p_j \cdot q) \tilde{\delta}(q) \tilde{\delta}(q-k) \delta(p_i \cdot (k-q))}{[k^2 + i0][-p_j \cdot k + i0][p_l \cdot q + i0]} \\
& + \frac{(2\pi i)^3 (p_j \cdot q) \tilde{\delta}(q-k) \delta(p_l \cdot q) \delta(p_i \cdot (k-q))}{[q^2 + i0][k^2 + i0][-p_j \cdot k + i0]} \\
& + \frac{(2\pi i)^3 (p_j \cdot q) \tilde{\delta}(k) \delta(p_l \cdot q) \delta(p_i \cdot (k-q))}{[(q-k)^2 + i0][q^2 + i0][-p_j \cdot k + i0]} \\
& + \frac{(2\pi i)^3 (p_j \cdot q) \tilde{\delta}(k) \tilde{\delta}(q-k) \delta(p_l \cdot q)}{[p_i \cdot (k-q) + i0][q^2 + i0][-p_j \cdot k + i0]} \Bigg\} \; .
\end{aligned}
\tag{5.53}
$$

One can rewrite the individual cuts by choosing a parametrisation of the loop momentum just like in the one-loop case. For three hard lines one can choose a frame in which two of them are pointing back-to-back, the third momentum points in a different direction. For instance, for the irreducible diagram one can take p_i and p_l as the forward/backward directions respectively, i.e.

$$
\begin{aligned}
p_i &= \sqrt{\frac{p_i \cdot p_l}{2}} \left(1, \vec{0}_\perp^{(d-2)}, 1\right) \; , \\
p_l &= \sqrt{\frac{p_i \cdot p_l}{2}} \left(1, \vec{0}_\perp^{(d-2)}, -1\right) \; ,
\end{aligned}
\tag{5.54}
$$

and thus, in terms of a Sudakov decomposition the loop momenta can be written as $k^\mu = \alpha p_i^\mu + \beta p_l^\mu + \hat{k}_\perp^\mu$ and $q^\mu = \hat{\alpha} p_i^\mu + \hat{\beta} p_l^\mu + \hat{q}_\perp^\mu$ with $\hat{k}_\perp^\mu = k_\perp (0, \vec{n}_{\perp,k}^{(d-2)}, 0)$ and $\vec{n}_\perp^2 = 1$, while for the hard momentum p_j one can use the general notation $p_j^\mu = E_j \left(1, \vec{n}_{j\perp}^{(d-2)} \sin\theta_j, \cos\theta_j\right) \equiv$

$\left(p_j^0, \vec{p}_{j\perp}^{\,(d-2)}, p_j^{(d)}\right)$. For example, consider one of the contributions in equation (5.53), choosing the coordinates in this way, one can evaluate the integrals with the delta functions to find

$$
\begin{aligned}
&\mu^{4\varepsilon} \int \frac{\text{đ}^d k}{i\pi^{d/2}} \frac{\text{đ}^d q}{i\pi^{d/2}} \frac{(2\pi i)^3 (p_j \cdot q)\tilde{\delta}(k)\delta(p_l \cdot q)\delta(p_i \cdot (k-q))}{[(q-k)^2 + i0][q^2 + i0][-p_j \cdot k + i0]} \\
&= -\frac{(2\pi i)^3}{(2\pi)^{2d}} \int_{-\infty}^{\infty} \mathrm{d}\beta \int_0^{\infty} \mathrm{d}k_\perp \left(\frac{\mu}{k_\perp}\right)^{2\varepsilon} \int_0^{\infty} \mathrm{d}q_\perp \left(\frac{\mu}{q_\perp}\right)^{2\varepsilon} \int \mathrm{d}\Omega_k^{(d-3)} \int \mathrm{d}\Omega_q^{(d-3)} \frac{1}{[-q_\perp^2 + i0]} \\
&\frac{k_\perp q_\perp \left[(p_j \cdot p_l)\beta - q_\perp \left(\vec{n}_{\perp,q}^{\,(d-2)} \vec{p}_{j\perp}^{\,(d-2)}\right)\right]}{2(p_i \cdot p_l)\beta} \frac{1}{\left[-q_\perp^2 - k_\perp^2 + 2k_\perp q_\perp \left(\vec{n}_{\perp,k}^{\,(d-2)} \vec{n}_{\perp,q}^{\,(d-2)}\right) + i0\right]} \\
&\frac{1}{\left[\frac{p_i \cdot p_j}{p_i \cdot p_l} \frac{1}{2\beta} k_\perp^2 + (p_j \cdot p_l)\beta - k_\perp \left(\vec{p}_{j\perp}^{\,(d-2)} \vec{n}_{\perp,k}^{\,(d-2)}\right) - i0\right]} \,.
\end{aligned}
\tag{5.55}
$$

In this way one can work through all of the cut-contributions in order to express them as integrals of the transverse momenta, alternatively one could also choose a different ordering variable, for instance energy.

5.4 Radiative cancellations

In this section the two-loop amplitudes squared are sorted with respect to their colour structure and the double radiative cuts of the virtual diagrams are brought together with the double real emission processes. In this way one can find out which diagrams have to be combined in order to observe the cancellation of IR divergences.

At first, consider the colour structure $\mathbf{T}_i^b \mathbf{T}_i^a \mathbf{T}_j^b \mathbf{T}_j^a$. The Abelian diagrams with two hard lines involved in the process of exchanging or emitting soft gluons are rewritten in terms of this colour structure by using the commutator relation (see equation (2.9)). Graphically, the cancellations for this type of colour structure can be depicted in the following way

$\sum_{i \neq j} \mathbf{T}_i^b \mathbf{T}_i^a \mathbf{T}_j^b \mathbf{T}_j^a \Bigg[\frac{1}{2} 2\mathrm{Re}\Bigg($ 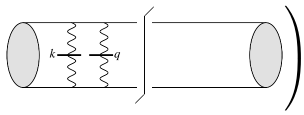 $\Bigg) + \frac{1}{2} 2\mathrm{Re}\Bigg($ 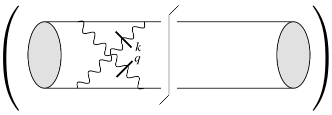 $\Bigg)$

$+2\mathrm{Re}\Bigg($ 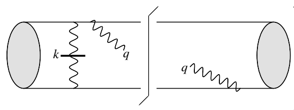 $\Bigg) + 2\mathrm{Re}\Bigg($ 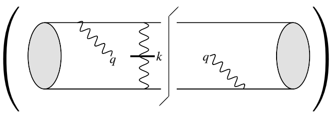 $\Bigg)$

$+\frac{1}{2} 2\mathrm{Re}\Bigg($ 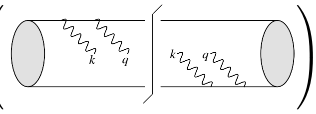 $\Bigg) + \frac{1}{2} 2\mathrm{Re}\Bigg($ 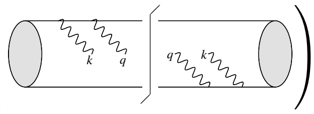 $\Bigg)$

$+\frac{1}{4} 2\mathrm{Re}\Bigg($ 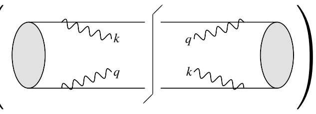 $\Bigg) + \frac{1}{4} 2\mathrm{Re}\Bigg($ 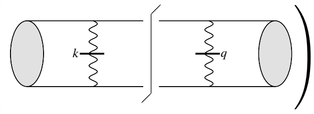 $\Bigg)\Bigg] = 0 \,,$

(5.56)

where the short black lines indicate which propagators are cut due to the application of the Feynman tree theorem. The cancellation is of course meant as an IR-divergence cancellation, i.e. the virtual lower and upper integration boundaries are taken to be 0 and μ_s in accordance with the real-emission phase-space integration. The contributions of the virtual integral from $[\mu_s, \infty]$ remain and thus there is still an UV divergence which has to be renormalised. The diagrams are drawn with photon lines in order to indicate that the colour structure has been taken out.

The sum over the hard parton lines i, j ensures that also diagrams with soft gluon emission from the opposite line with respect to the one which is depicted in the upper equation are included. In the sum it holds that $i \neq j$, since in the case that the real soft gluons are emitted from the same hard line in the amplitude and the conjugated amplitude the diagram does not give a contribution for massless hard lines in Feynman gauge.

The factors in front of the diagrams in equation (5.56) are written in this way as they arise due to different reasons:

The virtual exchange diagrams in the first line get a factor of 1/2 in order to avoid overcounting, since, if in the colour sum i and j are swapped, the diagrams do not change. Of course also the conjugated process has to be taken into account, the tree-level amplitude and the conjugated double exchange, this is encoded in taking the real part twice. For the one-loop/one-emission diagrams the colour sum takes into account the soft emission from the line j and writing two times the real part again takes care of the conjugated diagrams. In the case of the real emission diagrams one has to take into account a factor of 1/2 due to the final state symmetry as there are two identical gluons in the final state. One has to include an additional factor of 1/2 for the first diagram in the last line of equation (5.56), since the conjugated diagram is already part of the colour sum. For the last diagram one has to multiply with an additional factor of 1/2 as well, although for a different reason: In this case one truly squares the amplitude, it is not an interference with a different diagram.

Rewriting the "pictorial cancellation" of equation (5.56) in terms of integrands one gets

$$
\begin{aligned}
&\sum_{i\neq j} \mathbf{T}_i^b \mathbf{T}_i^a \mathbf{T}_j^b \mathbf{T}_j^a (p_i \cdot p_j)^2 \mu^{4\varepsilon} \int_0^{\mu_s} \mathrm{d}\Pi_k \, \mathrm{d}\Pi_q \\
&\left[\frac{1}{[p_i \cdot (k+q)][-p_j \cdot (k+q)][p_i \cdot q][-p_j \cdot q]} + \frac{1}{[p_i \cdot (k+q)][-p_j \cdot (k+q)][p_i \cdot q][-p_j \cdot k]} \right. \\
&+ \frac{2}{[p_i \cdot (k+q)][p_i \cdot q][-p_j \cdot k][p_j \cdot q]} + \frac{2}{[p_i \cdot (k+q)][p_i \cdot k][-p_j \cdot k][p_j \cdot q]} \\
&+ \frac{1}{[p_i \cdot (k+q)][p_i \cdot q][p_j \cdot (k+q)][p_j \cdot k]} + \frac{1}{[p_i \cdot (k+q)][p_i \cdot q][p_j \cdot q][p_j \cdot (k+q)]} \\
&\left. + \frac{1}{2} \frac{1}{[p_i \cdot k][p_i \cdot q][p_j \cdot q][p_j \cdot k]} + \frac{1}{2} \frac{1}{[p_i \cdot k][-p_i \cdot q][p_j \cdot q][-p_j \cdot k]} \right] = 0 \, .
\end{aligned}
\tag{5.57}
$$

Notice that the phase-space integration measure $\mathrm{d}\Pi_i$ has been written, since all of the virtual loop integrals have been reformulated as phase-space integrals by using the FTT. Furthermore, in equation (5.57) the i0-prescription has been omitted, since one is only interested in the real part in this case.

When bringing the colour structure into the form $\mathbf{T}_i^b \mathbf{T}_i^a \mathbf{T}_j^b \mathbf{T}_j^a$ for all the diagrams in equation (5.56) one also has to consider the subclass of diagrams for which the commutator of the colour-charge operators has to be applied. These diagrams thus have contributions proportional to the colour structure $\frac{C_A}{2}(\mathbf{T}_i \cdot \mathbf{T}_j)$, it turns out that the following cancellation occurs

$\sum_{i\neq j} \frac{C_A}{2}(\mathbf{T}_i \cdot \mathbf{T}_j) \Big[\frac{1}{2} 2\mathrm{Re} \Big($ 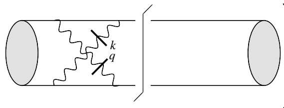 $\Big) + 2\mathrm{Re} \Big($ 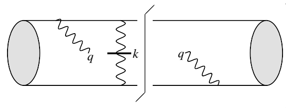 $\Big)$

$+ \frac{1}{2} 2\mathrm{Re} \Big($ 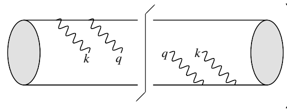 $\Big) + \frac{1}{4} 2\mathrm{Re} \Big($ 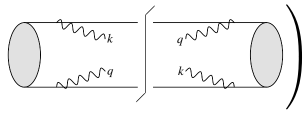 $\Big) \Big] = 0 \; .$ (5.58)

For the non-Abelian diagrams with two external lines one finds a colour structure of $\frac{C_A}{2}(\mathbf{T}_i \cdot \mathbf{T}_j)$ as well. The cancellation of the IR divergences proceeds in the following way:

$\sum_{i\neq j} \frac{C_A}{2}(\mathbf{T}_i \cdot \mathbf{T}_j) \Big[2\mathrm{Re} \Big($ 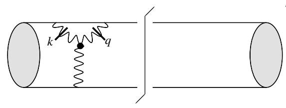 $\Big)$

$+ 2\mathrm{Re} \Big($ 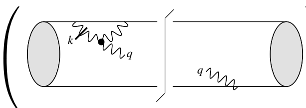 $\Big) + 2\mathrm{Re} \Big($ 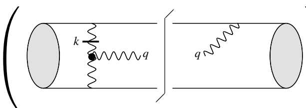 $\Big)$

$+ \frac{1}{2} 4\mathrm{Re} \Big($ 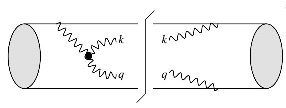 $\Big) + \frac{1}{2} 4\mathrm{Re} \Big($ 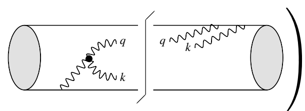 $\Big) \Big] = 0 \; ,$ (5.59)

where the cuts of the two-loop and one-loop/one-emission diagrams stand for the three/two different radiative double cuts which one obtains when applying the FTT. The unordered colour sum with $i \neq j$ ensures that also diagrams with swapped lines are taken into account. Furthermore, for the double emission processes, the prefactor is chosen such that the diagrams with exchanged momenta, i.e. $k \leftrightarrow q$, in the conjugated amplitude are included.

The structure of the IR cancellation of equation (5.59) is the following: The second diagram in the second line completely cancels with the first emission diagram in the third line. The whole contribution of the first diagram in the second line cancels with some of the terms in the virtual diagram in the first line and the remaining terms of the latter cancel with the second emission diagram in the third line. This pattern of cancellation can be observed when the squared amplitudes are explicitly written at the integrand level for each of the diagrams,

$$\begin{aligned}
&2\sum_{i\neq j} \frac{C_A}{2}(\mathbf{T}_i \cdot \mathbf{T}_j)\, \mu^{4\varepsilon} \int_0^{\mu_s} \mathrm{d}\Pi_k \, \mathrm{d}\Pi_q \, p_i^\mu p_i^\nu p_j^\tau \Bigg[-\frac{[(2q-k)_\mu g_{\nu\tau} - (k+q)_\nu g_{\mu\tau}]}{[p_i\cdot(q-k)][2k\cdot q][p_i\cdot q][p_j\cdot q]} \\
&-\frac{[(k+q)_\mu g_{\nu\tau} + (k-2q)_\nu g_{\mu\tau}]}{[p_i\cdot q][p_i\cdot k][2k\cdot q][p_j\cdot q]} - \frac{[(2q+k)_\nu g_{\mu\tau} - (2k+q)_\mu g_{\nu\tau}]}{[p_i\cdot(k+q)][p_j\cdot(k+q)][2k\cdot q][p_i\cdot q]} \\
&+\frac{[(2q-k)_\mu g_{\nu\tau} - (k+q)_\nu g_{\mu\tau}]}{[p_i\cdot(q-k)][2k\cdot q][p_i\cdot q][p_j\cdot q]} + \frac{[(k+q)_\mu g_{\nu\tau} + (k-2q)_\nu g_{\mu\tau}]}{[p_i\cdot q][p_i\cdot k][2k\cdot q][p_j\cdot q]} \\
&+\frac{[(k-q)_\mu g_{\nu\tau} - (2k+q)_\nu g_{\mu\tau}]}{[p_i\cdot(k+q)][2k\cdot q][p_i\cdot q][p_j\cdot k]} + \frac{[-(2q+k)_\mu g_{\nu\tau} + (2k+q)_\nu g_{\mu\tau}]}{[p_j\cdot(k+q)][2k\cdot q][p_i\cdot q][p_i\cdot k]} \\
&-\frac{[(k-q)_\mu g_{\nu\tau} - (2k+q)_\nu g_{\mu\tau}]}{[p_i\cdot(k+q)][2k\cdot q][p_i\cdot q][p_j\cdot k]} + \frac{[(k+2q)_\nu g_{\mu\tau} - (2k+q)_\mu g_{\nu\tau}]}{[p_i\cdot(k+q)][p_j\cdot(k+q)][2k\cdot q][p_i\cdot q]} \Bigg] = 0 \; ,
\end{aligned} \tag{5.60}$$

where the terms of the triple gluon vertices which equal to zero due to the on-shellness of the external lines are already neglected. In the first and second line of equation (5.60) the three radiative double cuts of the virtual diagram are given, in the third and fourth line the radiative cuts of the one-loop/one-emission diagrams are written and in the last line there are the contributions pertaining to the emission diagrams.

Similarly, if there are three hard parton lines involved in the process of exchanging and emitting soft gluons one can decompose the colour structures of the diagrams into $\mathbf{T}_i^b\mathbf{T}_i^a\mathbf{T}_j^b\mathbf{T}_l^a$ and $if_{abc}\mathbf{T}_i^a\mathbf{T}_j^b\mathbf{T}_l^c$ (colour charge operators pertaining to different hard lines commute). In Figure 19 the diagrams with colour structure $\mathbf{T}_i^b\mathbf{T}_i^a\mathbf{T}_j^b\mathbf{T}_l^a$ are depicted. Due to the propagator structure of the diagrams it is convenient to specify the colour sum for three lines in the form $[i,j][i,l]$, i.e. one can sum over the pairs i,j and i,l (notice that one of the lines necessarily carries two vertices) and then sum over i, such that all the possible (unordered) combinations of external lines are included. Here it is assumed that $i \neq j \neq l$ holds. In particular, this formulation of the colour sum is convenient in this case, since the propagators can be nicely combined for the diagrams in Figure 19, for instance one can rewrite the propagator structure of diagram 19(b) as

$$\frac{1}{[p_i\cdot k][p_j\cdot k][p_i\cdot q][p_l\cdot q]} = \frac{1}{[p_i\cdot (k+q)][p_j\cdot k][p_i\cdot q][p_l\cdot q]} + \frac{1}{[p_i\cdot (k+q)][p_i\cdot k][p_j\cdot k][p_l\cdot q]}\ , \tag{5.61}$$

and this is exactly the propagator structure of diagram 19(a). The same applies to the one-loop/one-emission diagrams in the second line of Figure 19, where equation (5.61) can be used for 19(e) to match the propagator structure of diagrams 19(c) and 19(d), and analogously for the double emission contributions.
As an illustration of the colour sum of pairs for three hard lines, consider Figure 20, which shows the counting for the one-loop/one-emission case when the sum over pairs is performed and thus numbers are assigned to the different lines. In this example only diagrams which have two vertices on line 1 are drawn and introducing the sum over $i = 1, ..., 3$ takes care of the other possibilities. The last two diagrams of Figure 20 have the two vertices on line 1 in the amplitude and conjugated amplitude respectively. Therefore one can aim to rewrite the counting of pairs in terms of the other diagrams, which always have the two vertices of line 1 in the amplitude. Due to the propagator structure (using equation (5.61)) the last two diagrams can be conveniently rewritten in terms of pairs $[1,2][1,3] + [1,3][1,2]$. The double emission and the virtual diagrams of Figure 19 can be treated analogously. As a result one can combine the different diagrams such that only the following types of diagrams have to be distinguished

$$\sum_i \sum_{[i,j][i,l]} \mathbf{T}_i^b\mathbf{T}_i^a\mathbf{T}_j^b\mathbf{T}_l^a \Bigg[4\mathrm{Re}\Bigg($$
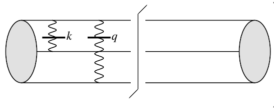
$$\Bigg) + 8\mathrm{Re}\Bigg($$
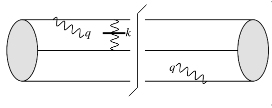
$$\Bigg)$$
$$+4\mathrm{Re}\Bigg($$
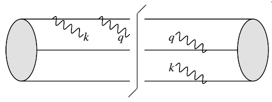
$$\Bigg)\Bigg] = 0\ , \tag{5.62}$$

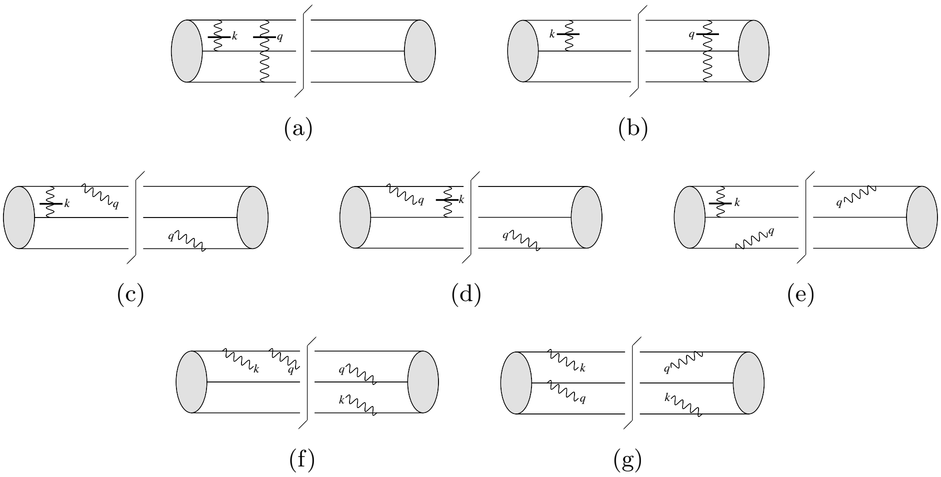

Figure 19: Diagrams with colour structure $\mathbf{T}_i^b\mathbf{T}_i^a\mathbf{T}_j^b\mathbf{T}_l^a$.

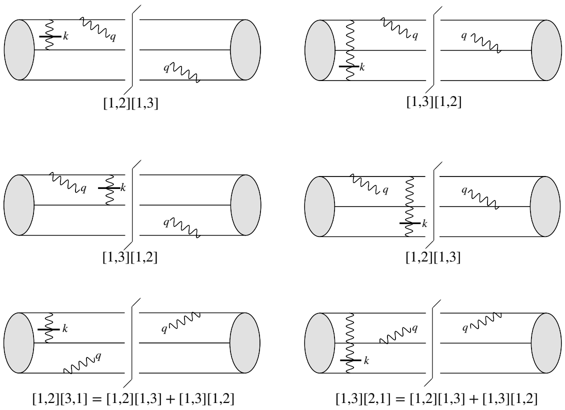

Figure 20: One-loop/one-emission diagrams with colour structure $\mathbf{T}_i^b\mathbf{T}_i^a\mathbf{T}_j^b\mathbf{T}_l^a$. Below each diagram the counting of pairs is written, due to the propagator structure it is possible to rewrite the colour sum of the last two diagrams in terms of pairs of structure $[i,j][i,l]$.

where combining the virtual contributions in the first line of Figure 19 leads to a factor of four for the first diagram in equation (5.62), similarly combining the one-loop/one-emission diagrams gives a factor of eight. Finally the combination of the emission diagrams gives rise to a factor four (where the symmetry factor 1/2 for the final state gluons has already been taken into account). As a result, the virtual diagram adds with the real emission, together cancelling the one-loop/one-emission contribution.

Furthermore, for the non-Abelian diagrams with the colour structure $if_{abc}\mathbf{T}_i^a\mathbf{T}_j^b\mathbf{T}_l^c$ the cancellation takes place between the following three diagrams

$$\sum_{i\neq j\neq l}\frac{1}{2}if_{abc}\mathbf{T}_i^a\mathbf{T}_j^b\mathbf{T}_l^c\Bigg[2\mathrm{Re}\Bigg($$
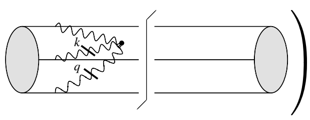
$$\Bigg)+2\mathrm{Re}\Bigg($$
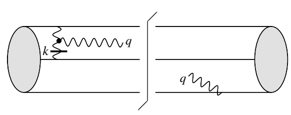
$$\Bigg)$$
$$+2\mathrm{Re}\Bigg($$
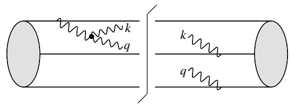
$$\Bigg)\Bigg]=0\;, \qquad (5.63)$$

where the cuts for the diagrams in the first line stand again for the three/two different radiative cuts which occur according to the rules of the FTT cutting procedure. Here the sum is performed by exchanging the lines with $i \neq j \neq l$, since for the diagrams considered here one does not have a line carrying two vertices. This introduces a factor of 1/2 for the diagrams. The one-loop/one-emission diagram combines with the emission diagram and together they cancel the contributions of the virtual diagram:

$$\begin{aligned}
&\sum_{i\neq j\neq l} i f_{abc} \mathbf{T}_i^a \mathbf{T}_j^b \mathbf{T}_l^c \, \mu^{4\varepsilon} \int_0^{\mu_s} \mathrm{d}\Pi_k \, \mathrm{d}\Pi_q \, p_i^\sigma p_j^\rho p_l^\nu \Bigg[-\frac{[(2q-k)_\rho g_{\sigma\nu} + (2k-q)_\sigma g_{\rho\nu} - (k+q)_\nu g_{\sigma\rho}]}{[p_i \cdot q][-2k \cdot q][-p_j \cdot k][p_l \cdot (k-q)]} \\
&-\frac{[(q+k)_\rho g_{\sigma\nu} + (q-2k)_\sigma g_{\rho\nu} + (k-2q)_\nu g_{\sigma\rho}]}{[p_i \cdot q][-2k \cdot q][p_j \cdot (k-q)][-p_l \cdot k]} + \frac{[(k+2q)_\rho g_{\sigma\nu} + (k-q)_\sigma g_{\rho\nu} - (2k+q)_\nu g_{\sigma\rho}]}{[p_i \cdot (k+q)][2k \cdot q][-p_j \cdot k][-p_l \cdot q]} \\
&+\frac{[(2q-k)_\rho g_{\sigma\nu} - (k+q)_\sigma g_{\rho\nu} + (2k-q)_\nu g_{\sigma\rho}]}{[p_i \cdot (q-k)][-2k \cdot q][p_j \cdot k][-p_l \cdot q]} + \frac{[(k+q)_\rho g_{\sigma\nu} + (k-2q)_\sigma g_{\nu\rho} + (q-2k)_\nu g_{\sigma\rho}]}{[p_i \cdot k][-2k \cdot q][p_j \cdot (q-k)][-p_l \cdot q]} \\
&+\frac{[(2k+q)_\nu g_{\sigma\rho} + (q-k)_\sigma g_{\rho\nu} - (2q+k)_\rho g_{\sigma\nu}]}{[p_i \cdot (k+q)][2k \cdot q][-p_j \cdot k][-p_l \cdot q]} \Bigg] = 0 \, ,
\end{aligned} \tag{5.64}$$

where the first three terms represent the three radiative double cuts of the virtual diagram, the fourth and the fifth term pertain to the one-loop/one-emission diagram and the last part corresponds to the emission diagram. One observes that the second contribution of the second line cancels with the term in the fourth line. The first term in the second line cancels against the one in the first line after performing the swaps of the hard parton lines ($i \leftrightarrow l$, $j \leftrightarrow l$) as well as renaming the momenta $k \leftrightarrow q$. It is noteworthy that swapping two hard lines, say $i \leftrightarrow l$, introduces a negative sign due to the antisymmetry of the colour structure under this action. Finally, the two contributions in the third line cancel when relabelling $k \leftrightarrow q$.

The IR-divergence cancellation can also be demonstrated for four hard partons involved, their momenta are labelled by p_i, p_j, p_l and p_m. The diagrams exhibit a colour structure of $\mathbf{T}_i^a \mathbf{T}_j^a \mathbf{T}_l^b \mathbf{T}_m^b$, the colour sum can be performed over two pairs of the (distinct) external lines ($[i,j][l,m]$ with $i \neq j \neq l \neq m$) such that one finds

$$\sum_{[i,j][l,m]} \mathbf{T}_i^a \mathbf{T}_j^a \mathbf{T}_l^b \mathbf{T}_m^b \Bigg[\frac{1}{4}\frac{1}{2} 2\mathrm{Re} \Bigg($$
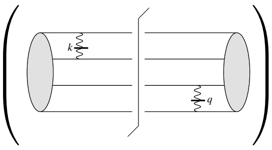

$$\Bigg) + \frac{1}{4}\frac{1}{2}2\frac{1}{2} 2\mathrm{Re} \Bigg($$
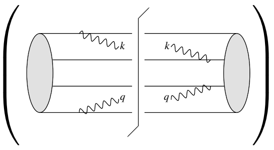

$$\Bigg) + \frac{1}{4} 2\mathrm{Re} \Bigg($$
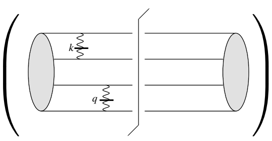

$$\Bigg) + \frac{1}{2} 2\mathrm{Re} \Bigg($$
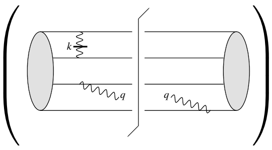

$$\Bigg) \Bigg] = 0 \, , \tag{5.65}$$

where the prefactors have the following origins:
The first diagram receives a factor of 1/4 in order to avoid overcounting when exchanging the order of the pairs. The diagram produces the real part only once, since the conjugated diagram is already included in the colour sum over pairs. The same is true for the second diagram, however, in addition one has to introduce a factor of two in order to include the diagrams with

the loop momenta exchanged, as well as the symmetry factor 1/2 for the final state gluons. For the diagrams in the second line one only needs to include factors to avoid overcounting, in particular for the virtual diagram this gives a factor of 1/4 for both gluon exchanges and consequently a factor of 1/2 for the one-loop/one-emission diagram.
When writing down the integrand structures one observes that the first three diagrams add up and cancel the contribution from the fourth diagram in equation (5.65),

$$\begin{aligned}&\sum_{[i,j][l,m]} \mathbf{T}_i^a \mathbf{T}_j^a \mathbf{T}_l^b \mathbf{T}_m^b (p_i \cdot p_j)(p_l \cdot p_m)\, \mu^{4\varepsilon} \int_0^{\mu_s} \mathrm{d}\Pi_k\, \mathrm{d}\Pi_q \\ &\left[\frac{1}{4}\frac{1}{[p_i \cdot k][-p_j \cdot k][-p_l \cdot q][p_m \cdot q]} + \frac{1}{4}\frac{1}{[p_i \cdot k][p_m \cdot q][p_j \cdot k][p_l \cdot q]}\right. \\ &\left.+\frac{1}{2}\frac{1}{[p_i \cdot k][-p_j \cdot k][-p_l \cdot q][p_m \cdot q]} - \frac{1}{[p_i \cdot k][p_j \cdot k][p_l \cdot q][p_m \cdot q]}\right] = 0\ .\end{aligned} \tag{5.66}$$

5.5 Self-energy contributions

The double propagators appearing in the self-energy diagrams ("bubble-diagrams") demand a modified formulation of the cutting procedure when applying the Feynman tree theorem. In this section a cutting rule for double propagators is presented which can be obtained by taking the derivative of the relation between the Feynman- and the advanced propagator with respect to a component of the loop momentum. It is then reformulated as the derivative of the squared loop momentum. Furthermore, the IR cancellations which take place for the radiative cuts of the self-energy diagrams are summarised.

To start with, the amplitude of the combined gluon- and ghost-loop self-energy (see Figure 21) is given by

$$\begin{aligned}\mathcal{M}_{21(\mathrm{a})+(\mathrm{b})} &= g^4 C_A (\mathbf{T}_i \cdot \mathbf{T}_j) \mu^{4\varepsilon} \int \frac{đ^d q}{i\pi^{d/2}} \frac{đ^d k}{i\pi^{d/2}} \\ &\quad \frac{p_{i\mu} p_{j\nu}}{[p_i \cdot q + i0][-p_j \cdot q + i0][k^2 + i0][(q-k)^2 + i0][q^2 + i0]^2} \Bigg\{ (4-2d) k^\mu k^\nu \\ &\quad + \left(3 - \frac{d}{2}\right) q^\mu q^\nu + \left(d - \frac{5}{2}\right) q^\mu k^\nu + \left(d - \frac{3}{2}\right) q^\nu k^\mu + g^{\mu\nu} \left(-\frac{5}{2} q^2 - k^2 + k \cdot q\right) \Bigg\} ,\end{aligned} \tag{5.67}$$

and when neglecting terms which vanish due to colour conservation one can rewrite the amplitude as

$$\begin{aligned}\mathcal{M}_{21(\mathrm{a})+(\mathrm{b})} &= g^4 C_A (\mathbf{T}_i \cdot \mathbf{T}_j) \mu^{4\varepsilon} \int \frac{đ^d q}{i\pi^{d/2}} \frac{đ^d k}{i\pi^{d/2}} \\ &\quad \Bigg\{ \frac{(4-2d)(p_i \cdot k)(p_j \cdot k)}{[p_i \cdot q + i0][-p_j \cdot q + i0][k^2 + i0][(q-k)^2 + i0][q^2 + i0]^2} \\ &\quad - \frac{2(p_i \cdot p_j)}{[p_i \cdot q + i0][-p_j \cdot q + i0][k^2 + i0][(q-k)^2 + i0][q^2 + i0]} \\ &\quad - \frac{(p_i \cdot p_j)}{[p_i \cdot q + i0][-p_j \cdot q + i0][k^2 + i0][q^2 + i0]^2} \Bigg\} .\end{aligned} \tag{5.68}$$

The loop integral in the second line does not have any double propagators anymore, it is identical to the integral (iii) of equation (5.44).
The amplitude of the fermion self-energy diagram, neglecting terms which vanish due to colour conservation, gives

$$\begin{aligned}\mathcal{M}_{21(\mathrm{c})} &= 4 g^4 \, T_R \, n_f (\mathbf{T}_i \cdot \mathbf{T}_j) \mu^{4\varepsilon} \int \frac{đ^d q}{i\pi^{d/2}} \frac{đ^d k}{i\pi^{d/2}} \\ &\quad \Bigg\{ \frac{2(p_i \cdot k)(p_j \cdot k)}{[p_i \cdot q + i0][-p_j \cdot q + i0][k^2 + i0][(k-q)^2 + i0][q^2 + i0]^2} \\ &\quad - \frac{1}{2} \frac{(p_i \cdot p_j)}{[p_i \cdot q + i0][-p_j \cdot q + i0][k^2 + i0][(k-q)^2 + i0][q^2 + i0]} \\ &\quad - \frac{(p_i \cdot p_j)}{[p_i \cdot q + i0][-p_j \cdot q + i0][k^2 + i0][q^2 + i0]^2} \Bigg\} .\end{aligned} \tag{5.69}$$

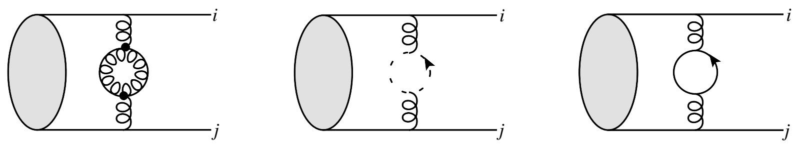

Figure 21: Gluon, ghost and fermion self-energy Feynman diagrams.

The fermion self-energy is needed when the full NLO correction is considered. In the evolution process the corrections as well as the renormalisation constants are being evolved, however the hard matrix element itself is not. Hence, the UV-counterterm is not written for the Born process since it does not start in a specific power of α_s but only for the whole, combined NLO correction. This counterterm is of the form β_0/ε_{UV} and thus the fermion bubble-diagram makes up exactly the part of the beta-function which is proportional to n_f.

5.5.1 The Feynman tree theorem for double propagators

In order to find an expression for a cutting rule for double propagators one can start with the identity which is introduced in equation (3.35)

$$\frac{1}{q^2 - i0(T \cdot q)^2} = \frac{1}{q^2 + i0(T \cdot q)^2} + 2\pi i \delta(q^2) \ , \tag{5.70}$$

where one can take the derivative with respect to a component of the loop momentum q^μ which then leads one to

$$\frac{q_\mu - i0\, T_\mu(T \cdot q)}{[q^2 - i0(T \cdot q)]^2} - \frac{q_\mu + i0\, T_\mu(T \cdot q)}{[q^2 + i0(T \cdot q)^2]^2} = -i\pi \frac{\partial}{\partial q^\mu} \delta(q^2) \ , \tag{5.71}$$

again with the timelike vector $(T^\mu) = (\sqrt{2}, \vec{0})$. By contracting with some spacelike vector S^μ, which is chosen to satisfy $S \cdot T = 0$, one can get rid of the dependence on the vector T in the numerator

$$\frac{1}{[q^2 - i0(T \cdot q)^2]^2} - \frac{1}{[q^2 + i0(T \cdot q)]^2} = -i\pi \frac{S^\mu}{S \cdot q} \frac{\partial}{\partial q^\mu} \delta(q^2) \ . \tag{5.72}$$

Using the relation $\frac{\partial}{\partial q^\mu} f(q^2) = 2q_\mu \frac{\partial}{\partial q^2} f(q^2)$ one can reformulate the upper equation in terms of q^2

$$\frac{1}{[q^2 - i0(T \cdot q)^2]^2} - \frac{1}{[q^2 + i0(T \cdot q)^2]^2} = -2\pi i\, \delta'(q^2) \ , \tag{5.73}$$

with the short-hand notation $\delta'(q^2) \equiv \frac{\partial}{\partial q^2} \delta(q^2)$.
Taking into account the Heaviside function in the formulation of the derivative cutting rule amounts to a small modification to equation (5.73), namely

$$\frac{1}{[q^2 - i0(T \cdot q)|T \cdot q|]^2} - \frac{1}{[q^2 + i0(T \cdot q)^2]^2} = -2\pi i\, \delta'(q^2) \theta(T \cdot q) \ . \tag{5.74}$$

Hence, if one has to cut the double propagator in a diagram where all the other propagators and possible numerator structures are encoded in the function $f(q, q^2)$, one can proceed to use integration by parts to "shift" the derivative from the delta function to the loop integrand

$f(q,q^2)$. This means that one has to calculate the derivative of $f(q,q^2)$ and it turns out to be convenient to parameterise the loop momentum with respect to which the derivative is evaluated in terms of a Sudakov decomposition expressed in the q^2 variable, for instance in the form

$$q^\mu = \alpha\, p_j^\mu + \frac{q^2+q_\perp^2}{2\alpha(p_i\cdot p_j)}\, p_i^\mu + q_\perp n_\perp^\mu \,, \tag{5.75}$$

where in this case p_j^μ defines the forward and p_i^μ the backward direction. It holds that $n_\perp^2 = -1$. Applying the FTT with this modification for double propagators to the loop integrals in the first and third line of equation (5.68) or equivalently to equation (5.69), i.e. to the integrals

$$\begin{aligned}
\text{(i)} &= \mu^{4\varepsilon}\int \frac{đ^d q}{i\pi^{d/2}}\frac{đ^d k}{i\pi^{d/2}}\frac{(p_i\cdot k)(p_j\cdot k)}{[p_i\cdot q+i0][-p_j\cdot q+i0][k^2+i0][(q-k)^2+i0][q^2+i0]^2}\\
\text{(ii)} &= \mu^{4\varepsilon}\int \frac{đ^d q}{i\pi^{d/2}}\frac{đ^d k}{i\pi^{d/2}}\frac{1}{[p_i\cdot q+i0][-p_j\cdot q+i0][k^2+i0][q^2+i0]^2}\,,
\end{aligned} \tag{5.76}$$

leads to the following cut-contributions

$$\begin{aligned}
\text{(i)} = \mu^{4\varepsilon}\int \frac{đ^d q}{i\pi^{d/2}}\frac{đ^d k}{i\pi^{d/2}}(p_i\cdot k)(p_j\cdot k)\Bigg\{ &-\frac{(2\pi i)^2\tilde\delta(q)\tilde\delta(k)}{[p_i\cdot(k+q)+i0][-p_j\cdot(k+q)+i0][(k+q)^2+i0]^2}\\
&+\frac{2(2\pi i)^2\tilde\delta(k)\delta(p_i\cdot q)}{[-p_j\cdot q+i0][(q-k)^2+i0][q^2+i0]^2}\\
&+\frac{2(2\pi i)^2(-\delta'(q^2)\theta(q^0))\,\tilde\delta(k)}{[p_i\cdot q+i0][-p_j\cdot q+i0][(q-k)^2+i0]}\\
&+\frac{2(2\pi i)^3\tilde\delta(k)\tilde\delta(q-k)\delta(p_i\cdot q)}{[-p_j\cdot q+i0][q^2+i0]^2}\\
&+\frac{2(2\pi i)^3(-\delta'(q^2)\theta(q^0))\,\tilde\delta(k)\delta(p_i\cdot q)}{[-p_j\cdot q+i0][(q-k)^2+i0]}\\
&+\frac{2(2\pi i)^3(-\delta'(q^2)\theta(q^0))\,\tilde\delta(k)\tilde\delta(q-k)}{[p_i\cdot q+i0][-p_j\cdot q+i0]}\\
&+\frac{2(2\pi i)^4(-\delta'(q^2)\theta(q^0))\,\tilde\delta(k)\tilde\delta(q-k)\delta(p_i\cdot q)}{[-p_j\cdot q+i0]}\Bigg\}\,,
\end{aligned} \tag{5.77}$$

and

$$\begin{aligned}
\text{(ii)} = \mu^{4\varepsilon}\int \frac{đ^d q}{i\pi^{d/2}}\frac{đ^d k}{i\pi^{d/2}}\Bigg\{&\frac{(2\pi i)^2\tilde\delta(k)\delta(p_i\cdot q)}{[-p_j\cdot q+i0][q^2+i0]^2}+\frac{(2\pi i)^2(-\delta'(q^2)\theta(q^0))\,\tilde\delta(k)}{[p_i\cdot q+i0][-p_j\cdot q+i0]}\\
&+\frac{(2\pi i)^3(-\delta'(q^2)\theta(q^0))\,\tilde\delta(k)\delta(p_i\cdot q)}{[-p_j\cdot q+i0]}\Bigg\}\,.
\end{aligned} \tag{5.78}$$

Due to the structure of cuts which appear in the equations (5.77) and (5.78) one can also observe why the parametrisation of the loop momentum in equation (5.75) is a convenient choice. In particular, for the terms with the triple cuts $\delta'(q^2)\tilde\delta(k)\delta(p_i\cdot q)$ the parametrisation allows one to express the $\delta(p_i\cdot q)$ without an explicit q^2 dependence. Hence, when using integration by parts to shift the derivative with respect to q^2 from the delta function to the other terms, it will not act on the delta function of eikonal momentum $(p_i\cdot q)$ but only on propagators dependent on

q^2.
Furthermore, for triple cuts of the form $\delta'(q^2)\tilde{\delta}(k)\tilde{\delta}(q-k)$ the integration of the loop momentum k has to be performed first using the delta functions $\tilde{\delta}(k)\tilde{\delta}(q-k)$. Afterwards, integration by parts can be conducted such that the derivative with respect to q^2 will once again act only on the loop integrand and not on delta functions.

5.5.2 Radiative cancellations for the self-energy diagrams

In order to demonstrate the IR cancellation of radiative cuts concerning the self-energy diagrams one has to consider the following diagrams

$$\sum_{i\neq j} C_A(\mathbf{T}_i\cdot\mathbf{T}_j)\Bigg[\frac{1}{2}\frac{1}{2}2\mathrm{Re}\Bigg(\text{[diagram 1]}\Bigg)+\frac{1}{2}2\mathrm{Re}\Bigg(\text{[diagram 2]}\Bigg)$$
$$+\frac{1}{2}2\mathrm{Re}\Bigg(\text{[diagram 3]}\Bigg)+\frac{1}{2}2\mathrm{Re}\Bigg(\text{[diagram 4]}\Bigg)\Bigg]=0\ . \tag{5.79}$$

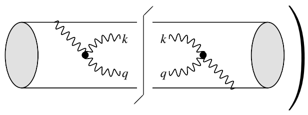

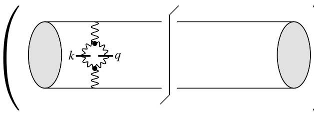

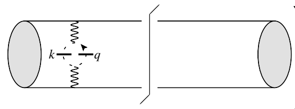

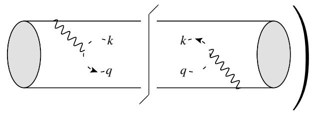

Again, the Feynman diagrams are drawn with photon-lines in order to indicate that the colour structure has been taken out and written as a global factor and the sum is once again understood to exclude the case $i=j$, i.e. it holds that $i\neq j$.
Notice that the radiative double cuts of the virtual diagrams receive a factor of (-1) from the FTT procedure (cf. equation 5.77).
For the virtual diagrams one has to multiply by a factor of 1/2 in order to avoid overcounting. Additionally, when determining the squared amplitude of the gluon bubble-diagram, the symmetry factor of 1/2 has to be taken into account. Furthermore, for the emission type diagram one needs to include the symmetry factor of the gluons as well as an additional factor of 1/2, since the conjugated diagram matches the one which is already part of the colour sum. For the amplitudes of the fermionic ghost-loops a factor of (-1) has to be included.
At the integrand level, equation (5.79) leads one to

$$\begin{aligned}
&\sum_{i\neq j}\frac{C_A}{2}(\mathbf{T}_i\cdot\mathbf{T}_j)\mu^{4\varepsilon}\int_0^{\mu_s}\mathrm{d}\Pi_k\mathrm{d}\Pi_q\,\frac{p_{i\alpha}p_j^{\delta}}{[p_i\cdot(k+q)][p_j\cdot(k+q)][(k+q)^2]^2}\\
&\Big\{-\Big[(2k+q)^{\sigma}g^{\alpha\beta}+(q-k)^{\alpha}g^{\beta\sigma}-(2q+k)^{\beta}g^{\alpha\sigma}\Big]\Big[(2k+q)_{\sigma}g_{\beta\delta}-(2q+k)_{\beta}g_{\sigma\delta}+(q-k)_{\delta}g_{\beta\sigma}\Big]\\
&+\Big[(2k+q)^{\sigma}g^{\alpha\beta}+(q-k)^{\alpha}g^{\sigma\beta}-(2q+k)^{\beta}g^{\alpha\sigma}\Big]\Big[(2k+q)_{\sigma}g_{\beta\delta}-(2q+k)_{\beta}g_{\delta\sigma}+(q-k)_{\delta}g_{\beta\sigma}\Big]\\
&+2k^{\alpha}q_{\delta}-2k^{\alpha}q_{\delta}\Big\}=0\ .
\end{aligned} \tag{5.80}$$

6 Conclusion and outlook

To summarise the main goal of this thesis was to determine some of the central ingredients to soft gluon evolution [2, 6, 9] at next-to-leading logarithmic order. These central ingredients are the colour structure and the kinematic part of the two-loop soft anomalous dimension. We aimed to determine both in an approach of algorithmic structure such that it is accessible to a numerical evolution and can thus be extended to higher orders and beyond the soft approximation.

In order to describe the colour structure within the framework of the colour-space formalism we chose the colour-flow basis [4, 6]. The formulation in terms of permutations of (anti-)colour labels is very well suited for a numerical approach. Furthermore, the colour-flow basis allowed us to efficiently determine subleading contributions in the number of colours and thus provide the possibility to go beyond the usual large-N limit. In particular, we found that this is desirable at two-loop level, since, in addition to the sum over two-parton correlations, a sum over three-parton correlations is introduced, leading to enhanced coefficients which would not be accounted for in the large-N limit.

Turning to the kinematical structure, the Feynman tree theorem [7, 8] allows one to take an algorithmic approach by systematically expressing the loop integrands in terms of cut-contributions. In this way the loop integrals are rewritten as phase-space type integrals. We reformulated the Feynman tree theorem to be able to apply it to eikonal propagators, propagators raised to second power and to the two-loop level integrals. Furthermore, it is convenient to express the loop integrals in terms of their cut-contributions since one can readily choose a parametrisation of the loop momenta (e.g. energy-ordering or perform a Sudakov decomposition) and analyse the imaginary parts in different orderings.

In order to uncover the cancellation of IR divergences we combined the real emission cross-sections with the double radiative cuts of the two-loop diagrams.

In the treatment of the amplitudes we have used a covariant gauge. This is possible here, since we have only considered soft gluons and the soft gluon current is gauge independent [10] for double emission. If collinear gluons are to be included in the framework, one has to switch to a physical gauge. When working for example in an axial gauge, the (linear) gauge propagators have to be assigned an $i0$-prescription, the so-called "Mandelstam-Leibbrandt" prescription (see [23]), which means that such types of propagators have to be cut in the course of the FTT cutting procedure. Furthermore, for "double gauge propagators" a cutting rule can be introduced, similar to the one presented in section 5.5.1.

In this way we have determined building blocks which hopefully give further insight to amplitude evolution at next-to-leading logarithmic order as well as to colour evolution beyond the large-N limit. Since we aimed for an algorithmic formulation of the procedures, the results are also relevant to branching algorithms.

A Jacobian determinants

In this appendix several Jacobian determinants for different coordinate choices are listed.
To obtain a logarithmic integration over the energy of the soft gluon, which leads to an energy ordering for multiple soft gluons, one may use the following parametrisation for the soft gluon momentum k

$$k = \left(k^0, E\,\vec{n}_\perp^{(d-2)}\sin\theta, E\cos\theta\right) \ , \tag{A.1}$$

where $\vec{n}_\perp^{(d-2)} \equiv \vec{n}_\perp^{(d-2)}(\varphi^{(d-3)})$ depends on the $(d-3)$ angular variables. In order to rewrite the measure $\mathrm{d}^d k = \mathrm{d}k^0\mathrm{d}^{d-1}k$ one has to determine the Jacobian determinant J_E

$$J_E = \begin{vmatrix} \frac{\partial k^d}{\partial E} & \frac{\partial k^d}{\partial \cos\theta} & \frac{\partial k^d}{\partial \varphi^{(d-3)}} \\ \frac{\partial \vec{k}_\perp^{(d-2)}}{\partial E} & \frac{\partial \vec{k}_\perp^{(d-2)}}{\partial \cos\theta} & \frac{\partial \vec{k}_\perp^{(d-2)}}{\partial \varphi^{(d-3)}} \end{vmatrix} = \begin{vmatrix} \cos\theta & E & (\vec{0}^{(d-3)})^\mathsf{T} \\ \vec{n}_\perp^{(d-2)}\sin\theta & -E\vec{n}_\perp^{(d-2)}\frac{\cos\theta}{\sin\theta} & E\sin\theta\frac{\partial\vec{n}_\perp^{(d-2)}}{\partial\varphi^{(d-3)}} \end{vmatrix} \ . \tag{A.2}$$

The determinant of this $[(d-1)\times(d-1)]$-dimensional matrix can now be expanded, such that one finds

$$J_E = -E^{d-2}\left(\cos^2\theta\sin^{d-4}\theta + \sin^{d-2}\theta\right)\begin{vmatrix}\vec{n}_\perp^{(d-2)} & \frac{\partial\vec{n}_\perp^{(d-2)}}{\partial\varphi^{(d-3)}}\end{vmatrix} = -E^{d-2}\sin^{-2\varepsilon}\theta\begin{vmatrix}\vec{n}_\perp^{(d-2)} & \frac{\partial\vec{n}_\perp^{(d-2)}}{\partial\varphi^{(d-3)}}\end{vmatrix} \ , \tag{A.3}$$

where it is used that the relation $|a\vec{x} \quad bY| = ab^{d-1}|\vec{x} \quad Y|$ holds for the determinant of a d-dimensional matrix, i.e. in this case for a $(d-1)$-dimensional matrix one has to adjust the power of b to $d-2$.
As a result the measure in terms of the parametrisation in equation (A.1) yields

$$\mu^{2\varepsilon}\mathrm{d}^d k = \mathrm{d}k^0\,\mathrm{d}E\,E^2\theta(E)\left(\frac{\mu}{E}\right)^{2\varepsilon}\left(1-\cos^2\theta\right)^{-\varepsilon}\mathrm{d}\cos\theta\,\mathrm{d}\Omega^{(d-3)} \ , \tag{A.4}$$

where

$$\mathrm{d}\Omega^{(d-3)} = \begin{vmatrix}\vec{n}_\perp^{(d-2)} & \frac{\partial\vec{n}_\perp^{(d-2)}}{\partial\varphi^{(d-3)}}\end{vmatrix}\mathrm{d}^{d-3}\varphi \ . \tag{A.5}$$

Note that

$$\int \mathrm{d}\Omega^{(d-3)} = \frac{2\pi}{\pi^\varepsilon\Gamma(1-\varepsilon)} \ . \tag{A.6}$$

If instead one would like to focus on transverse momentum ordering one can express the loop momentum in terms of a Sudakov decomposition/light-cone coordinates, i.e.

$$k^\mu = \alpha p_i^\mu + \beta p_j^\mu + k_\perp^\mu \ , \tag{A.7}$$

where $p_i\cdot p_j > 0$ and the transverse components have to satisfy $k_\perp\cdot p_i = k_\perp\cdot p_j = 0$.
Therefore one can choose a frame in which

$$p_i = \sqrt{\frac{p_i\cdot p_j}{2}}\left(1, \vec{0}_\perp^{(d-2)}, 1\right) \ ,$$
$$p_j = \sqrt{\frac{p_i\cdot p_j}{2}}\left(1, \vec{0}_\perp^{(d-2)}, -1\right) \ ,$$

and for the transverse components $k_\perp = p_\perp(0, \vec{n}_\perp^{(d-2)}, 0)$. As a result the Jacobian determinant reads

$$J_{p_\perp} = \begin{vmatrix} \frac{\partial k^0}{\partial \alpha} & \frac{\partial k^0}{\partial \beta} & \frac{\partial k^0}{\partial p_\perp} & \frac{\partial k^0}{\partial \varphi^{(d-3)}} \\ \frac{\partial k^d}{\partial \alpha} & \frac{\partial k^d}{\partial \beta} & \frac{\partial k^d}{\partial p_\perp} & \frac{\partial k^d}{\partial \varphi^{(d-3)}} \\ \frac{\partial \vec{k}_\perp^{(d-2)}}{\partial \alpha} & \frac{\partial \vec{k}_\perp^{(d-2)}}{\partial \beta} & \frac{\partial \vec{k}_\perp^{(d-2)}}{\partial p_\perp} & \frac{\partial \vec{k}_\perp^{(d-2)}}{\partial \varphi^{(d-3)}} \end{vmatrix} = \begin{vmatrix} \sqrt{\frac{p_i \cdot p_j}{2}} & \sqrt{\frac{p_i \cdot p_j}{2}} & 0 & (\vec{0}^{(d-3)})^\mathsf{T} \\ \sqrt{\frac{p_i \cdot p_j}{2}} & -\sqrt{\frac{p_i \cdot p_j}{2}} & 0 & (\vec{0}^{(d-3)})^\mathsf{T} \\ \vec{0}^{(d-2)} & \vec{0}^{(d-2)} & \vec{n}_\perp^{(d-2)} & p_\perp \frac{\partial \vec{n}_\perp^{(d-2)}}{\partial \varphi^{(d-3)}} \end{vmatrix} . \tag{A.8}$$

Expanding the determinant one finds

$$J_{p_\perp} = -\left(p_i \cdot p_j\right)\, p_\perp^{d-3} \begin{vmatrix} \vec{n}_\perp^{(d-2)} & \frac{\partial \vec{n}_\perp^{(d-2)}}{\partial \varphi^{(d-3)}} \end{vmatrix} , \tag{A.9}$$

which leads to

$$\mu^{2\varepsilon} \mathrm{d}^d k = \mathrm{d}p_\perp p_\perp \theta(p_\perp)\, \left(p_i \cdot p_j\right) \left(\frac{\mu}{p_\perp}\right)^{2\varepsilon} \mathrm{d}\alpha\, \mathrm{d}\beta\, \mathrm{d}\Omega^{(d-3)} , \tag{A.10}$$

for the integration measure expressed in terms of light-cone coordinates. In high-energy collisions of hadrons one has to deal with particles boosted along a preferred axis, the beam axis. Light-cone coordinates are very convenient for such cases since they have simple transformation properties when a boost is applied and one can also identify which components of momentum dominate [19].

In order to translate back to energy-ordering one can make use of

$$\begin{aligned} p_\perp &= E \sin\theta , \\ \alpha &= \frac{1}{\sqrt{2 p_i \cdot p_j}} \left(k^0 + E\cos\theta\right) , \\ \beta &= \frac{1}{\sqrt{2 p_i \cdot p_j}} \left(k^0 - E\cos\theta\right) , \end{aligned} \tag{A.11}$$

and hence, the Jacobian determinant for reformulating in terms of energy-ordering can be written as

$$J_{(p_\perp \Rightarrow E)} = \begin{vmatrix} \frac{\partial p_\perp}{\partial k^0} & \frac{\partial p_\perp}{\partial E} & \frac{\partial p_\perp}{\partial \cos\theta} \\ \frac{\partial \alpha}{\partial k^0} & \frac{\partial \alpha}{\partial E} & \frac{\partial \alpha}{\partial \cos\theta} \\ \frac{\partial \beta}{\partial k^0} & \frac{\partial \beta}{\partial E} & \frac{\partial \beta}{\partial \cos\theta} \end{vmatrix} = \begin{vmatrix} 0 & \sin\theta & -E\frac{\cos\theta}{\sin\theta} \\ \frac{1}{\sqrt{2 p_i \cdot p_j}} & \frac{\cos\theta}{\sqrt{2 p_i \cdot p_j}} & \frac{E}{\sqrt{2 p_i \cdot p_j}} \\ \frac{1}{\sqrt{2 p_i \cdot p_j}} & -\frac{\cos\theta}{\sqrt{2 p_i \cdot p_j}} & -\frac{E}{\sqrt{2 p_i \cdot p_j}} \end{vmatrix} = \frac{E}{\sin\theta} \frac{1}{p_i \cdot p_j} . \tag{A.12}$$

Making use of the Jacobian in equation (A.12) one correctly obtains the result given in equation (A.4).

Another convenient variable change which is used in section 4.3 is $(\vec{k}_\perp^{(d-2)}, k^d) \to (p_\perp, \eta, \varphi^{(d-3)})$, where η is rapidity. The variables are related by

$$\begin{aligned} \vec{k}_\perp^{(d-2)} &= p_\perp \vec{n}_\perp^{(d-2)}(\varphi^{(d-3)}) , \\ k^d &= p_\perp \sinh\eta . \end{aligned} \tag{A.13}$$

The Jacobian determinant for this translation reads

$$J_\eta = \begin{vmatrix} \frac{\partial k^d}{\partial p_\perp} & \frac{\partial k^d}{\partial \eta} & \frac{\partial k^d}{\partial \varphi^{(d-3)}} \\ \frac{\partial \vec{k}_\perp^{(d-2)}}{\partial p_\perp} & \frac{\partial \vec{k}_\perp^{(d-2)}}{\partial \eta} & \frac{\partial \vec{k}^{(d-2)}}{\partial \varphi^{(d-3)}} \end{vmatrix} = \begin{vmatrix} \sinh\eta & p_\perp \cosh\eta & (\vec{0}^{(d-3)})^\mathsf{T} \\ \vec{n}_\perp^{(d-2)}(\varphi^{(d-3)}) & \vec{0}^{(d-2)} & p_\perp \frac{\partial \vec{n}_\perp^{(d-2)}}{\partial \varphi^{(d-3)}} \end{vmatrix}$$
$$= -p_\perp^{d-2} \cosh\eta \begin{vmatrix} \vec{n}_\perp^{(d-2)}(\varphi^{(d-3)}) & \frac{\partial \vec{n}_\perp^{(d-2)}}{\partial \varphi^{(d-3)}} \end{vmatrix} . \tag{A.14}$$

As a result one obtains for the integral measure

$$\mu^{2\varepsilon} \mathrm{d}^d k = \mathrm{d}k^0 \mathrm{d}p_\perp p_\perp^2 \left(\frac{\mu}{p_\perp}\right)^{2\varepsilon} \mathrm{d}\eta \, \cosh\eta \, \mathrm{d}\Omega^{(d-3)} . \tag{A.15}$$

In collisions of highly energetic hadrons the variable of (pseudo-)rapidity instead of polar angle is commonly used. When applying a boost with respect to the beam axis, the variable of rapidity conveniently transforms just as a translation [19]. In hadron collisions the production of hadrons in the final state is in approximation not changed by such boosts along the beam axis.

One can rewrite the zeroth component of the four-momentum in an exponential form, namely $(\alpha, \beta) = p_\perp (e^\eta, e^{-\eta})$ [19]. Therefore, one finds together with equation (A.11)

$$\alpha + \beta = 2p_\perp \cosh\eta = \frac{2k^0}{\sqrt{2p_i \cdot p_j}} \equiv \frac{2k^0}{\sqrt{s_{ij}}} . \tag{A.16}$$

If one now considers the process of a quark/anti-quark pair (momenta p_i/p_j) radiating a soft gluon (momentum k), one can make use of the typical energy fraction variables $x_a = \frac{2p_a \cdot Q}{Q^2}$ for $Q^\mu = p_i^\mu + p_j^\mu + k^\mu$ [24]. The energy fraction is equal to the energy of the parton a divided by the centre of mass energy of the process. In this case it holds that $x_i + x_j + x_k = 2$. With the energy fraction of the gluon x_k one can reformulate equation (A.16) to get

$$2p_\perp \cosh\eta = x_k \sqrt{s_{ij}} , \tag{A.17}$$

and thus, since the energy fraction lies in the interval $[0, 1]$, one is lead to [24]

$$\ln\left(\frac{\sqrt{s_{ij}}}{p_\perp}\right) \geq \ln(2\cosh\eta) \simeq |\eta| . \tag{A.18}$$

This corresponds to a triangle-shaped region in a phase space expressed in the variables of rapidity η and $\kappa = \frac{1}{2}\ln\left(\frac{p_\perp}{\Lambda}\right)$, where Λ is some cut-off scale. This region of phase space defines the so-called Lund-plane.

B QCD-Feynman rules

In this appendix the QCD Feynman rules are listed, in particular in order to establish the convention of momentum flow of the triple gluon vertex which is used throughout this work.

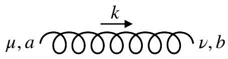

$$= \frac{-i\left(g^{\mu\nu} - (1-\xi)\frac{k^\mu k^\nu}{k^2}\right)}{k^2 + i0}\delta^{ab}$$

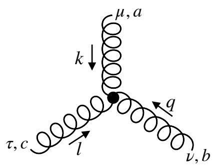

$$= -gf^{abc}\left[(k-q)^\tau g^{\mu\nu} + (q-l)^\mu g^{\nu\tau} + (l-k)^\nu g^{\mu\tau}\right]$$

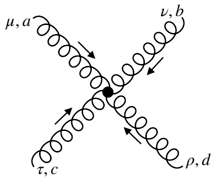

$$= -ig^2\Big[f^{eac}f^{ebd}\left(g^{\mu\nu}g^{\tau\rho} - g^{\mu\rho}g^{\nu\tau}\right) + f^{ead}f^{ebc}\left(g^{\mu\nu}g^{\tau\rho} - g^{\mu\tau}g^{\nu\rho}\right)$$
$$+ f^{eab}f^{ecd}\left(g^{\mu\tau}g^{\rho\nu} - g^{\mu\rho}g^{\nu\tau}\right)\Big]$$

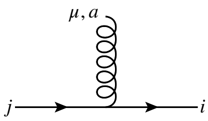

$$= ig\gamma^\mu(t^a)^i{}_j$$

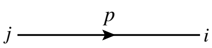

$$= \frac{i(\not{p} + m)}{p^2 - m^2 + i0}\delta^i_j$$

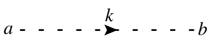

$$= \frac{i}{k^2 + i0}\delta^{ab}$$

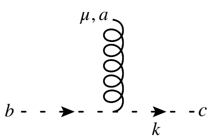

$$= gf^{abc}k^\mu$$

Note that in this work the mass of the fermion propagator has been neglected, all hard partons are considered to be massless in the high energy scatterings (which is a valid approximation for up-, down- and strange-quarks).

C Colour-flow Feynman rules

In this part of the appendix the colour-flow Feynman rules are motivated and listed. As an alternative to the method presented in section 3.2 one may immediately use Feynman rules where the part which concerns the colour structure is already expressed in terms of colour-flow Kronecker deltas.

In order to reformulate the part concerning the colour structure of the usual QCD Feynman rules one aims to convert adjoint indices into fundamental ones. This can be performed by using the replacement rule

$$A^{a\cdots} \to (A^{\cdots})^i{}_j = \frac{1}{\sqrt{T_R}} A^{a\cdots} (t^a)^i{}_j \ , \tag{C.1}$$

where the ellipsis in the exponent of the general object A stand for possible other adjoint indices in addition to a. Further, the Fierz identity and the trace identity of equation (3.12) are convenient for rewriting.

For the quark-gluon vertex, only focusing on the colour structure, one finds when using equation (C.1)

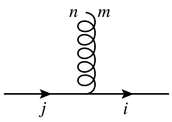

$$= (t^a)^i{}_j \to \frac{1}{\sqrt{T_R}} (t^a)^i{}_j (t^a)^m_n = \frac{T_R}{\sqrt{T_R}} \left(\delta^i_n \delta^m_j - \frac{1}{N} \delta^i_j \delta^m_n \right) \ , \tag{C.2}$$

where the term proportional to $1/N$ can be dropped for the coupling, due to the fact the whole term in the round brackets is a projector, i.e. $P^{im}_{jn} = \delta^i_n \delta^m_j - \frac{1}{N} \delta^i_j \delta^m_n$ [4]. However, if there are external gluons one needs to multiply by the projector such that the colour sum evaluates to $N^2 - 1$ instead of N^2, which would otherwise be the case. The factor of T_R in equation (C.2) is written in this way, since it may be convenient to absorb the factor of $1/\sqrt{T_R}$ into the coupling.

For the gluon propagator one finds

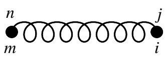

$$= \delta^{ab} = \delta^{ac}\delta^{cb} = \left(\frac{1}{\sqrt{T_R}} (t^a)^i{}_j \right) \left(\frac{1}{\sqrt{T_R}} (t^b)^n{}_m \right) \left(\delta^j_n \delta^m_i - \frac{1}{N} \delta^j_i \delta^m_n \right) \ , \tag{C.3}$$

where the factors with the generators are to be taken out of the Feynman rule for the gluon propagator, since they are already part of the quark-gluon vertex by using the replacement rule in equation (C.1).

For the triple gluon vertex one can rewrite

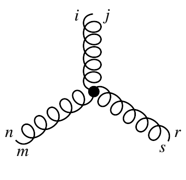

$$= f^{abc} \to \frac{1}{\sqrt{T_R}} \frac{1}{T_R} f^{abc} (t^a)^i{}_j (t^b)^m{}_n (t^c)^r{}_s = \frac{T_R}{\sqrt{T_R}} \left(\delta^i_n \delta^r_j \delta^m_s - \delta^i_s \delta^m_j \delta^r_n \right) \ . \tag{C.4}$$

The colour-flow Feynman rules are listed in the following [4]

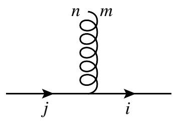

$$\propto \delta_n^i \delta_j^m$$

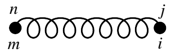

$$\propto \left(\delta_n^j \delta_i^m - \frac{1}{N} \delta_i^j \delta_n^m \right)$$

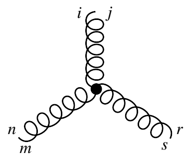

$$\propto \left(\delta_n^i \delta_j^r \delta_s^m - \delta_s^i \delta_j^m \delta_n^r \right)$$

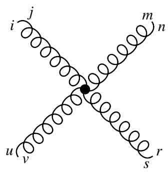

$$\propto \left(\delta_n^i \delta_s^m \delta_v^r \delta_j^u + \delta_n^i \delta_j^r \delta_s^u \delta_v^m + \delta_n^r \delta_s^u \delta_v^i \delta_j^m \right.$$
$$\left. - \delta_s^i \delta_j^u \delta_v^m \delta_n^r - \delta_n^u \delta_v^r \delta_s^i \delta_j^m - \delta_s^m \delta_n^u \delta_v^i \delta_j^r \right)$$

As an illustration one may evaluate the gluon emission from the different types of parton lines once again with this procedure and compare the results to equations (3.13)-(3.15). For the gluon emission off a quark line one finds

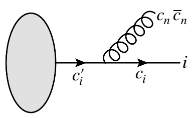

$$= \sqrt{T_R}\, \delta_n^{\alpha_{c_i}} \delta^m_{\beta_{c_i'}} P^{n,\alpha_{c_n}}_{m,\beta_{\bar{c}_n}} = \sqrt{T_R} \left(\delta^{\alpha_{c_i}}_{\beta_{\bar{c}_n}} \delta^{\alpha_{c_n}}_{\beta_{c_i'}} - \frac{1}{N} \delta^{\alpha_{c_i}}_{\beta_{c_i'}} \delta^{\alpha_{c_n}}_{\beta_{\bar{c}_n}} \right) , \tag{C.5}$$

where the projection operator has to be applied due to the presence of the external gluon. A gluon emission off an anti-quark line leads to

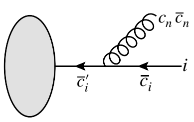

$$= -\sqrt{T_R}\, \delta^m_{\beta_{\bar{c}_i}} \delta_n^{\alpha_{\bar{c}_i'}} P^{n,\alpha_{c_n}}_{m,\beta_{\bar{c}_n}} = -\sqrt{T_R} \left(\delta^{\alpha_{\bar{c}_i'}}_{\beta_{\bar{c}_n}} \delta^{\alpha_{c_n}}_{\beta_{\bar{c}_i}} - \frac{1}{N} \delta^{\alpha_{\bar{c}_i'}}_{\beta_{\bar{c}_i}} \delta^{\alpha_{c_n}}_{\beta_{\bar{c}_n}} \right) . \tag{C.6}$$

Finally, for a gluon emission off a gluon line one does not have to multiply by the projection operator, since all of the $1/N$-terms have to cancel. Hence, one obtains

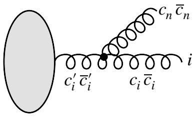

$$
\begin{aligned}
&= \left(\delta^{\alpha_{c'_i}}_{\beta_{c'_i}} \delta^{\alpha_{\bar{c}'_i}}_{\beta_{\bar{c}'_i}} - \frac{1}{N} \delta^{\alpha c'_i}_{\beta_{\bar{c}'_i}} \delta^{\alpha_{\bar{c}'_i}}_{\beta_{c'_i}} \right) \left(\delta^{\alpha_{c_n}}_{\alpha_{c'_i}} \delta^{\alpha_{c_i}}_{\beta_{\bar{c}_n}} \delta^{\beta_{\bar{c}'_i}}_{\beta_{\bar{c}_i}} - \delta^{\alpha_{c_i}}_{\alpha_{c'_i}} \delta^{\alpha_{c_n}}_{\beta_{\bar{c}_i}} \delta^{\beta_{\bar{c}'_i}}_{\beta_{\bar{c}_n}} \right) \\
&= \sqrt{T_R} \left(\delta^{\alpha_{c_n}}_{\beta_{c'_i}} \delta^{\alpha_{c_i}}_{\beta_{\bar{c}_n}} \delta^{\alpha_{\bar{c}'_i}}_{\beta \bar{c}_i} - \delta^{\alpha_{c_i}}_{\beta_{c'_i}} \delta^{\alpha_{c_n}}_{\beta_{\bar{c}_i}} \delta^{\alpha_{\bar{c}'_i}}_{\beta \bar{c}_n} \right) \ .
\end{aligned}
\tag{C.7}
$$

These results match the expressions found in equations (3.13)-(3.15).

D Two-loop current in Feynman gauge

In this appendix the calculation of squaring the two-loop current in Feynman-t'Hooft gauge is given in detail and the result of [10] can be reproduced. For convenience the two-loop current is written here once again (cf. equation (5.41)) [10]

$$\begin{aligned}\mathbf{J}^{\mu\nu}_{bc}(q,k) &= \frac{1}{2}\{\mathbf{J}^{\mu}_{b}(q),\mathbf{J}^{\nu}_{c}(k)\}\\ &+ if_{abc}\sum_{l}\mathbf{T}^{a}_{l}\left\{\frac{p_i^\nu q^\mu - p_i^\mu k^\nu}{(k\cdot q)(p_i\cdot(q+k))} - \frac{p_i\cdot(q-k)}{2(p_i\cdot(q+k))}\left[\frac{p_i^\mu p_i^\nu}{(p_i\cdot q)(p_i\cdot k)} + \frac{g^{\mu\nu}}{k\cdot q}\right]\right\} .\end{aligned} \tag{D.1}$$

Squaring this expression in Feynman gauge amounts to evaluating $(\mathbf{J}^{a_1a_2}_{\mu\tau}(q,k))^\dagger(-g^{\mu\nu})(-g^{\tau\lambda})$ $\mathbf{J}^{a_1a_2}_{\nu\lambda}(q,k)$, which consists of four contributions. The first one is

$$\begin{aligned}&\frac{1}{4}\left\{\mathbf{J}^{a_1}_{\mu}(q),\mathbf{J}^{a_2}_{\tau}(k)\right\}\left\{\mathbf{J}^{\mu\,a_1}(q),\mathbf{J}^{\tau\,a_2}(k)\right\} =\\ &\frac{1}{2}\{\mathbf{J}^2(q),\mathbf{J}^2(k)\} + \frac{1}{4}\left(\mathbf{J}^{a_1}_{\mu}(q)\left[\mathbf{J}^{a_2}_{\tau}(k),\mathbf{J}^{\mu\,a_1}(q)\right]\mathbf{J}^{\tau\,a_2}(k) + \mathbf{J}^{a_2}_{\tau}(k)\left[\mathbf{J}^{a_1}_{\mu}(q),\mathbf{J}^{\tau\,a_2}(k)\right]\mathbf{J}^{\mu\,a_1}(q)\right)\\ &+\frac{1}{4}\left(\mathbf{J}^{a_1}_{\mu}(q)\left[\mathbf{J}^2(k),\mathbf{J}^{\mu\,a_1}(q)\right] + \mathbf{J}^{a_2}_{\tau}(k)\left[\mathbf{J}^2(q),\mathbf{J}^{\tau\,a_2}(k)\right]\right)\\ &= \frac{1}{2}\{\mathbf{J}^2(q),\mathbf{J}^2(k)\} + \frac{3}{4}C_A\sum_{i,j}(\mathbf{T}_i\cdot\mathbf{T}_j)\frac{(p_i\cdot p_j)^2}{(p_i\cdot q)(p_i\cdot k)(p_j\cdot q)(p_j\cdot k)} ,\end{aligned} \tag{D.2}$$

where the second term of the result above can be found by carefully evaluating the colour algebra of the commutators of the one-loop currents in the first and second line of equation (D.2). Since it holds that

$$[\mathbf{J}^{a_2}_{\tau}(k),\mathbf{J}^{\mu\,a_1}(q)] = \sum_{i,j}\left[\mathbf{T}^{a_2}_{i},\mathbf{T}^{a_1}_{j}\right]\frac{p_{i\tau}p_j^\mu}{(p_i\cdot k)(p_j\cdot q)} = \begin{cases}0, & \text{if i}\neq\text{j}\\ \sum_i if^{a_2a_1c}\mathbf{T}^{c}_{i}\frac{p_{i\tau}p_i^\mu}{(p_i\cdot k)(p_i\cdot q)}, & \text{else} ,\end{cases} \tag{D.3}$$

the terms with the commutators in the second line of equation (D.2) can be written as

$$\begin{aligned}&\frac{1}{4}\left(\mathbf{J}^{a_1}_{\mu}(q)\left[\mathbf{J}^{a_2}_{\tau}(k),\mathbf{J}^{\mu\,a_1}(q)\right]\mathbf{J}^{\tau\,a_2}(k) + \mathbf{J}^{a_2}_{\tau}(k)\left[\mathbf{J}^{a_1}_{\mu}(q),\mathbf{J}^{\tau\,a_2}(k)\right]\mathbf{J}^{\mu\,a_1}(q)\right)\\ &= \frac{1}{4}\sum_{i,j,l}if^{a_1a_2c}\left(\mathbf{T}^{a_2}_{l}\mathbf{T}^{c}_{i}\mathbf{T}^{a_1}_{j} - \mathbf{T}^{a_1}_{j}\mathbf{T}^{c}_{i}\mathbf{T}^{a_2}_{l}\right)\frac{(p_i\cdot p_j)(p_i\cdot p_l)}{(p_i\cdot k)(p_i\cdot q)(p_j\cdot q)(p_l\cdot k)} .\end{aligned} \tag{D.4}$$

By performing a case analysis one finds that for $i = j \neq l$, $i = l \neq j$ and $i = j = l$ the result vanishes due to the fact that the hard momenta are on-shell. Furthermore for $i \neq j \neq l$ the colour charge operators commute and one gets a vanishing result as well. Only in the case $j = l \neq i$ one obtains a non-vanishing contribution which can be cast into the form

$$\begin{aligned}&\frac{1}{4}\left(\mathbf{J}^{a_1}_{\mu}(q)\left[\mathbf{J}^{a_2}_{\tau}(k),\mathbf{J}^{\mu\,a_1}(q)\right]\mathbf{J}^{\tau\,a_2}(k) + \mathbf{J}^{a_2}_{\tau}(k)\left[\mathbf{J}^{a_1}_{\mu}(q),\mathbf{J}^{\tau\,a_2}(k)\right]\mathbf{J}^{\mu\,a_1}(q)\right)\\ &= \frac{1}{4}\sum_{i,j}C_A(\mathbf{T}_i\cdot\mathbf{T}_j)\frac{(p_i\cdot p_j)^2}{(p_i\cdot q)(p_i\cdot k)(p_j\cdot q)(p_j\cdot k)} .\end{aligned} \tag{D.5}$$

Similarly, one can proceed for the contribution of the third line in equation (D.2) which leads one to

$$\begin{aligned} &\frac{1}{4}\left(\mathbf{J}_{\mu}^{a_1}(q)\left[\mathbf{J}^2(k),\mathbf{J}^{\mu\, a_1}(q)\right]+\mathbf{J}_{\tau}^{a_2}(k)\left[\mathbf{J}^2(q),\mathbf{J}^{\tau\, a_2}(k)\right]\right)\\ &=\frac{1}{2}\sum_{i,j}C_A(\mathbf{T}_i\cdot\mathbf{T}_j)\frac{(p_i\cdot p_j)^2}{(p_i\cdot q)(p_i\cdot k)(p_j\cdot q)(p_j\cdot k)}\ . \end{aligned} \tag{D.6}$$

In this way one finds the result in equation (D.2).

When multiplying the term of the second line of equation (D.1) with its adjoint counterpart and contracting the indices one finds

$$\begin{aligned} C_A\sum_{i,j}(\mathbf{T}_i\cdot\mathbf{T}_j)\Bigg\{&\frac{(p_i\cdot p_j)^2\, p_i\cdot(q-k)\, p_j\cdot(q-k)}{4p_i\cdot(k+q)\, p_j\cdot(k+q)(p_i\cdot q)(p_i\cdot k)(p_j\cdot k)(p_j\cdot q)}\\ &+\frac{d\, p_i\cdot(q-k)\, p_j\cdot(q-k)}{4(k\cdot q)^2 p_i\cdot(k+q)p_j\cdot(k+q)}-\frac{(p_i\cdot q)(p_i\cdot k)+(p_i\cdot k)(p_j\cdot k)}{2(k\cdot q)^2 p_i\cdot(k+q)p_j\cdot(k+q)}\\ &+\frac{p_i\cdot p_j}{2(k\cdot q)p_i\cdot(k+q)\, p_j\cdot(k+q)}\left(4-\frac{p_i\cdot k}{p_i\cdot q}-\frac{p_i\cdot q}{p_i\cdot k}-\frac{p_j\cdot q}{p_j\cdot k}-\frac{p_j\cdot k}{p_j\cdot q}\right)\Bigg\}\ , \end{aligned} \tag{D.7}$$

which can be rewritten as

$$\begin{aligned} C_A\sum_{i,j}(\mathbf{T}_i\cdot\mathbf{T}_j)\Bigg\{&-\frac{(1-\varepsilon)((p_i\cdot k)(p_j\cdot q)+(p_i\cdot q)(p_j\cdot k))}{(k\cdot q)^2 p_i\cdot(k+q)\, p_j\cdot(k+q)}\\ &+\frac{(p_i\cdot p_j)^2}{2(p_i\cdot q)(p_i\cdot k)(p_j\cdot q)(p_j\cdot k)}\left[\frac{1}{2}-\frac{(p_i\cdot q)(p_j\cdot k)+(p_i\cdot k)(p_j\cdot q)}{p_i\cdot(k+q)\, p_j\cdot(k+q)}\right]\\ &+\frac{p_i\cdot p_j}{2(k\cdot q)}\Bigg[\frac{6}{p_i\cdot(k+q)\, p_j\cdot(k+q)}-\frac{p_j\cdot q}{p_i\cdot(k+q)\, p_j\cdot(k+q)(p_j\cdot k)}\\ &-\frac{p_j\cdot k}{p_i\cdot(k+q)\, p_j\cdot(k+q)(p_j\cdot q)}-\frac{1}{p_j\cdot(k+q)(p_i\cdot q)}-\frac{1}{p_j\cdot(k+q)(p_i\cdot k)}\Bigg]\Bigg\}\ . \end{aligned} \tag{D.8}$$

Finally, the last two terms of the product of currents (i.e. the product of the anti-commutator with the adjoint contribution of the second line of equation (D.1) and vice versa) contributes a factor of

$$\frac{1}{2}if^{a_1a_2c}\sum_{i,j,l}\frac{p_j^{\mu}p_l^{\tau}}{(p_j\cdot q)(p_l\cdot k)}\Gamma_{\mu\tau}\left(\mathbf{T}_j^{a_1}\mathbf{T}_l^{a_2}\mathbf{T}_i^{c}+\mathbf{T}_l^{a_2}\mathbf{T}_j^{a_1}\mathbf{T}_i^{c}-\mathbf{T}_i^{c}\mathbf{T}_j^{a_1}\mathbf{T}_l^{a_2}-\mathbf{T}_i^{c}\mathbf{T}_l^{a_2}\mathbf{T}_j^{a_1}\right)\ , \tag{D.9}$$

where $\Gamma_{\mu\tau}$ refers to the second line of equation (D.1) without the colour structure. Distinguishing the different cases for labels of the hard lines i,j and l one obtains the following result for equation (D.9)

$$-C_A\sum_{i,j}\frac{p_i\cdot p_j}{2(k\cdot q)}\left[\frac{1}{(p_i\cdot q)(p_j\cdot k)}+\frac{1}{(p_i\cdot k)(p_j\cdot q)}\right]\ , \tag{D.10}$$

since non-vanishing contributions only occur for the cases $(j \neq l, i = j)$ and $(j \neq l, i = l)$. Combining equations (D.2), (D.8) and (D.10) leads one to

$$(\mathbf{J}^{a_1 a_2}_{\mu\tau}(q,k))^{\dagger}\mathbf{J}^{\mu\tau\, a_1 a_2}(q,k) = \frac{1}{2}\{\mathbf{J}^2(q), \mathbf{J}^2(k)\} + C_A \sum_{i,j}(\mathbf{T}_i \cdot \mathbf{T}_j) S_{ij} \ , \tag{D.11}$$

where the factor S_{ij} has the following form

$$\begin{aligned} S_{ij} = & \frac{(p_i \cdot p_j)^2}{2(p_i \cdot k)(p_i \cdot q)(p_j \cdot k)(p_j \cdot q)} \left[2 - \frac{(p_i \cdot q)(p_j \cdot k) + (p_i \cdot k)(p_j \cdot q)}{p_i \cdot (k+q)\, p_j \cdot (k+q)} \right] \\ & - \frac{(1-\varepsilon)((p_i \cdot k)(p_j \cdot q) + (p_i \cdot q)(p_j \cdot k))}{(k \cdot q)^2 p_i \cdot (k+q)\, p_j \cdot (k+q)} - \frac{p_i \cdot p_j}{2(k \cdot q)} \left[\frac{2}{(p_i \cdot q)(p_j \cdot k)} + \frac{2}{(p_i \cdot k)(p_j \cdot q)} \right. \\ & \left. - \frac{1}{p_i \cdot (k+q)\, p_j \cdot (k+q)} \left(4 + \frac{((p_i \cdot q)(p_j \cdot k) + (p_i \cdot k)(p_j \cdot q))^2}{(p_i \cdot q)(p_i \cdot k)(p_j \cdot q)(p_j \cdot k)} \right) \right] \ , \end{aligned} \tag{D.12}$$

which coincides with the expression in equation (5.43) and thus one can reproduce the result in [10].

E Colour structures in the colour-flow basis

In this appendix the detailed results for the matrix elements in the colour-flow basis of the colour structures from the one-loop/one-emission Feynman diagrams depicted in Figure 13 are given. To find these results, the colour structures of the diagrams have been analysed in analogy to the one-loop case described in section 4.2.

E.1 One-loop/one-emission order

Writing the colour structure of diagram (a) in Figure 13 as a matrix element in the colour-flow basis leads to

$$
\begin{aligned}
[\tau|\mathbf{T}_i(\mathbf{T}_i\cdot\mathbf{T}_j)\,|\sigma\rangle = N^2\delta_{\sigma\tau\backslash n}\Bigg[&\frac{1}{N^2}(\lambda_i-\bar{\lambda}_i)\left(\lambda_i\bar{\lambda}_j\delta_{c_i\sigma^{-1}(\bar{c}_j)}\delta_{c_n\tau^{-1}(\bar{c}_n)}+\bar{\lambda}_i\lambda_j\delta_{c_j\sigma^{-1}(\bar{c}_i)}\delta_{c_n\tau^{-1}(\bar{c}_n)}\right)\\
&+\frac{1}{N^4}(\lambda_i-\bar{\lambda}_i)^2(\lambda_j-\bar{\lambda}_j)\delta_{c_n\tau^{-1}(\bar{c}_n)}\Bigg]\\
&+\sum_{(a,b)}\delta_{\sigma\tau_{(a,b)}\backslash n}\Big[N\left(\bar{\lambda}_i^2\lambda_j\delta_{c_j\sigma^{-1}(\bar{c}_i)}\delta_{(a,b)(c_j,c_n)}-\lambda_i^2\bar{\lambda}_j\delta_{c_i\sigma^{-1}(\bar{c}_j)}\delta_{(a,b)(c_i,c_n)}\right.\\
&\left.+\lambda_i\bar{\lambda}_i\lambda_j\delta_{c_i\sigma^{-1}(\bar{c}_j)}\delta_{(a,b)(\sigma^{-1}(\bar{c}_i),c_n)}-\lambda_i\bar{\lambda}_i\lambda_j\delta_{c_j\sigma^{-1}(\bar{c}_i)}\delta_{(a,b)(c_i,c_n)}\right)\\
&+\frac{1}{N}\delta_{c_n\tau^{-1}(\bar{c}_n)}(\lambda_i-\bar{\lambda}_i)\left(\lambda_i\bar{\lambda}_j\delta_{(a,b)(c_i,\sigma^{-1}(\bar{c}_j))}+\bar{\lambda}_i\lambda_j\delta_{(a,b)(c_j,\sigma^{-1}(\bar{c}_i))}\right.\\
&\left.-\lambda_i\lambda_j\delta_{(a,b)(c_i,c_j)}-\bar{\lambda}_i\bar{\lambda}_j\delta_{(a,b)(\sigma^{-1}(\bar{c}_j),\sigma^{-1}(\bar{c}_i))}\right)\\
&-\frac{1}{N}(\lambda_i-\bar{\lambda}_i)(\lambda_j-\bar{\lambda}_j)\left(\lambda_i\delta_{(a,b)(c_i,c_n)}-\bar{\lambda}_i\delta_{(a,b)(\sigma^{-1}(\bar{c}_i),c_n)}\right)\Big]\\
&+\sum_{(a,b)}\sum_{(b,c)}\delta_{\sigma\tau_{(a,b)(b,c)}\backslash n}\\
&\Big[\lambda_i^2\lambda_j\delta_{(a,b)(c_n,c_i)}\delta_{(b,c)(c_i,c_j)}+\bar{\lambda}_i^2\lambda_j\delta_{(a,b)(c_n,c_j)}\delta_{(b,c)(c_j,\sigma^{-1}(\bar{c}_i))}\\
&-\lambda_i^2\bar{\lambda}_j\delta_{(a,b)(c_n,c_i)}\delta_{(b,c)(c_i,\sigma^{-1}(\bar{c}_j))}-\bar{\lambda}_i^2\bar{\lambda}_j\delta_{(a,b)(c_n,\sigma^{-1}(\bar{c}_j))}\delta_{(b,c)(\sigma^{-1}(\bar{c}_j),\sigma^{-1}(\bar{c}_i))}\Big]\\
&+\sum_{(a,b)}\sum_{(c,d)}\delta_{\sigma\tau_{(a,b)(c,d)}\backslash n}\lambda_i\bar{\lambda}_i\left[\delta_{(a,b)(\sigma^{-1}(\bar{c}_i),c_n)}\left(\bar{\lambda}_j\delta_{(c,d)(c_i,\sigma^{-1}(\bar{c}_j))}-\lambda_j\delta_{(c,d)(c_i,c_j)}\right)\right.\\
&\left.+\delta_{(a,b)(c_i,c_n)}\left(\bar{\lambda}_j\delta_{(c,d)(\sigma^{-1}(\bar{c}_i),\sigma^{-1}(\bar{c}_j))}-\lambda_j\delta_{(c,d)(c_j,\sigma^{-1}(\bar{c}_i))}\right)\right]\ ,
\end{aligned}
\tag{E.1}
$$

where this result, as in the one-loop case, includes all of the different combinations of types of partons for the external lines encoded in the factors of $\lambda_{i,j}$. Compared to the one-loop result, there are several new structures appearing. First of all, there are not only single swaps of the colour labels, but also double swaps of the form $(a,b)(b,c)$ have to be performed such that the colour labels of the emitted gluon are merged and the permutations σ and τ match. Further, one finds terms which involve two swaps of different colour labels, which are, however, only present for a hard gluon line i. This is another difference to the one-loop case, at one-loop/one-emission level one finds terms which exclusively contribute for external gluon lines.

For the colour structure of diagram 13(b) where the emission of the soft gluon takes place after the virtual exchange one finds a different matrix element

$$
\begin{aligned}
[\tau|(\mathbf{T}_i\cdot\mathbf{T}_j)\mathbf{T}_i\,|\sigma\rangle = {} & N^2\delta_{\sigma\tau\backslash n}\delta_{c_n\tau^{-1}(\bar{c}_n)}\left[\frac{1}{N^2}\left(\lambda_i\bar{\lambda}_i\lambda_j\delta_{c_j\sigma^{-1}(\bar{c}_i)}-\lambda_i\bar{\lambda}_i\bar{\lambda}_j\delta_{c_i\sigma^{-1}(\bar{c}_j)}\right)\right.\\
&\left.+\frac{1}{N^4}(\lambda_i-\bar{\lambda}_i)^2(\lambda_j-\bar{\lambda}_j)\right]\\
&+\sum_{(a,b)}\delta_{\sigma\tau_{(a,b)}\backslash n}\left[N\lambda_i\bar{\lambda}_i\left(\bar{\lambda}_j\delta_{c_i\sigma^{-1}(\bar{c}_j)}\delta_{(a,b)(\sigma^{-1}(\bar{c}_i),c_n)}-\lambda_j\delta_{c_j\sigma^{-1}(\bar{c}_i)}\delta_{(a,b)(c_i,c_n)}\right)\right.\\
&+\frac{1}{N}\delta_{c_n\tau^{-1}(\bar{c}_n)}(\lambda_i-\bar{\lambda}_i)\left(\bar{\lambda}_j\lambda_i\delta_{(a,b)(c_i,\sigma^{-1}(\bar{c}_j))}+\bar{\lambda}_i\lambda_j\delta_{(a,b)(\sigma^{-1}(\bar{c}_i),c_j)}\right.\\
&\left.-\lambda_i\lambda_j\delta_{(a,b)(c_i,c_j)}-\bar{\lambda}_i\bar{\lambda}_j\delta_{(a,b)(\sigma^{-1}(\bar{c}_i),\sigma^{-1}(\bar{c}_j))}\right)\\
&\left.-\frac{1}{N}\lambda_i(\lambda_i-\bar{\lambda}_i)(\lambda_j-\bar{\lambda}_j)\delta_{(a,b)(c_i,c_n)}+\frac{1}{N}\bar{\lambda}_i(\lambda_i-\bar{\lambda}_i)(\lambda_j-\bar{\lambda}_j)\delta_{(a,b)(\sigma^{-1}(\bar{c}_i),c_n)}\right]\\
&+\sum_{(a,b)}\sum_{(b,c)}\delta_{\sigma\tau_{(a,b)(b,c)}\backslash n}\\
&\left[\lambda_i^2\lambda_j\delta_{(a,b)(c_n,c_j)}\delta_{(b,c)(c_j,c_i)}+\bar{\lambda}_i^2\lambda_j\delta_{(a,b)(c_n,\sigma^{-1}(\bar{c}_i))}\delta_{(b,c)(\sigma^{-1}(\bar{c}_i),c_j)}\right.\\
&-\lambda_i^2\bar{\lambda}_j\delta_{(a,b)(c_n,\sigma^{-1}(\bar{c}_j))}\delta_{(b,c)(\sigma^{-1}(\bar{c}_j),c_i)}-\bar{\lambda}_i^2\bar{\lambda}_j\delta_{(a,b)(c_n,\sigma^{-1}(\bar{c}_i))}\delta_{(b,c)(\sigma^{-1}(\bar{c}_i),\sigma^{-1}(\bar{c}_j))}\\
&\left.-\lambda_i\bar{\lambda}_i\lambda_j\delta_{c_j\sigma^{-1}(\bar{c}_i)}\delta_{(a,b)(c_n,c_i)}\delta_{(b,c)(c_i,c_j)}+\lambda_i\bar{\lambda}_i\bar{\lambda}_j\delta_{c_i\sigma^{-1}(\bar{c}_j)}\delta_{(a,b)(c_n,c_i)}\delta_{(b,c)(c_i,\sigma^{-1}(\bar{c}_i))}\right]\\
&+\sum_{(a,b)}\sum_{(c,d)}\delta_{\sigma\tau_{(a,b)(c,d)}\backslash n}\lambda_i\bar{\lambda}_i\left[\bar{\lambda}_j\left(\delta_{(a,b)(\sigma^{-1}(\bar{c}_i),c_n)}\delta_{(c,d)(c_i,\sigma^{-1}(\bar{c}_j))}\right.\right.\\
&\left.-\delta_{(a,b)(c_i,c_n)}\delta_{(c,d)(\sigma^{-1}(\bar{c}_i),\sigma^{-1}(\bar{c}_j))}\right)\\
&\left.-\lambda_j\left(\delta_{(a,b)(\sigma^{-1}(\bar{c}_i),c_n)}\delta_{(c,d)(c_i,c_j)}+\delta_{(a,b)(c_i,c_n)}\delta_{(c,d)(\sigma^{-1}(\bar{c}_i),c_j)}\right)\right]\ .
\end{aligned}
\tag{E.2}
$$

The diagram with the the triple gluon vertex in Figure 13(c) gives a much shorter result than the previous two colour structures, since in this case there are no U(1)-gluon contributions and therefore also no $1/N$ suppressed terms occur

$$
\begin{aligned}
[\tau|\mathbf{T}_g\mathbf{T}_i\mathbf{T}_j\,|\sigma\rangle = {} & \sqrt{T_R}\left\{\delta_{\sigma\tau\backslash n}\delta_{c_n\tau^{-1}(\bar{c}_n)}\left[-\lambda_i\bar{\lambda}_j\delta_{c_i\sigma^{-1}(\bar{c}_j)}+\bar{\lambda}_i\lambda_j\delta_{c_j\sigma^{-1}(\bar{c}_i)}\right]\right.\\
&+N\sum_{(a,b)}\delta_{\sigma\tau_{(a,b)}\backslash n}\left[\lambda_i\bar{\lambda}_j\delta_{c_i\sigma^{-1}(\bar{c}_j)}\delta_{(a,b)(c_i,c_n)}-\bar{\lambda}_i\lambda_j\delta_{c_j\sigma^{-1}(\bar{c}_i)}\delta_{(a,b)(c_j,c_n)}\right]\\
&+\sum_{(a,b)}\sum_{(b,c)}\delta_{\sigma\tau_{(a,b)(b,c)}\backslash n}\\
&\left[\lambda_i\bar{\lambda}_j\left(\delta_{(a,b)(c_n,c_i)}\delta_{(b,c)(c_i,\sigma^{-1}(\bar{c}_j))}-\delta_{(a,b)(c_n,\sigma^{-1}(\bar{c}_j))}\delta_{(b,c)(\sigma^{-1}(\bar{c}_j),c_i)}\right)\right.\\
&+\bar{\lambda}_i\lambda_j\left(\delta_{(a,b)(c_n,\sigma^{-1}(\bar{c}_i))}\delta_{(b,c)(\sigma^{-1}(\bar{c}_i),c_j)}-\delta_{(a,b)(c_n,c_j)}\delta_{(b,c)(c_j,\sigma^{-1}(\bar{c}_i))}\right)\\
&+\lambda_i\lambda_j\left(\delta_{(a,b)(c_n,c_j)}\delta_{(b,c)(c_j,c_i)}-\delta_{(a,b)(c_n,c_i)}\delta_{(b,c)(c_i,c_j)}\right)\\
&+\bar{\lambda}_i\bar{\lambda}_j\left(\delta_{(a,b)(c_n,\sigma^{-1}(\bar{c}_j))}\delta_{(b,c)(\sigma^{-1}(\bar{c}_j),\sigma^{-1}(\bar{c}_i))}\right.\\
&\left.\left.\left.-\delta_{(a,b)(c_n,\sigma^{-1}(\bar{c}_i))}\delta_{(b,c)(\sigma^{-1}(\bar{c}_i),\sigma^{-1}(\bar{c}_j))}\right)\right]\right\}\ ,
\end{aligned}
\tag{E.3}
$$

where $\mathbf{T}_g = if_{abc}$ and there is an overall factor of $\sqrt{T_R}$, since for the gluon vertex one does not encode this factor with the $\lambda_{i,j}$ variables. For the diagram with three hard lines (see Figure 13(d)) one finds

$$
\begin{aligned}
[\tau|(\mathbf{T}_i \cdot \mathbf{T}_j)\mathbf{T}_l|\sigma\rangle =& N^2 \delta_{\sigma\tau\backslash n}\delta_{c_n\tau^{-1}(\bar{c}_n)} \Bigg[\frac{1}{N^4}(\lambda_i - \bar{\lambda}_i)(\lambda_j - \bar{\lambda}_j)(\lambda_l - \bar{\lambda}_l) \\
&+ \frac{1}{N^2}\left(\bar{\lambda}_i\lambda_j(\lambda_l - \bar{\lambda}_l)\delta_{c_j\sigma^{-1}(\bar{c}_i)} + \lambda_i\bar{\lambda}_j(\lambda_l - \bar{\lambda}_l)\delta_{c_i\sigma^{-1}(\bar{c}_j)}\right)\Bigg] \\
&+ \sum_{(a,b)} \delta_{\sigma\tau_{(a,b)}\backslash n}\Big[N\delta_{(a,b)(\sigma^{-1}(\bar{c}_l),c_n)}\left(\lambda_i\bar{\lambda}_j\bar{\lambda}_l\delta_{c_i\sigma^{-1}(\bar{c}_j)} + \bar{\lambda}_i\lambda_j\bar{\lambda}_l\delta_{c_j\sigma^{-1}(\bar{c}_i)}\right) \\
&- N\delta_{(a,b)(c_l,c_n)}\left(\lambda_i\bar{\lambda}_j\lambda_l\delta_{c_i\sigma^{-1}(\bar{c}_j)} + \bar{\lambda}_i\lambda_j\lambda_l\delta_{c_j\sigma^{-1}(\bar{c}_i)}\right) \\
&+ \frac{1}{N}(\lambda_i - \bar{\lambda}_i)(\lambda_j - \bar{\lambda}_j)\left(\bar{\lambda}_l\delta_{(a,b)(\sigma^{-1}(\bar{c}_l),c_n)} - \lambda_l\delta_{(a,b)(c_l,c_n)}\right) \\
&+ \frac{1}{N}\delta_{c_n\tau^{-1}(\bar{c}_n)}(\lambda_l - \bar{\lambda}_l)\Big(\lambda_i\bar{\lambda}_j\delta_{(a,b)(c_i,\sigma^{-1}(\bar{c}_j))} + \bar{\lambda}_i\lambda_j\delta_{(a,b)(\sigma^{-1}(\bar{c}_i),c_j)} \\
&- \lambda_i\lambda_j\delta_{(a,b)(c_i,c_j)} - \bar{\lambda}_i\bar{\lambda}_j\delta_{(a,b)(\sigma^{-1}(\bar{c}_i),\sigma^{-1}(\bar{c}_j))}\Big)\Big] \\
&+ \sum_{(a,b)}\sum_{(c,d)} \delta_{\sigma\tau_{(a,b)(c,d)}\backslash n} \\
&\Big[-\lambda_i\bar{\lambda}_l\delta_{(a,b)(\sigma^{-1}(\bar{c}_l),c_n)}\left(\lambda_j\delta_{(c,d)(c_i,c_j)} - \bar{\lambda}_j\delta_{(c,d)(c_i,\sigma^{-1}(\bar{c}_j))}\right) \\
&+ \bar{\lambda}_i\bar{\lambda}_l\delta_{(a,b)(\sigma^{-1}(\bar{c}_l),c_n)}\left(\lambda_j\delta_{(c,d)(\sigma^{-1}(\bar{c}_i),c_j))} - \bar{\lambda}_j\delta_{(c,d)(\sigma^{-1}(\bar{c}_i),\sigma^{-1}(\bar{c}_j))}\right) \\
&+ \lambda_i\lambda_l\delta_{(a,b)(c_l,c_n)}\left(\lambda_j\delta_{(c,d)(c_i,c_j)} - \bar{\lambda}_j\delta_{(c,d)(c_i,\sigma^{-1}(\bar{c}_j))}\right) \\
&- \bar{\lambda}_i\lambda_l\delta_{(a,b)(c_l,c_n)}\left(\lambda_j\delta_{(c,d)(\sigma^{-1}(\bar{c}_i),c_j)} - \bar{\lambda}_j\delta_{(c,d)(\sigma^{-1}(\bar{c}_i),\sigma^{-1}(\bar{c}_j))}\right)\Big] \quad ,
\end{aligned}
\tag{E.4}
$$

where in this case there are, apart from the ρ-terms, only single swaps or two swaps of different colour-labels. Note that for all of the one-loop/one-emission colour structures the "open" adjoint index has been contracted with a polarisation vector, i.e. for instance for equation (E.4) one defines $(\mathbf{T}_i \cdot \mathbf{T}_j)\mathbf{T}_l = (\mathbf{T}_i \cdot \mathbf{T}_j)\mathbf{T}_l^a \cdot \varepsilon_a^*$.

In Table 1 the one-loop/one-emission diagrams, which contribute in the soft limit are listed. The diagrams are stripped off their colour factors, for this reason they are drawn with photon instead of gluon lines. The kinematical factors are obtained by evaluating the Feynman rules for these QED-type diagrams. Note that the colour structure for the bubble and self-energy diagram in Table 1 is written as $T_R\mathbf{T}_i^a$ according to the convention introduced in equation (5.8). Furthermore, Table 2 gives an overview to be able to identify which diagrams contribute to which coefficient of the soft anomalous dimension matrix element in the colour-flow basis (cf. equation (5.9)).

E.2 Two-loop order

In this part of the appendix the detailed results of the matrix elements of the colour-correlators of the two-loop diagrams which contribute in the soft limit are given.

The virtual double exchange diagram (see Figure 15(a)) has a colour structure of $(\mathbf{T}_i{\cdot}\mathbf{T}_j)(\mathbf{T}_i{\cdot}\mathbf{T}_j)$,

Coefficient	Diagram	Colour factor
$\Omega_{ij}^{(1,1)}$	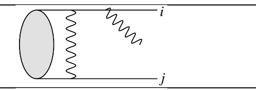	$\mathbf{T}_i^a(\mathbf{T}_i \cdot \mathbf{T}_j)$
$\tilde{\Omega}_{ij}^{(1,1)}$	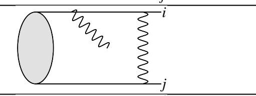	$(\mathbf{T}_i \cdot \mathbf{T}_j)\mathbf{T}_i^a$
$\hat{\Omega}_{ij}^{(1,1)}$	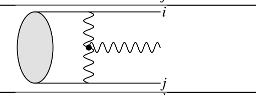	$f^{abc}\mathbf{T}_i^b\mathbf{T}_j^c$
$\Omega_{ijl}^{(1,1)}$	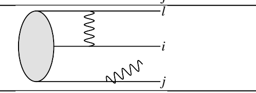	$\mathbf{T}_l^a(\mathbf{T}_i \cdot \mathbf{T}_j)$
$\Omega_{i,\mathrm{self-en.}}^{(1,1)}$	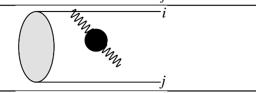	$T_R\mathbf{T}_i^a$
$\Omega_{i,\mathrm{vertex-corr.}}^{(1,1)}$	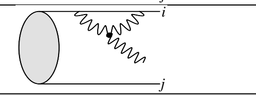	$T_R\mathbf{T}_i^a$

Table 1: Amplitudes of the one-loop/one-emission diagrams contributing in the soft limit. In each case the diagram is split into its respective colour structure and into the kinematical part which is abbreviated by the $\Omega^{(1,1)}$-coefficients. The latter are obtained by using QED-type Feynman rules.

Structure	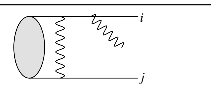	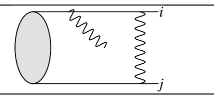	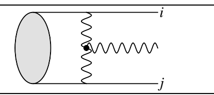	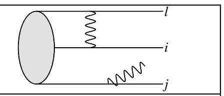
$\rho_{\sigma\tau}$	✓	✓	✓	✓
ρ_{τ}	✓	✓	×	✓
$\hat{\Sigma}_{\sigma\tau}^{(1,1)}$	✓	✓	✓	✓
$\tilde{\Sigma}_{\sigma\tau}^{(1,1)}$	✓	✓	×	✓
$\hat{\hat{\Sigma}}_{\sigma\tau}^{(1,1)}$	✓	✓	×	✓
$\Sigma_{\sigma\tau}^{\prime(1,1)}$	✓	✓	✓	×
$\Sigma_{\sigma\tau}^{\prime\prime(1,1)}$	✓	✓	×	✓

Table 2: Overview of which one-loop/one-emission diagrams contribute to which structure of the soft anomalous dimension matrix in the colour-flow basis.

as a matrix element in the colour-flow basis one finds the following expression

$$
\begin{aligned}
[\tau|(\mathbf{T}_i\cdot\mathbf{T}_j)(\mathbf{T}_i\cdot\mathbf{T}_j)|\sigma\rangle = {} & N^2\delta_{\sigma\tau} \\
& \Big[\lambda_i^2\bar\lambda_j^2\delta_{c_i\sigma^{-1}(\bar c_j)} + \bar\lambda_i^2\lambda_j^2\delta_{c_j\sigma^{-1}(\bar c_i)} + 2\lambda_i\bar\lambda_i\lambda_j\bar\lambda_j\delta_{c_i\sigma^{-1}(\bar c_j)}\delta_{c_j\sigma^{-1}(\bar c_i)} \\
& + \frac{2}{N^2}(\lambda_i-\bar\lambda_i)(\lambda_j-\bar\lambda_j)\left(\bar\lambda_i\lambda_j\delta_{c_j\sigma^{-1}(\bar c_i)} + \lambda_i\bar\lambda_j\delta_{c_i\sigma^{-1}(\bar c_j)}\right) \\
& + \frac{1}{N^2}\left(\lambda_i^2\lambda_j^2+\bar\lambda_i^2\bar\lambda_j^2\right) + \frac{1}{N^4}(\lambda_i-\bar\lambda_i)^2(\lambda_j-\bar\lambda_j)^2\Big] \\
& + N\sum_{(a,b)}\delta_{\sigma\tau_{(a,b)}}\Big[\lambda_i^2\bar\lambda_j^2\delta_{(a,b)(c_i,\sigma^{-1}(\bar c_j))} + \bar\lambda_i^2\lambda_j^2\delta_{(a,b)(\sigma^{-1}(\bar c_i),c_j)} \\
& +\frac{2}{N^2}(\lambda_i-\bar\lambda_i)(\lambda_j-\bar\lambda_j)\Big(\lambda_i\bar\lambda_j\delta_{(a,b)(c_i,\sigma^{-1}(\bar c_j))} + \bar\lambda_i\lambda_j\delta_{(a,b)(\sigma^{-1}(\bar c_i),c_j)} \\
& -\lambda_i\lambda_j\delta_{(a,b)(c_i,c_j)} - \bar\lambda_i\bar\lambda_j\delta_{(a,b)(\sigma^{-1}(\bar c_i),\sigma^{-1}(\bar c_j))}\Big) \\
& -\lambda_i\bar\lambda_i\left(\lambda_j^2\delta_{(a,b)(c_i,c_j)}\delta_{c_j\sigma^{-1}(\bar c_i)} + \bar\lambda_j^2\delta_{(a,b)(c_i,\sigma^{-1}(\bar c_i))}\delta_{c_i\sigma^{-1}(\bar c_j)}\right) \\
& -\lambda_j\bar\lambda_j\left(\lambda_i^2\delta_{(a,b)(c_i,c_j)}\delta_{c_i\sigma^{-1}(\bar c_j)} + \bar\lambda_i^2\delta_{(a,b)(c_j,\sigma^{-1}(\bar c_j))}\delta_{c_j\sigma^{-1}(\bar c_i)}\right) \\
& +2\lambda_i\bar\lambda_i\lambda_j\bar\lambda_j\left(\delta_{(a,b)(\sigma^{-1}(\bar c_i),c_j)}\delta_{c_i\sigma^{-1}(\bar c_j)} + \delta_{(a,b)(c_i,\sigma^{-1}(\bar c_j))}\delta_{c_j\sigma^{-1}(\bar c_i)}\right)\Big] \\
& - \sum_{(a,b)}\sum_{(b,c)}\delta_{\sigma\tau_{(a,b)(b,c)}} \\
& \Big[\lambda_i\bar\lambda_i\lambda_j^2\left(\delta_{(a,b)(c_i,\sigma^{-1}(\bar c_i))}\delta_{(b,c)(\sigma^{-1}(\bar c_i),c_j)} + \delta_{(a,b)(c_i,c_j)}\delta_{(b,c)(c_j,\sigma^{-1}(\bar c_i))}\right) \\
& +\lambda_j\bar\lambda_j\lambda_i^2\left(\delta_{(a,b)(c_i,\sigma^{-1}(\bar c_j))}\delta_{(b,c)(\sigma^{-1}(\bar c_j),c_j))} + \delta_{(a,b)(c_i,c_j)}\delta_{(b,c)(c_j,\sigma^{-1}(\bar c_j))}\right) \\
& +\lambda_i\bar\lambda_i\bar\lambda_j^2\Big(\delta_{(a,b)(c_i,\sigma^{-1}(\bar c_i))}\delta_{(b,c)(\sigma^{-1}(\bar c_i),\sigma^{-1}(\bar c_j))} \\
& +\delta_{(a,b)(c_i,\sigma^{-1}(\bar c_j))}\delta_{(b,c)(\sigma^{-1}(\bar c_j),\sigma^{-1}(\bar c_i))}\Big) \\
& +\lambda_j\bar\lambda_j\bar\lambda_i^2\Big(\delta_{(a,b)(\sigma^{-1}(\bar c_i),\sigma^{-1}(\bar c_j))}\delta_{(b,c)(\sigma^{-1}(\bar c_j),c_j)} \\
& +\delta_{(a,b)(\sigma^{-1}(\bar c_i),c_j)}\delta_{(b,c)(c_j,\sigma^{-1}(\bar c_j))}\Big)\Big] \\
& + 2\sum_{(a,b)}\sum_{(c,d)}\delta_{\sigma\tau_{(a,b)(c,d)}}\lambda_i\bar\lambda_i\lambda_j\bar\lambda_j \\
& \Big[\delta_{(a,b)(c_i,\sigma^{-1}(\bar c_j))}\delta_{(c,d)(\sigma^{-1}(\bar c_i),c_j)} + \delta_{(a,b)(c_i,c_j)}\delta_{(c,d)(\sigma^{-1}(\bar c_i),\sigma^{-1}(\bar c_j))}\Big] \ .
\end{aligned}
\tag{E.5}
$$

The "crossed" double gluon exchange in Figure 15(b) leads to a different result

$$
\begin{aligned}
[\tau|\mathbf{T}_i\mathbf{T}_i\mathbf{T}_j\mathbf{T}_j|\sigma\rangle = {} & N^2\delta_{\sigma\tau}\Bigg[2\lambda_i\bar{\lambda}_i\lambda_j\bar{\lambda}_j\delta_{c_i\sigma^{-1}(\bar{c}_j)}\delta_{c_j\sigma^{-1}(\bar{c}_i)} \\
& + \frac{2}{N^2}(\lambda_i-\bar{\lambda}_i)(\lambda_j-\bar{\lambda}_j)(\lambda_i\bar{\lambda}_j\delta_{c_i\sigma^{-1}(\bar{c}_j)}+\bar{\lambda}_i\lambda_j\delta_{c_j\sigma^{-1}(\bar{c}_i)}) \\
& + \frac{1}{N^2}\left(\lambda_i^2\bar{\lambda}_j^2+\bar{\lambda}_i^2\lambda_j^2\right)+\frac{1}{N^4}(\lambda_i-\bar{\lambda}_i)^2(\lambda_j-\bar{\lambda}_j)^2\Bigg] \\
& + \sum_{(a,b)}\delta_{\sigma\tau_{(a,b)}}\Big[N\lambda_i^2\lambda_j^2\delta_{(a,b)(c_i,c_j)}+N\bar{\lambda}_i^2\bar{\lambda}_j^2\delta_{(a,b)(\sigma^{-1}(\bar{c}_i),\sigma^{-1}(\bar{c}_j))} \\
& +2N\lambda_i\bar{\lambda}_i\lambda_j\bar{\lambda}_j\left(\delta_{c_i\sigma^{-1}(\bar{c}_j)}\delta_{(a,b)(\sigma^{-1}(\bar{c}_i),c_j)}+\delta_{c_j\sigma^{-1}(\bar{c}_i)}\delta_{(a,b)(c_i,\sigma^{-1}(\bar{c}_j))}\right) \\
& +\frac{2}{N}(\lambda_i-\bar{\lambda}_i)(\lambda_j-\bar{\lambda}_j)\Big(\lambda_i\bar{\lambda}_j\delta_{(a,b)(c_i,\sigma^{-1}(\bar{c}_j))}+\bar{\lambda}_i\lambda_j\delta_{(a,b)(c_j,\sigma^{-1}(\bar{c}_i))} \\
& -\lambda_i\lambda_j\delta_{(a,b)(c_i,c_j)}-\bar{\lambda}_i\bar{\lambda}_j\delta_{(a,b)(\sigma^{-1}(\bar{c}_i),\sigma^{-1}(\bar{c}_j))}\Big)\Big] \\
& -\sum_{(a,b)}\sum_{(b,c)}\delta_{\sigma\tau_{(a,b)(b,c)}} \\
& \Big[\lambda_j^2\lambda_i\bar{\lambda}_i\left(\delta_{(a,b)(c_i,c_j)}\delta_{(b,c)(c_j,\sigma^{-1}(\bar{c}_i)))}+\delta_{(a,b)(c_i,\sigma^{-1}(\bar{c}_i))}\delta_{(b,c)(\sigma^{-1}(\bar{c}_i),c_j)}\right) \\
& +\bar{\lambda}_j^2\lambda_i\bar{\lambda}_i\Big(\delta_{(a,b)(c_i,\sigma^{-1}(\bar{c}_i))}\delta_{(b,c)(\sigma^{-1}(\bar{c}_i),\sigma^{-1}(\bar{c}_j))}+\delta_{(a,b)(c_i,\sigma^{-1}(\bar{c}_j))}\delta_{(b,c)(\sigma^{-1}(\bar{c}_j),\sigma^{-1}(\bar{c}_i))}\Big) \\
& +\bar{\lambda}_i^2\lambda_j\bar{\lambda}_j\left(\delta_{(a,b)(\sigma^{-1}(\bar{c}_i),c_j)}\delta_{(b,c)(c_j,\sigma^{-1}(\bar{c}_j))}+\delta_{(a,b)(\sigma^{-1}(\bar{c}_i),\sigma^{-1}(\bar{c}_j))}\delta_{(b,c)(\sigma^{-1}(\bar{c}_j),c_j)}\right) \\
& +\lambda_i^2\lambda_j\bar{\lambda}_j\left(\delta_{(a,b)(c_i,\sigma^{-1}(\bar{c}_j))}\delta_{(b,c)(\sigma^{-1}(\bar{c}_j),c_j)}+\delta_{(a,b)(c_i,c_j)}\delta_{(b,c)(c_j,\sigma^{-1}(\bar{c}_j))}\right)\Big] \\
& +2\sum_{(a,b)}\sum_{(c,d)}\delta_{\sigma\tau_{(a,b)(c,d)}}\lambda_i\bar{\lambda}_i\lambda_j\bar{\lambda}_j\Big[\delta_{(a,b)(c_i,\sigma^{-1}(\bar{c}_j))}\delta_{(c,d)(c_j,\sigma^{-1}(\bar{c}_i))} \\
& +\delta_{(a,b)(c_i,c_j)}\delta_{(c,d)(\sigma^{-1}(\bar{c}_i),\sigma^{-1}(\bar{c}_j))}\Big]\ .
\end{aligned}
\tag{E.6}
$$

The structures in equation (E.5) and (E.6) have many terms in common, there are, however, also some differences. As an example for the latter, consider the diagonal structure of $1/N^2(\lambda_i^2\lambda_j^2+\bar{\lambda}_i^2\bar{\lambda}_j^2)$ for the double gluon exchange, while one finds that this term appears for a different parton content in the case of the crossed exchange, namely $1/N^2(\lambda_i^2\bar{\lambda}_j^2+\bar{\lambda}_i^2\lambda_j^2)$. Furthermore, there is a difference in parton content for certain off-diagonal single-swap terms; for the double exchange there is a contribution of the form

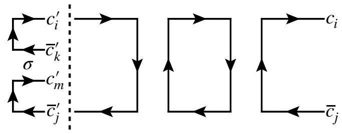

$$\rightarrow \lambda_i^2\bar{\lambda}_j^2N\delta_{\sigma\tau_{(a,b)}}\delta_{(a,b)(c_i,\sigma^{-1}(\bar{c}_j))}\ , \tag{E.7}$$

for a hard quark and anti-quark line. The corresponding part from the crossed exchange originates from two hard quark lines i and j

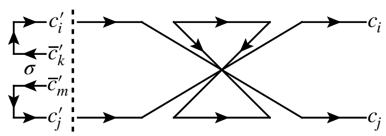

$$\rightarrow \lambda_i^2\lambda_j^2N\delta_{\sigma\tau_{(a,b)}}\delta_{(a,b)(c_i,c_j)}\ . \tag{E.8}$$

From this it also follows that for the double exchange in equation (E.7) one gets a term with a colour-connection in the basis σ for i and j, while there is no such term for the crossed exchange. It turns out that there are some contributions for the double exchange concerning hard gluon lines, which do not appear for the crossed exchange. For instance, for the double exchange in equation (E.5) one finds for a hard gluon line j and a quark line i a contribution of

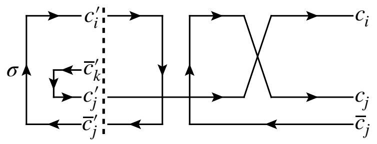

$$\rightarrow -\lambda_i \lambda_j \bar{\lambda}_j N \delta_{\sigma\tau_{(a,b)}} \delta_{(a,b)(c_i,c_j)} \delta_{c_i \sigma^{-1}(\bar{c}_j)} \ . \tag{E.9}$$

However, for the crossed exchange diagram the structure which corresponds to the contribution in equation (E.9), namely,

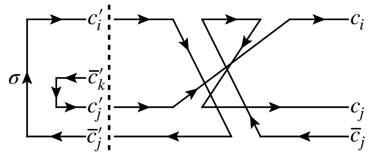

$$\rightarrow -\lambda_i \lambda_j \bar{\lambda}_j N \delta_{\sigma\tau_{(a,b)}} \delta_{(a,b)(c_i,c_j)} \delta_{c_i \sigma^{-1}(\bar{c}_j)} \ , \tag{E.10}$$

is cancelled by the following structure

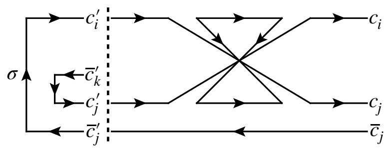

$$\rightarrow \lambda_i \lambda_j \bar{\lambda}_j N \delta_{\sigma\tau_{(a,b)}} \delta_{(a,b)(c_i,c_j)} \delta_{c_i \sigma^{-1}(\bar{c}_j)} \ . \tag{E.11}$$

The same argument applies to the cases with a hard gluon line j and an anti-quark line i, as well as to a gluon line i and (anti-)quark line j.

For Figure 15(c) one obtains in the colour-flow basis

$$
\begin{aligned}
[\tau|(\mathbf{T}_i\cdot\mathbf{T}_j)(\mathbf{T}_l\cdot\mathbf{T}_i)|\sigma\rangle = N^2\delta_{\sigma\tau}\Big[&-\lambda_i\bar\lambda_i\left(\lambda_j\bar\lambda_l\delta_{c_i\sigma^{-1}(\bar c_l)}\delta_{c_j\sigma^{-1}(\bar c_i)}+\bar\lambda_j\lambda_l\delta_{c_i\sigma^{-1}(\bar c_j)}\delta_{c_l\sigma^{-1}(\bar c_i)}\right)\\
&+\frac{1}{N^2}\lambda_i\bar\lambda_i(\lambda_l-\bar\lambda_l)\left(\bar\lambda_j\delta_{c_i\sigma^{-1}(\bar c_j)}-\lambda_j\delta_{c_j\sigma^{-1}(\bar c_i)}\right)\\
&+\frac{1}{N^2}(\lambda_i-\bar\lambda_i)(\lambda_j-\bar\lambda_j)\left(\lambda_i\bar\lambda_l\delta_{c_i\sigma^{-1}(\bar c_l)}+\bar\lambda_i\lambda_l\delta_{c_l\sigma^{-1}(\bar c_i)}\right)\\
&-\frac{1}{N^2}\left(\lambda_i^2\lambda_j\bar\lambda_l\delta_{c_j\sigma^{-1}(\bar c_l)}-\bar\lambda_i^2\bar\lambda_j\lambda_l\delta_{c_l\sigma^{-1}(\bar c_j)}\right)\\
&+\frac{1}{N^4}(\lambda_i-\bar\lambda_i)^2(\lambda_j-\bar\lambda_j)(\lambda_l-\bar\lambda_l)\Big]\\
&+\sum_{(a,b)}\delta_{\sigma\tau_{(a,b)}}\Bigg\{\frac{1}{N}(\lambda_i-\bar\lambda_i)\Big[(\lambda_l-\bar\lambda_l)\Big(\lambda_i\bar\lambda_j\delta_{(a,b)(c_i,\sigma^{-1}(\bar c_j))}\\
&+\bar\lambda_i\lambda_j\delta_{(a,b)(\sigma^{-1}(\bar c_i),c_j)}-\bar\lambda_i\bar\lambda_j\delta_{(a,b)(\sigma^{-1}(\bar c_i),\sigma^{-1}(\bar c_j))}-\lambda_i\lambda_j\delta_{(a,b)(c_i,c_j)}\Big)\\
&+(\lambda_j-\bar\lambda_j)\left(\lambda_i\bar\lambda_l\delta_{(a,b)(c_i,\sigma^{-1}(\bar c_l))}-\lambda_i\lambda_l\delta_{(a,b)(c_i,c_l)}+\bar\lambda_i\lambda_l\delta_{(a,b)(\sigma^{-1}(\bar c_i),c_l)}\right.\\
&\left.-\bar\lambda_i\bar\lambda_l\delta_{(a,b)(\sigma^{-1}(\bar c_i),\sigma^{-1}(\bar c_l))}\right)\Big]\\
&+N\Big[-\lambda_i^2\bar\lambda_l\delta_{c_i\sigma^{-1}(\bar c_l)}\left(\lambda_j\delta_{(a,b)(c_i,c_j)}-\bar\lambda_j\delta_{(a,b)(c_i,\sigma^{-1}(\bar c_j))}\right)\\
&+\bar\lambda_i^2\lambda_l\delta_{c_l\sigma^{-1}(\bar c_i)}\left(\lambda_j\delta_{(a,b)(c_j,c_l)}-\bar\lambda_j\delta_{(a,b)(\sigma^{-1}(\bar c_j),c_l)}\right)\\
&-\lambda_i^2\lambda_l\bar\lambda_j\delta_{c_l\sigma^{-1}(\bar c_j)}\delta_{(a,b)(c_i,c_l)}-\bar\lambda_i^2\lambda_j\bar\lambda_l\delta_{c_j\sigma^{-1}(\bar c_l)}\delta_{(a,b)(\sigma^{-1}(\bar c_i),c_j)}\Big]\\
&+N\lambda_i\bar\lambda_i\Big[\lambda_l\delta_{c_l\sigma^{-1}(\bar c_i)}\left(\lambda_j\delta_{(a,b)(c_i,c_j)}-\bar\lambda_j\delta_{(a,b)(c_i,\sigma^{-1}(\bar c_j))}\right)\\
&+\lambda_j\delta_{c_j\sigma^{-1}(\bar c_i)}\left(\lambda_l\delta_{(a,b)(c_i,c_l)}-\bar\lambda_l\delta_{(a,b)(c_i,\sigma^{-1}(\bar c_l))}\right)\\
&-\bar\lambda_j\delta_{c_i\sigma^{-1}(\bar c_j)}\left(\lambda_l\delta_{(a,b)(\sigma^{-1}(\bar c_i),c_l)}-\bar\lambda_l\delta_{(a,b)(\sigma^{-1}(\bar c_i),\sigma^{-1}(\bar c_l))}\right)\\
&-\bar\lambda_l\delta_{c_i\sigma^{-1}(\bar c_l)}\left(\lambda_j\delta_{(a,b)(\sigma^{-1}(\bar c_i),c_j)}-\bar\lambda_j\delta_{(a,b)(\sigma^{-1}(\bar c_i),\sigma^{-1}(\bar c_j))}\right)\Big]\Bigg\}\\
&+\sum_{(a,b)}\sum_{(b,c)}\delta_{\sigma\tau_{(a,b)(b,c)}}\Big[\lambda_i^2\lambda_l\delta_{(a,b)(c_i,c_l)}\left(\lambda_j\delta_{(b,c)(c_l,c_j)}-\bar\lambda_j\delta_{(b,c)(c_l,\sigma^{-1}(\bar c_j))}\right)\\
&-\lambda_i^2\bar\lambda_l\delta_{(a,b)(c_i,\sigma^{-1}(\bar c_l))}\left(\lambda_j\delta_{(b,c)(\sigma^{-1}(\bar c_l),c_j)}-\bar\lambda_j\delta_{(b,c)(\sigma^{-1}(\bar c_l),\sigma^{-1}(\bar c_j))}\right)\\
&+\bar\lambda_i^2\lambda_j\delta_{(a,b)(\sigma^{-1}(\bar c_i),c_j)}\left(\lambda_l\delta_{(b,c)(c_j,c_l)}-\bar\lambda_l\delta_{(b,c)(c_j,\sigma^{-1}(\bar c_l))}\right)\\
&-\bar\lambda_i^2\bar\lambda_j\delta_{(a,b)(\sigma^{-1}(\bar c_i),\sigma^{-1}(\bar c_j))}\left(\lambda_l\delta_{(b,c)(\sigma^{-1}(\bar c_j),c_l)}-\bar\lambda_l\delta_{(b,c)(\sigma^{-1}(\bar c_j),\sigma^{-1}(\bar c_l))}\right)\Big]\\
&+\sum_{(a,b)}\sum_{(c,d)}\delta_{\sigma\tau_{(a,b)(c,d)}}\lambda_i\bar\lambda_i\\
&\Big[\lambda_l\delta_{(a,b)(c_i,c_l)}\left(\lambda_j\delta_{(c,d)(\sigma^{-1}(\bar c_i),c_j)}-\bar\lambda_j\delta_{(c,d)(\sigma^{-1}(\bar c_i),\sigma^{-1}(\bar c_j))}\right)\\
&+\lambda_j\delta_{(a,b)(c_i,c_j)}\left(\lambda_l\delta_{(c,d)(\sigma^{-1}(\bar c_i),c_l)}-\bar\lambda_l\delta_{(c,d)(\sigma^{-1}(\bar c_i),\sigma^{-1}(\bar c_l))}\right)\\
&-\bar\lambda_l\delta_{(a,b)(c_i,\sigma^{-1}(\bar c_l))}\left(\lambda_j\delta_{(c,d)(\sigma^{-1}(\bar c_i),c_j)}-\bar\lambda_j\delta_{(c,d)(\sigma^{-1}(\bar c_i),\sigma^{-1}(\bar c_j))}\right)\\
&-\bar\lambda_j\delta_{(a,b)(c_i,\sigma^{-1}(\bar c_j))}\left(\lambda_l\delta_{(c,d)(\sigma^{-1}(\bar c_i),c_l)}-\bar\lambda_l\delta_{(c,d)(\sigma^{-1}(\bar c_i),\sigma^{-1}(\bar c_l))}\right)\Big]\ ,
\end{aligned}
\tag{E.12}
$$

while the colour structure for swapping the order of the two exchanges leads to (a diagram which is contained in the colour sum)

$$
\begin{aligned}
[\tau|(\mathbf{T}_l\cdot\mathbf{T}_i)(\mathbf{T}_i\cdot\mathbf{T}_j)|\sigma\rangle = N^2\delta_{\sigma\tau}\Bigg[&-\lambda_i\bar\lambda_i\left(\lambda_j\bar\lambda_l\delta_{c_i\sigma^{-1}(\bar c_l)}\delta_{c_j\sigma^{-1}(\bar c_i)}+\bar\lambda_j\lambda_l\delta_{c_i\sigma^{-1}(\bar c_j)}\delta_{c_l\sigma^{-1}(\bar c_i)}\right)\\
&+\frac{1}{N^2}(\lambda_i-\bar\lambda_i)(\lambda_l-\bar\lambda_l)\left(\lambda_i\bar\lambda_j\delta_{c_i\sigma^{-1}(\bar c_j)}+\bar\lambda_i\lambda_j\delta_{c_j\sigma^{-1}(\bar c_i)}\right)\\
&-\frac{1}{N^2}\left(\lambda_i^2\bar\lambda_j\lambda_l\delta_{c_l\sigma^{-1}(\bar c_j)}+\bar\lambda_i^2\lambda_j\bar\lambda_l\delta_{c_j\sigma^{-1}(\bar c_l)}\right)\\
&+\frac{1}{N^2}\lambda_i\bar\lambda_i(\lambda_j-\bar\lambda_j)\left(\bar\lambda_l\delta_{c_i\sigma^{-1}(\bar c_l)}-\lambda_l\delta_{c_l\sigma^{-1}(\bar c_i)}\right)\\
&+\frac{1}{N^4}(\lambda_i-\bar\lambda_i)^2(\lambda_j-\bar\lambda_j)(\lambda_l-\bar\lambda_l)\Bigg]\\
&+\sum_{(ab)}\delta_{\sigma\tau_{(a,b)}}\Big\{N\lambda_i\bar\lambda_i\Big[\lambda_j\delta_{c_j\sigma^{-1}(\bar c_i)}\left(\lambda_l\delta_{(a,b)(c_i,c_l)}-\bar\lambda_l\delta_{(a,b)(c_i,\sigma^{-1}(\bar c_l))}\right)\\
&+\lambda_l\delta_{c_l\sigma^{-1}(\bar c_i)}\left(\lambda_j\delta_{(a,b)(c_i,c_j)}-\bar\lambda_j\delta_{(a,b)(c_i,\sigma^{-1}(\bar c_j))}\right)\\
&-\bar\lambda_l\delta_{c_i\sigma^{-1}(\bar c_l)}\left(\lambda_j\delta_{(a,b)(\sigma^{-1}(\bar c_i),c_j)}-\bar\lambda_j\delta_{(a,b)(\sigma^{-1}(\bar c_i),\sigma^{-1}(\bar c_j))}\right)\\
&-\bar\lambda_j\delta_{c_i\sigma^{-1}(\bar c_j)}\left(\lambda_l\delta_{(a,b)(\sigma^{-1}(\bar c_i),c_l)}-\bar\lambda_l\delta_{(a,b)(\sigma^{-1}(\bar c_i),\sigma^{-1}(\bar c_l))}\right)\Big]\\
&+N\Big[-\lambda_i^2\bar\lambda_j\delta_{c_i\sigma^{-1}(\bar c_j)}\left(\lambda_l\delta_{(a,b)(c_i,c_l)}-\bar\lambda_l\delta_{(a,b)(c_i,\sigma^{-1}(\bar c_l))}\right)\\
&+\bar\lambda_i^2\lambda_j\delta_{c_j\sigma^{-1}(\bar c_i)}\left(\lambda_l\delta_{(a,b)(c_j,c_l)}-\bar\lambda_l\delta_{(a,b)(c_j,\sigma^{-1}(\bar c_l))}\right)\\
&-\bar\lambda_i^2\bar\lambda_j\lambda_l\delta_{c_l\sigma^{-1}(\bar c_j)}\delta_{(a,b)(\sigma^{-1}(\bar c_i),c_l)}-\lambda_i^2\lambda_j\bar\lambda_l\delta_{c_j\sigma^{-1}(\bar c_i)}\delta_{(a,b)(c_i,c_j)}\Big]\\
&+\frac{1}{N}(\lambda_i-\bar\lambda_i)\Big[(\lambda_j-\bar\lambda_j)\left(\lambda_i\bar\lambda_l\delta_{(a,b)(c_i,\sigma^{-1}(\bar c_l))}-\lambda_i\lambda_l\delta_{(a,b)(c_i,c_l)}\right.\\
&\left.+\bar\lambda_i\lambda_l\delta_{(a,b)(\sigma^{-1}(\bar c_i),c_l)}-\bar\lambda_i\bar\lambda_l\delta_{(a,b)(\sigma^{-1}(\bar c_i),\sigma^{-1}(\bar c_l))}\right)\\
&+(\lambda_l-\bar\lambda_l)\left(\lambda_i\bar\lambda_j\delta_{(a,b)(c_i,\sigma^{-1}(\bar c_j))}+\bar\lambda_i\lambda_j\delta_{(a,b)(\sigma^{-1}(\bar c_i),c_j)}\right.\\
&\left.-\lambda_i\lambda_j\delta_{(a,b)(c_i,c_j)}-\bar\lambda_i\bar\lambda_j\delta_{(a,b)(\sigma^{-1}(\bar c_i),\sigma^{-1}(\bar c_j))}\right)\Big]\Big\}\\
&+\sum_{(a,b)}\sum_{(b,c)}\delta_{\sigma\tau_{(a,b)(b,c)}}\Big\{\lambda_i^2\lambda_j\delta_{(a,b)(c_i,c_j)}\left(\lambda_l\delta_{(b,c)(c_j,c_l)}-\bar\lambda_l\delta_{(b,c)(c_j,\sigma^{-1}(\bar c_l))}\right)\\
&+\bar\lambda_i^2\lambda_l\delta_{(a,b)(\sigma^{-1}(\bar c_i),c_l)}\left(\lambda_j\delta_{(b,c)(c_l,c_j)}-\bar\lambda_j\delta_{(b,c)(c_l,\sigma^{-1}(\bar c_j))}\right)\\
&-\bar\lambda_i^2\bar\lambda_l\delta_{(a,b)(\sigma^{-1}(\bar c_i),\sigma^{-1}(\bar c_l))}\left(\lambda_j\delta_{(b,c)(\sigma^{-1}(\bar c_l),c_j)}-\bar\lambda_j\delta_{(b,c)(\sigma^{-1}(\bar c_l),\sigma^{-1}(\bar c_j))}\right)\\
&-\lambda_i^2\bar\lambda_j\delta_{(a,b)(c_i,\sigma^{-1}(\bar c_j))}\left(\lambda_l\delta_{(b,c)(\sigma^{-1}(\bar c_j),c_l)}-\bar\lambda_l\delta_{(b,c)(\sigma^{-1}(\bar c_j),\sigma^{-1}(\bar c_l))}\right)\Big\}\\
&+\sum_{(a,b)}\sum_{(c,d)}\delta_{\sigma\tau_{(a,b)(c,d)}}\lambda_i\bar\lambda_i\\
&\Big[\lambda_j\delta_{(a,b)(c_i,c_j)}\left(\lambda_l\delta_{(c,d)(\sigma^{-1}(\bar c_i),c_l)}-\bar\lambda_l\delta_{(c,d)(\sigma^{-1}(\bar c_i),\sigma^{-1}(\bar c_l))}\right)\\
&-\bar\lambda_j\delta_{(a,b)(c_i,\sigma^{-1}(\bar c_j))}\left(\lambda_l\delta_{(c,d)(\sigma^{-1}(\bar c_i),c_l)}-\bar\lambda_l\delta_{(c,d)(\sigma^{-1}(\bar c_i),\sigma^{-1}(\bar c_l))}\right)\\
&+\lambda_l\delta_{(a,b)(c_i,c_l)}\left(\lambda_j\delta_{(c,d)(\sigma^{-1}(\bar c_i),c_j)}-\bar\lambda_j\delta_{(c,d)(\sigma^{-1}(\bar c_i),\sigma^{-1}(\bar c_j))}\right)\\
&-\bar\lambda_l\delta_{(a,b)(c_i,\sigma^{-1}(\bar c_l))}\left(\lambda_j\delta_{(c,d)(\sigma^{-1}(\bar c_i),c_j)}-\bar\lambda_j\delta_{(c,d)(\sigma^{-1}(\bar c_i),\sigma^{-1}(\bar c_j))}\right)\Big]\,.
\end{aligned}
\tag{E.13}
$$

One can readily get from equation (E.12) to (E.13) by swapping the l and j labels of the hard lines. There are some structures which are symmetric under this swap, thus these remain the same for both cases. However, there are also parts which do not show this symmetry under the exchange, these then do not coincide.
Finally, the colour structure of Figure 15(f) in terms of a matrix element in the colour-flow basis can be written as

$$
\begin{aligned}
[\tau|\mathbf{T}_g\mathbf{T}_l\mathbf{T}_i\mathbf{T}_j|\sigma\rangle = {} & \sqrt{T_R}N^2\delta_{\sigma\tau}\Bigg[\frac{1}{N^2}\left((\lambda_l-\bar{\lambda}_l)\left(\lambda_i\bar{\lambda}_j\delta_{c_i\sigma^{-1}(\bar{c}_j)}-\lambda_j\bar{\lambda}_i\delta_{c_j\sigma^{-1}(\bar{c}_i)}\right)\right.\\
& +(\lambda_j-\bar{\lambda}_j)\left(\bar{\lambda}_i\lambda_l\delta_{c_l\sigma^{-1}(\bar{c}_i)}-\lambda_i\bar{\lambda}_l\delta_{c_i\sigma^{-1}(\bar{c}_l)}\right)\\
& \left.+(\lambda_i-\bar{\lambda}_i)\left(\bar{\lambda}_l\lambda_j\delta_{c_j\sigma^{-1}(\bar{c}_l)}-\bar{\lambda}_j\lambda_l\delta_{c_l\sigma^{-1}(\bar{c}_j)}\right)\right)\Bigg]\\
& +\sum_{(a,b)}\delta_{\sigma\tau_{(a,b)}}N\sqrt{T_R}\\
& \Big[\lambda_i\bar{\lambda}_j\lambda_l\delta_{(a,b)(c_i,c_l)}\left(\delta_{c_l\sigma^{-1}(\bar{c}_j)}-\delta_{c_i\sigma^{-1}(\bar{c}_j)}\right)\\
& +\bar{\lambda}_i\lambda_j\lambda_l\delta_{(a,b)(c_j,c_l)}\left(\delta_{c_j\sigma^{-1}(\bar{c}_i)}-\delta_{c_l\sigma^{-1}(\bar{c}_i)}\right)\\
& +\lambda_i\lambda_j\bar{\lambda}_l\delta_{(a,b)(c_i,c_j)}\left(\delta_{c_i\sigma^{-1}(\bar{c}_l)}-\delta_{c_j\sigma^{-1}(\bar{c}_l)}\right)\\
& +\lambda_i\bar{\lambda}_j\bar{\lambda}_l\left(\delta_{(a,b)(c_i,\sigma^{-1}(\bar{c}_l))}\delta_{c_i\sigma^{-1}(\bar{c}_j)}-\delta_{(a,b)(c_i,\sigma^{-1}(\bar{c}_j))}\delta_{c_i\sigma^{-1}(\bar{c}_l)}\right)\\
& +\bar{\lambda}_i\lambda_j\bar{\lambda}_l\left(\delta_{(a,b)(\sigma^{-1}(\bar{c}_i),c_j)}\delta_{c_j\sigma^{-1}(\bar{c}_l)}-\delta_{(a,b)(c_j,\sigma^{-1}(\bar{c}_l))}\delta_{c_j\sigma^{-1}(\bar{c}_i)}\right)\\
& +\bar{\lambda}_i\bar{\lambda}_j\lambda_l\left(\delta_{(a,b)(\sigma^{-1}(\bar{c}_j),c_l)}\delta_{c_l\sigma^{-1}(\bar{c}_i)}-\delta_{(a,b)(\sigma^{-1}(\bar{c}_i),c_l)}\delta_{c_l\sigma^{-1}(\bar{c}_j)}\right)\Big]\\
& +\sum_{(a,b)}\sum_{(b,c)}\delta_{\sigma\tau_{(a,b)(b,c)}}\sqrt{T_R}\\
& \Big[\lambda_i\lambda_j\delta_{(a,b)(c_i,c_j)}\left(\lambda_l\delta_{(b,c)(c_j,c_l)}-\bar{\lambda}_l\delta_{(b,c)(c_j,\sigma^{-1}(\bar{c}_l))}\right)\\
& -\lambda_i\lambda_l\delta_{(a,b)(c_i,c_l)}\left(\lambda_j\delta_{(b,c)(c_l,c_j)}-\bar{\lambda}_j\delta_{(b,c)(c_l,\sigma^{-1}(\bar{c}_j))}\right)\\
& -\lambda_i\bar{\lambda}_j\delta_{(a,b)(c_i,\sigma^{-1}(\bar{c}_j))}\left(\lambda_l\delta_{(b,c)(\sigma^{-1}(\bar{c}_j),c_l)}-\bar{\lambda}_l\delta_{(b,c)(\sigma^{-1}(\bar{c}_j),\sigma^{-1}(\bar{c}_l))}\right)\\
& +\bar{\lambda}_i\lambda_l\delta_{(a,b)(\sigma^{-1}(\bar{c}_i),c_l)}\left(\lambda_j\delta_{(b,c)(c_l,c_j)}-\bar{\lambda}_j\delta_{(b,c)(c_l,\sigma^{-1}(\bar{c}_j))}\right)\\
& -\bar{\lambda}_i\lambda_j\delta_{(a,b)(\sigma^{-1}(\bar{c}_i),c_j)}\left(\lambda_l\delta_{(b,c)(c_j,c_l)}-\bar{\lambda}_l\delta_{(b,c)(c_j,\sigma^{-1}(\bar{c}_l))}\right)\\
& -\bar{\lambda}_i\bar{\lambda}_l\delta_{(a,b)(\sigma^{-1}(\bar{c}_i),\sigma^{-1}(\bar{c}_l))}\left(\lambda_j\delta_{(b,c)(\sigma^{-1}(\bar{c}_l),c_j)}-\bar{\lambda}_j\delta_{(b,c)(\sigma^{-1}(\bar{c}_l),\sigma^{-1}(\bar{c}_j))}\right)\\
& +\lambda_i\bar{\lambda}_l\delta_{(a,b)(c_i,\sigma^{-1}(\bar{c}_l))}\left(\lambda_j\delta_{(b,c)(\sigma^{-1}(\bar{c}_l),c_j)}-\bar{\lambda}_j\delta_{(b,c)(\sigma^{-1}(\bar{c}_l),\sigma^{-1}(\bar{c}_j))}\right)\\
& +\bar{\lambda}_i\bar{\lambda}_j\delta_{(a,b)(\sigma^{-1}(\bar{c}_i),\sigma^{-1}(\bar{c}_j))}\left(\lambda_l\delta_{(b,c)(\sigma^{-1}(\bar{c}_j),c_l)}-\bar{\lambda}_l\delta_{(b,c)(\sigma^{-1}(\bar{c}_j),\sigma^{-1}(\bar{c}_l))}\right)\Big]\ .
\end{aligned}
\tag{E.14}
$$

In Table 3 one finds an overview of the two-loop diagrams and their respective colour factors as well as their corresponding kinematical parts. For an overview to determine which two-loop diagrams contribute to which structure of the soft anomalous dimension matrix in the colour-flow basis consider Table 4.

Coefficient	Diagram	Colour factor
$\Omega_{ij}^{(2)}$	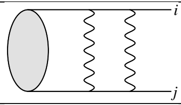	$(\mathbf{T}_i \cdot \mathbf{T}_j)(\mathbf{T}_i \cdot \mathbf{T}_j)$
$\tilde{\Omega}_{ij}^{(2)}$	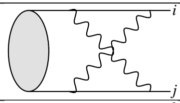	$\mathbf{T}_i^a \mathbf{T}_i^b \mathbf{T}_j^b \mathbf{T}_j^a$
$\Omega_{ijl}^{(2)}$	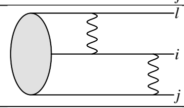	$(\mathbf{T}_i \cdot \mathbf{T}_l)(\mathbf{T}_i \cdot \mathbf{T}_j)$
$\hat{\Omega}_{ijl}^{(2)}$	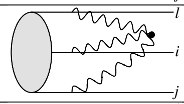	$f^{abc} \mathbf{T}_i^a \mathbf{T}_j^b \mathbf{T}_l^c$
$\Omega_{ij,\mathrm{self-en.}}^{(2)}$	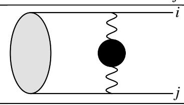	$T_R (\mathbf{T}_i \cdot \mathbf{T}_j)$
$\Omega_{ij,\mathrm{vertex-corr.}}^{(2)}$	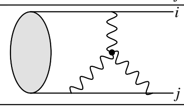	$T_R (\mathbf{T}_i \cdot \mathbf{T}_j)$

Table 3: Amplitudes of the two-loop diagrams contributing in the soft limit. In each case the diagram is split into its respective colour structure and into the kinematical part which is abbreviated by the $\Omega^{(2)}$-coefficients. The latter are obtained by using QED-type Feynman rules.

Structure	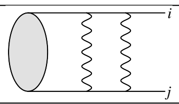	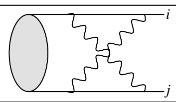	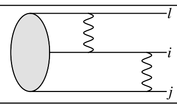	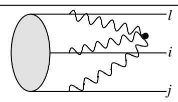
$\Gamma_\sigma^{(2)}$	✓	✓	✓	×
$\rho^{(2)}$	✓	✓	✓	×
ρ_σ	✓	✓	✓	✓
$\tilde{\rho}$	✓	✓	×	×
$\Sigma_{\sigma\tau}^{(2)}$	✓	✓	×	×
$\hat{\Sigma}_{\sigma\tau}^{(2)}$	✓	✓	✓	✓
$\tilde{\Sigma}_{\sigma\tau}^{(2)}$	✓	✓	✓	×
$\Sigma_{\sigma\tau}^{\prime(2)}$	✓	✓	✓	✓
$\Sigma_{\sigma\tau}^{\prime\prime(2)}$	✓	✓	✓	×

Table 4: Overview of which two-loop diagrams contribute to which coefficients of the soft anomalous dimension matrix in the colour-flow basis.

F List of kinematically forbidden cuts for one-loop/one-emission and two-loop order

When applying the Feynman tree theorem to the diagrams of one-loop/one-emission and two-loop order several cuts occur which do not give a contribution due to kinematic constraints which cannot be satisfied simultaneously or due to the form of the integral in the transverse momentum variable (cf. equation (4.24)). In this appendix such cuts are identified and listed for each of the two-loop diagrams.

In dimensional regularisation the following integral vanishes

$$\int_0^\infty \mathrm{d}q_\perp^2 \left(\frac{\mu}{q_\perp}\right)^{2\varepsilon} \delta(q_\perp^2)\, I = 0 \;, \tag{F.1}$$

if the integrand I either does not depend on the transverse momentum $q_\perp$ or if it is a regular function for $q_\perp \to 0$. Due to the presence of the $\delta(q_\perp^2)$ one can cut off the upper integral boundary at an arbitrary value, such that there is no UV divergence anymore. Consequently, the ε parameter is smaller than zero since one only has to deal with the infrared behaviour of the integrand and as a result the integral vanishes. This property can be used to neglect several cuts which occur when applying the Feynman tree theorem to the loop integrals.

In the following, the vanishing cuts are listed for each of the diagrams:

Two-loop double exchange diagram (equation (5.45))

- $\mathrm{d}^d k\, \mathrm{d}^d q\; \tilde{\delta}(k)\tilde{\delta}(q)\delta(p_i \cdot (k+q))\delta(p_i \cdot q)$
- $\mathrm{d}^d k\, \mathrm{d}^d q\; \tilde{\delta}(k)\tilde{\delta}(q)\delta(p_i \cdot (k+q))$
- $\mathrm{d}^d k\, \mathrm{d}^d q\; \tilde{\delta}(k)\delta(p_i \cdot (k+q))\delta(p_i \cdot q)$
- $\mathrm{d}^d k\, \mathrm{d}^d q\; \tilde{\delta}(k)\tilde{\delta}(q)\delta(p_i \cdot q)$
- $\mathrm{d}^d k\, \mathrm{d}^d q\; \tilde{\delta}(q)\delta(p_i \cdot q)\delta(p_i \cdot k)$
- $\mathrm{d}^d k\, \mathrm{d}^d q\; \tilde{\delta}(q)\delta(p_i \cdot q)\delta(p_i \cdot k)\tilde{\delta}(k-q)$

The first as well as the third cut evaluate to zero since, using the parametrisation $q^\mu = \alpha p_i^\mu + \beta k^\mu + n_\perp^\mu q_\perp$, one finds a both a $\delta(\beta)$ and a $\delta(1+\beta)$. All of the other cuts vanish since they lead to a contribution of the form of equation (F.1). This can be observed by decomposing the loop momenta in terms of light-cone coordinates, i.e. $k^\mu = \alpha p_i^\mu + \beta p_j^\mu + n_{\perp,k}^\mu k_\perp$ and $q^\mu = \hat{\alpha} p_i^\mu + \hat{\beta} p_j^\mu + n_{\perp,q}^\mu q_\perp$. For instance, for the fifth cut in the list, one gets $\delta(\beta)\delta(\hat{\beta})\delta(2\hat{\alpha}\hat{\beta}(p_i \cdot p_j) - q_\perp^2)\theta(\hat{\alpha}+\hat{\beta})$ and the remaining integrand is of the form $([-\alpha + i0][-\hat{\alpha}+i0])^{-1}$. This gives a vanishing contribution according to equation (F.1) for an integrand independent of $q_\perp$. Similarly the other cuts can be shown to vanish.

Two-loop crossed double exchange diagram (equation (5.46)):

- $\mathrm{d}^d k\, \mathrm{d}^d q\ \tilde{\delta}(k)\delta(p_i \cdot q)\delta(p_i \cdot (k+q))$
- $\mathrm{d}^d k\, \mathrm{d}^d q\ \tilde{\delta}(q)\tilde{\delta}(k)\delta(p_i \cdot (k+q))$
- $\mathrm{d}^d k\, \mathrm{d}^d q\ \tilde{\delta}(q)\tilde{\delta}(k)\delta(p_i \cdot (k+q))\delta(p_i \cdot q)$
- $\mathrm{d}^d k\, \mathrm{d}^d q\ \tilde{\delta}(k)\tilde{\delta}(q)\delta(p_i \cdot q)$
- $\mathrm{d}^d k\, \mathrm{d}^d q\ \tilde{\delta}(q)\delta(p_i \cdot k)\delta(p_i \cdot q)$
- $\mathrm{d}^d k\, \mathrm{d}^d q\ \tilde{\delta}(q)\tilde{\delta}(k-q)\delta(p_i \cdot k)\delta(p_i \cdot q)$
- $\mathrm{d}^d k\, \mathrm{d}^d q\ \tilde{\delta}(q)\delta(p_i \cdot k)\delta(p_i \cdot q)\delta(p_j \cdot (q-k))$
- $\mathrm{d}^d k\, \mathrm{d}^d q\ \tilde{\delta}(q)\tilde{\delta}(k-q)\delta(p_i \cdot k)\delta(p_j \cdot (q-k))$
- $\mathrm{d}^d k\, \mathrm{d}^d q\ \tilde{\delta}(q)\tilde{\delta}(k-q)\delta(p_i \cdot k)\delta(p_i \cdot q)\delta(p_j \cdot (q-k))$

The cuts of the first and the third point evaluate to zero due to kinematic constraints, as already described for the double exchange diagram.
All of the other cuts can be brought into a form of the integral in equation (F.1) and thus vanish as well. For instance, in light-cone coordinates, one finds for the eighth cut a contribution of $\delta(2\hat{\alpha}\hat{\beta}(p_i \cdot p_j) - q_\perp^2)\theta(\hat{\alpha}+\hat{\beta})\delta(\alpha-\hat{\alpha})\delta(2\alpha\beta(p_i \cdot p_j) - k_\perp^2 - 2(\alpha\hat{\beta}(p_i \cdot p_j) + \hat{\alpha}\beta(p_i \cdot p_j) + k_\perp q_\perp (n_{\perp,k} \cdot n_{\perp,q})))\theta(\alpha+\beta-\hat{\alpha}-\hat{\beta})\delta(\beta)$. Due to the restriction $\theta(q_\perp)$ from the measure, the first delta function implies $\theta(\hat{\alpha})\theta(\hat{\beta})$, while there is also a $\theta(-\hat{\beta})$ when setting $\beta = 0$ and $\alpha = \hat{\alpha}$ according to the other delta functions. Thus, one has to demand that $\delta(q_\perp^2)$ holds, which leads to the conclusion that the cut vanishes.

Two-loop vertex-correction diagram (equations (5.47) and (5.48)):

After the reduction of the two-loop vertex diagram two integrals remain. Their analysis (cf. equation (5.47) and (5.48)) leads one to the following cuts which give a vanishing contribution:

- $\mathrm{d}^d k\, \mathrm{d}^d q\ \tilde{\delta}(q)\tilde{\delta}(k)\tilde{\delta}(q-k)\delta(p_i \cdot k)$
- $\mathrm{d}^d k\, \mathrm{d}^d q\ \tilde{\delta}(q)\tilde{\delta}(k)\delta(p_i \cdot k)$
- $\mathrm{d}^d k\, \mathrm{d}^d q\ \tilde{\delta}(q)\tilde{\delta}(k)\tilde{\delta}(k+q)\delta(p_i \cdot k)$

These three cuts all give an integral of the form of equation (F.1).

Two-loop double exchange diagram with three hard lines (equation (5.50)):

- $\mathrm{d}^d k\, \mathrm{d}^d q\ \tilde{\delta}(k)\delta(p_i \cdot (k+q))\delta(p_i \cdot q)$

- $\mathrm{d}^d k\, \mathrm{d}^d q\ \tilde{\delta}(k)\tilde{\delta}(q)\delta(p_i \cdot (k+q))$
- $\mathrm{d}^d k\, \mathrm{d}^d q\ \tilde{\delta}(k)\tilde{\delta}(q)\delta(p_i \cdot (k+q))\delta(p_i \cdot q)$
- $\mathrm{d}^d k\, \mathrm{d}^d q\ \tilde{\delta}(k)\tilde{\delta}(q)\delta(p_i \cdot q)$
- $\mathrm{d}^d k\, \mathrm{d}^d q\ \tilde{\delta}(q)\delta(p_i \cdot q)\delta(p_i \cdot k)$
- $\mathrm{d}^d k\, \mathrm{d}^d q\ \tilde{\delta}(k-q)\tilde{\delta}(q)\delta(p_i \cdot k)\delta(p_i \cdot q)$
- $\mathrm{d}^d k\, \mathrm{d}^d q\ \tilde{\delta}(k-q)\tilde{\delta}(q)\delta(p_i \cdot k)\delta(p_j \cdot (q-k))$
- $\mathrm{d}^d k\, \mathrm{d}^d q\ \tilde{\delta}(q)\delta(p_i \cdot q)\delta(p_i \cdot k)\delta(p_j \cdot (q-k))$
- $\mathrm{d}^d k\, \mathrm{d}^d q\ \tilde{\delta}(k-q)\tilde{\delta}(q)\delta(p_i \cdot k)\delta(p_i \cdot q)\delta(p_j \cdot (q-k))$

Two-loop triple gluon diagram with three hard lines (equations (5.51)-(5.53)):

- $\mathrm{d}^d k\, \mathrm{d}^d q\ \tilde{\delta}(q)\tilde{\delta}(k)\tilde{\delta}(k+q)\delta(p_l \cdot (k+q))$
- $\mathrm{d}^d k\, \mathrm{d}^d q\ \tilde{\delta}(q)\tilde{\delta}(k)\tilde{\delta}(q-k)\delta(p_i \cdot (k-q))$
- $\mathrm{d}^d k\, \mathrm{d}^d q\ \tilde{\delta}(k)\tilde{\delta}(q-k)\delta(p_i \cdot (k-q))\delta(p_l \cdot q)$
- $\mathrm{d}^d k\, \mathrm{d}^d q\ \tilde{\delta}(q)\tilde{\delta}(k)\delta(p_l \cdot q)$
- $\mathrm{d}^d k\, \mathrm{d}^d q\ \tilde{\delta}(q)\delta(p_i \cdot (k-q))\delta(p_l \cdot q)$
- $\mathrm{d}^d k\, \mathrm{d}^d q\ \tilde{\delta}(q)\tilde{\delta}(q-k)\delta(p_i \cdot (k-q))\delta(p_l \cdot q)$
- $\mathrm{d}^d k\, \mathrm{d}^d q\ \tilde{\delta}(q)\tilde{\delta}(k)\delta(p_i \cdot (k-q))\delta(p_l \cdot q)$
- $\mathrm{d}^d k\, \mathrm{d}^d q\ \tilde{\delta}(q)\tilde{\delta}(k)\tilde{\delta}(q-k)\delta(p_l \cdot q)$
- $\mathrm{d}^d k\, \mathrm{d}^d q\ \tilde{\delta}(q)\tilde{\delta}(k)\tilde{\delta}(q-k)\delta(p_l \cdot q)\delta(p_i \cdot (k-q))$

References

1. Dasgupta, M. & Salam, G. Resummation of nonglobal QCD observables. *Phys. Lett. B* **512,** 323–330 (Apr. 2001).
2. Martínez, R. Á., De Angelis, M., Forshaw, J. R., Plätzer, S. & Seymour, M. H. Soft gluon evolution and non-global logarithms. *Journal of High Energy Physics* **2018** (2018).
3. Forshaw, J., Holguin, J. & Plätzer, S. Parton branching at amplitude level. *Journal of High Energy Physics* **2019** (Aug. 2019).
4. Maltoni, F., Paul, K., Stelzer, T. & Willenbrock, S. Color-flow decomposition of QCD amplitudes. *Physical Review D* **67** (Sept. 2002).
5. Catani, S. & Grazzini, M. The soft-gluon current at one-loop order. *Nuclear Physics B* **591** (Dec. 2000).
6. Plätzer, S. Summing large-N towers in colour flow evolution. *The European Physical Journal C* **74** (2014).
7. Catani, S., Gleisberg, T., Krauss, F., Rodrigo, G. & Winter, J.-C. From loops to trees by-passing Feynman's theorem. *Journal of High Energy Physics* **2008,** 065 (2008).
8. Bierenbaum, I., Catani, S., Draggiotis, P. & Rodrigo, G. Feynman's Tree Theorem and Loop-Tree Dualities. *Proceedings of Science* (Nov. 2010).
9. Plätzer, S. *Soft Gluon Evolution* ,Unpublished. (2020).
10. Catani, S. & Grazzini, M. Infrared factorization of tree level QCD amplitudes at the next-to-next-to-leading order and beyond. *Nucl. Phys. B* **570,** 287–325 (Mar. 2000).
11. Binosi, D., Collins, J., Kaufhold, C. & Theussl, L. JaxoDraw: A graphical user interface for drawing Feynman diagrams. Version 2.0 release notes. *Computer Physics Communications* **180,** 1709–1715 (2009).
12. Muta, T. *Foundations of quantum chromodynamics: an introduction to perturbative methods in gauge theories* (World Scientific Publishing Company, 2009).
13. Schwartz, M. D. *Quantum field theory and the standard model* (Cambridge University Press, 2014).
14. Böhm, M., Denner, A. & Joos, H. *Gauge theories of the strong and electroweak interaction* (Springer Science & Business Media, 2012).
15. Plätzer, S. *Lecture notes of the course "Particle Physics III"* ,Unpublished. (2020).
16. Kilian, W., Ohl, T., Reuter, J. & Speckner, C. QCD in the Color-Flow Representation. *Journal of High Energy Physics* **2012** (June 2012).
17. Hagiwara, K. & Takaesu, Y. Generating QCD amplitudes in the color-flow basis with MadGraph. *European Physical Journal C* **71** (Oct. 2010).
18. Ángeles Martínez, R., Forshaw, J. R. & Seymour, M. H. Coulomb gluons and the ordering variable. *Journal of High Energy Physics* **12** (Oct. 2015).
19. Collins, J. C. Light cone variables, rapidity and all that. arXiv: `hep-ph/9705393` (May 1997).

20. Plätzer, S. *Amplitude Level Evolution* URL: `https://indico.cern.ch/event/876082/contributions/3876212/subcontributions/307838/attachments/2068117/3471188/slides.pdf`. July 2020.

21. Forshaw, J. R., Kyrieleis, A. & Seymour, M. H. Super-leading logarithms in non-global observables in QCD? *Journal of High Energy Physics* **2006,** 059–059 (Aug. 2006).

22. Forshaw, J. & Seymour, M. Soft gluons and superleading logarithms in QCD. *Nuclear Physics B - Proceedings Supplements,* 257–267 (Feb. 2009).

23. Leibbrandt, G. *Noncovariant gauges: quantization of Yang-Mills and Chern-Simons theory in axial-type gauges* (World Scientific, 1994).

24. Dissertori, G., Knowles, I. G. & Schmelling, M. *Quantum chromodynamics: high energy experiments and theory* (Oxford University Press, 2003).